Scalable Computing:
Practice and Experience

Scientific International Journal
for Parallel and Distributed Computing

ISSN: 1895-1767

Universitatea de Vest din Timişoara

Volume 19(1) March 2018

SUBSCRIPTION INFORMATION: please visit http://www.scpe.org

Scalable Computing: Practice and Experience

Volume 19, Number 1, March 2018

TABLE OF CONTENTS

DOI 10.12694/scpe.v19i1.1389
Scalable Computing: Practice and Experience ISSN 1895-1767
Volume 19, Number 1, pp. 1–14. http://www.scpe.org

A SOLUTION TO IMAGE PROCESSING WITH PARALLEL MPI I/O AND DISTRIBUTED NVRAM CACHE

ARTUR MALINOWSKI AND PAWEŁ CZARNUL*

Abstract. The paper presents a new approach to parallel image processing using byte addressable, non-volatile memory (NVRAM). We show that our custom built MPI I/O implementation of selected functions that use a distributed cache that incorporates NVRAMs located in cluster nodes can be used for efficient processing of large images. We demonstrate performance benefits of such a solution compared to a traditional implementation without NVRAM for various sizes of buffers used to read image parts, process and write back to storage. We also show that our implementation benefits from overlapping reading subsequent images while processing already loaded ones. We present results obtained in a cluster environment for three parallel implementation of blur, multipass blur and Sobel filters, for various NVRAM parameters such as latencies and bandwidth values.

Key words: image processing, high performance computing, NVRAM, distributed cache, Sobel, blur filter

AMS subject classifications. 68U10, 68W10

1. Introduction. For many customers the number of recorded megapixels is a key factor when choosing digital cameras. Assuming that engineers properly matched the size of an image sensor to its resolution, it is completely justified – each pixel contains additional information that could be used in order to improve quality of an image. The first affordable, commercially available digital cameras started from the resolution of about one megapixel, like Kodak DCS or NASA's Nikon F4 that was used during Space Shuttle missions [26]. The megapixel race led to about 20 megapixel sensors in modern smartphones and more than 50 megapixel sensors in DSLR equipment for professional photographers. Some digital cameras take things even a step further, like the recently announced Hasselblad device with effective resolution of 400 megapixels [11]. The scale grows even bigger for specialized devices, such as Hawaii telescopes of the project Pan-STARRS that are equipped with sensors of a resolution more than one gigapixel [13].

Apart from better sensors, the final image resolution could be obtained by combining multiple smaller parts. The sharpest view of the Andromeda Galaxy, created by NASA/ESA using data from Hubble telescope, contains 1.5 billion pixels [27]. This technique is useful not only in scientific research – in 2016 Bentley Motors created a 53 gigapixel photo only for demonstration of the companys commitment to technological innovation [38].

Large images are more difficult during processing. The size of a file could exceed the amount of RAM installed within a single node. Moreover, more demanding algorithms involve complex computations. It is possible to offload some processing to GPU (compatible with GPGPU technologies, e.g. NVIDIA CUDA, OpenCL) or computational accelerators (e.g. Intel® Xeon Phi®), but it may require many round trips between a host memory and a device due to limited memory on such compute devices.

An alternative solution for high data volume (especially with multiple images) and demanding computations is changing the processing application from running on a single node to the one distributed among several nodes. With such an approach, an application designer can include all of the techniques and methods of High Performance Computing (HPC) in the application. It should be especially convenient for processing used in scientific applications, where developers are familiar with HPC tools and technologies.

Within this paper we propose a distributed architecture for a large image processing application based on HPC tools. The solution is created using Message Passing Interface (MPI), image file access is accelerated by a byte-addressable non-volatile RAM (NVRAM) distributed cache. Initially, the framework consists of three exemplary image filters, but it can be easily extended further. A set of experiments proved that the architecture is capable to process large images (single or multiple) in reasonable time.

2. Related work and motivation. Firstly, parallel image processing, as a way to decrease execution times of image filtering, important in many fields, has been analyzed and used for many years already.

*Faculty of Electronics, Telecommunications and Informatics, Gdansk University of Technology, Poland, artur.malinowski@pg.edu.pl, pczarnul@eti.pg.edu.pl

2.1. Parallel image processing. Parallel programming with Message Passing Interface (MPI) traditionally allows utilization of clusters but MPI-based programs can be also run successfully on powerful workstations with multi- (such as Intel Xeon) and many-core processors (such as Intel Xeon Phi x200) or many-core coprocessors (such as Intel Xeon Phi x100). Parallel image processing with MPI has been analyzed in many works. Paper [29] presents design and results of a C+MPI framework for low-level image processing, run on a cluster of up to 64 nodes connected with Myrinet. An example of a multi-baseline stereo vision application is used for which speed-ups up to around 10 have been obtained on 32 nodes. In work [28] authors demonstrated parallel extensions, also using MPI, to the Delft Image Processing LIBrary (DIPLIB) library. For geometric mean filters and larger window sizes and image sizes (15x15 for an 256x256 and 9x9 and 15x15 for 1024x1024 images) the authors have obtained linear speed-ups up to 24 machines. Paper [33] introduced Parallel Image Processing Toolkit (PIPT) that uses MPI, with load balancing schemes in the framework for transparent distribution of computations. Paper [2] deals with parallel image processing and considers data distribution for heterogeneous machines with scalability results for an active contour algorithm. Website [5] provides a C/C++ with MPI implementation of several operations on images: contrast an image, filtering: smooth, blur, sharpen, mean_removal, emboss as well as computing image entropy.

Other parallel programming APIs allowing execution on clusters have also been used for image processing. In paper [6] the authors extended the well known image processing tool GIMP with a possibility to use a cluster based system for pipelined image processing. Paper [32] presents parallel processing of pressure-sensitive paint images on a multiprocessor machine or a cluster with multiple nodes, however implemented with forks/pipes and TCP/IP.

Recently, parallel image processing with GPUs has been explored deeper in many fields, for example: plant growth analysis [30], medical applications such as cancer research [31] object recognition [35], embedded systems [4]. Several frameworks for image processing with GPUs have been developed [1, 16] along with a possibility to perform GPU image processing from higher level systems such as MATLAB [10]. However, GPUs have limitations in terms of maximum memory capacity – currently up to 16GB in the latest and expensive cards such as NVIDIA V100 or 12GB in NVIDIA Titan X. Consumer grade cards offer up to 8GB of memory. In view of this, processing of very large images might require several communications over PCI Express and the overall performance will suffer. Because of this, we explore the possibility of using NVRAM in parallel image processing, especially in a cluster environment, in which NVRAMs from various nodes might offer even higher capacities.

2.2. NVRAM applications. Non-volatile byte-addressable memory has several potential advantages that make it an interesting solution in increasing performance of demanding applications [19]. These include byte-addressability, sizes larger than RAM and persistence. There are several examples of applications analyzed in the literature.

One is low overhead checkpointing. Paper [14] proposes NVM-checkpoints for storing checkpoints locally and remotely. Authors propose checkpointing based on a hybrid memory model. An application uses an NVM interface for provision of information regarding checkpointed data. While data remains in RAM, it can be copied to NVM. NVM is used for local and less frequent remote checkpoints. Apart from an NVM kernel manager, the provided NVM user library for handling checkpointed data: allocation, moving data from DRAM to NVM and restart. Checkpointing using NVRAM was also proposed by us in [7] where wrappers to MPI functions for use with NVRAM were proposed. We demonstrated that for expected performance characteristics of actual NVRAM devices (latencies and bandwidth) NVRAM based checkpointing performs considerably better than the traditional disk based approach for applications such as the HPCCG benchmark and the PageRank algorithm.

In terms of storage oriented solutions, several contributions have been made. Paper [17] presents NVWAL that uses NVRAM for maintaining a write-ahead log that benefits from byte addressability of NVRAM, provides a transaction-aware persistency and shows that NVWAL provides considerably better performance for SQLite compared to using flash memory. In paper [39] authors present Mojim which is a two-tier system where the first one contains a mirrored pair of nodes and the second tier encompasses secondary backup nodes with weakly consistent data copies. The system provides reliability and availability. The paper demonstrates that a solution with replication with non-volatile memory provides similar or better performance than a version with non-volatile memory without replication. In paper [9] authors propose Phoenix (PHX) which is an NVRAM-

bandwidth aware object store for persistent objects. What is interesting is the fact that it can use NVRAM and DRAM simultaneously as well as incorporate information such as bandwidths of devices, distances and energy costs. The authors have presented that their solution reduced checkpoint/restart times for three tested HPC benchmarks such as GTC, CM1 and S3D HPC compared to NVRAM only solutions.

Work [18] demonstrates how NVRAM can be used in order to improve performance of a browser. This includes making use of NVRAM for placement of files for startup. Furthermore, perceived performance is increased through caching of web resources in NVRAM.

Another application that can benefit from NVRAM is online transaction processing. Paper [12] presents how NVRAM can be used for a logging subsystem and justifies that it provides better performance to cost ratio than replacing the whole storage with NVRAM.

Paper [8], on the other hand, provides a study of impact of NVRAM on a Breadth-First Search (BFS) graph traversal algorithm. An NVRAM simulator called PerMA has been used which allows to model latencies and bandwidths of memory types from flash to RAM. The authors came to the conclusion that with sufficient concurrency, with NVRAM the analyzed algorithm will be able to approach the performance of an in-memory algorithm.

In paper [15] authors investigate benefits from using NVRAM for large scale data intensive (I/O) applications and demonstrated gains such as 3.85x I/O throughput and 1.6x for ort based data post processing over a disk only approach.

Paper [36] demonstrates benefits through an average of 2.7x performance improvement of the map phase of Map Reduce from using NVRAM. Benchmarks and workloads included those from Intel HiBench and PUMA. Low level optimization of processing using NVRAM is analyzed in work [20] in which authors presents a software cache in which lines to be flushed are buffered first and flushed later. Cache size is adapted at run time.

So far image processing with NVRAM has been addressed to a certain degree in the literature in terms of energy efficiency. For instance, paper [25] presents that power consumption for parallel image processing can be reduced greatly with the use of non-volatile memory. Work [37] presents energy efficient in memory machine learning for image processing and corresponding benefits when using non-volatile memory.

2.3. Motivation and goal. Taking into account the aforementioned contributions, in this work we propose to integrate usage of NVRAM for parallel image processing, especially large images, and demonstrate benefits of this approach. With expected adoption of NVRAM in the nearest future, we believe that it will be an asset applicable to a variety of fields and users.

3. Proposed solution.

3.1. Assumptions. From the HPC perspective, image processing could be regarded as performing a set of operations on a two-dimensional matrix in which each element corresponds to a pixel of a selected color. In the most straightforward approach an application performs the following steps:

1. The application opens an image file and reads an image as a matrix.
2. The matrix is split into submatrices.
3. Submatrices are assigned to processes (one to one or many to one depending on the processing paradigm)
4. Each process reads required data, performs its computations on the assigned part and writes output.
5. The application closes the file.

We believe that these steps make the application as simple as possible from a developer point of view. Our solution sticks to this in order to make it easy to implement own image processing algorithms. On the other hand, our solution uses NVRAM in an intermediate layer between files and the MPI I/O functions invoked within the application.

Such an approach should be efficient with images of a size limited to the sum of all RAM capacities in a cluster. In such case a file is read once at the beginning of processing and written back after computations have been completed. The situation changes when the size of an image increases. The greater the size of a file, the smaller image part can be processed at once and the application requires more read/write requests. Finally, the application that used to be computationally bound becomes data intensive and I/O operations appear to be a bottleneck.

Taking everything into account, the task is to design the application as simple as possible, keeping in mind that in order to provide good application performance, it is required to perform I/O operations efficiently.

3.2. Design of the solution. As a base for our application we used the C programming language and MPI which is the de facto standard for message passing parallel programming allowing to run applications on clusters but also within nodes with multi-core CPUs. Choosing MPI ensures a wide knowledge of a platform among HPC application programmers – e.g. MVAPICH, one of most popular MPI implementation, declares being used by more than 2,750 organizations[1]. Many MPI implementations also offer additional advantages like built-in Infiniband integration, efficient process managers, several levels of threads support or dynamic process management routines.

In order to provide file access for all nodes within a cluster, in a typical HPC environment a parallel file system (PFS) is used. Most popular PFSes provide POSIX support, but applications based on MPI can use MPI I/O – a set of functions that allow accessing a file in a way convenient for a programmer. Popular MPI I/O implementations also include many different optimizations, e.g. data sieving and two-phase I/O in ROMIO [34].

One of the conditions for comfortable file usage is the possibility to read and write a data chunk efficiently independently from its location and size. As we will show in experiments, performance of specific operations in regular MPI I/O and PFS could be significantly improved using our byte-addressable NVRAM distributed cache [23].

The NVRAM cache, previously proposed by us, is a transparent component placed between an application and MPI I/O. Its transparency is achieved through reimplementing selected MPI I/O API, so no additional effort is needed from a developer. The most important requirements of this extension are installation of a NVRAM device in each node of a cluster and the size of a file limited to the sum of all NVRAM capacities. As justified in related work, NVRAM capacities are expected to far exceed RAM properties, so it should not be a problem in the nearest future. The main distinguishing features of the cache are fully decentralized management, prefetching the whole file during opening, synchronizing the whole file during closing and keeping minimal metadata. A set of tests with synthetic benchmarks and real-life applications like map searching, crowd simulation or graph processing proved I/O improved performance, especially for long running applications [21, 22, 23]. An additional feature of the cache that naturally benefits from NVRAM persistence is safety of the data during processing [24]. The cache can also run using volatile RAM as its storage. Such a configuration forces reducing RAM available for the application and does not offer any fail-safe mechanisms, but can be successfully applied in order to enhance the efficiency of I/O.

Figure 3.1 presents the most important architecture components and their dependencies. As previously stated, image files are served by a PFS. An application accesses it using MPI I/O API. The NVRAM cache is a transparent component that improves efficiency of file access. Optionally, an application can use computational accelerators.

3.3. Performance optimization. According to the description of the NVRAM based cache, overhead for opening and closing a file may have a significant impact on application execution time. In a typical HPC case this issue is negligible – in long running applications the gain from faster data access fully compensates the initialization and deinitialization phases. However, omitting this overhead for fast and simple image processing algorithms would be noticeable. The proposed application is prepared to be used as a service that is able to process requested images one by one. The common idea in HPC used for avoidance of waiting for a data is overlapping communication and computation. In our application we implemented a similar approach – image processing overlaps with opening/closing a file.

Another important task was tuning the PFS. Our cluster was equipped both with Infiniband and 10Gb/s Ethernet, so we were able to separate the application and the PFS traffic. Internal MPI communication was based on Infiniband, while our cache was connected to PFS using Ethernet. The OrangeFS setting that has the most impact on significant reduction of application execution time was turning off TroveSyncData option. It allowed to omit costly data synchronization after each operation at the cost of increased risk of loosing data. Instead of protection offered by OrangeFS we can use the fail-safe mode built into the NVRAM cache mechanism or take the risk – in the worst case the application will process a lost image once more.

[1] `http://mvapich.cse.ohio-state.edu/`

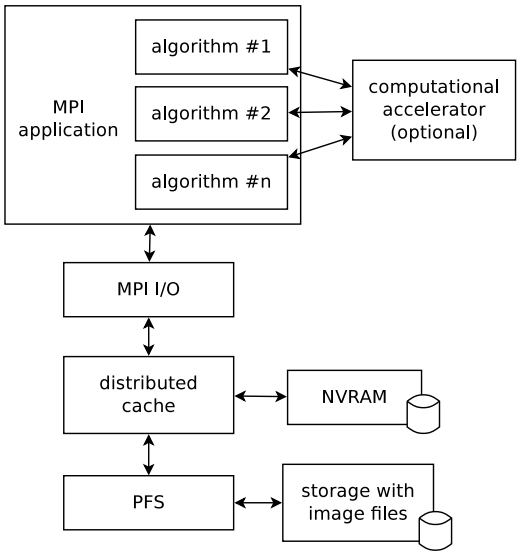

FIG. 3.1. *Architecture of the application for large image processing*

Application optimizations included also, among others, tuning buffer sizes, reducing number of round-trips between PFS and NVRAM cache or proper usage of MPI I/O flags like `MPI_MODE_READONLY`.

3.4. Exemplary filters. Our implementation contains code for parallel execution of three different filters. Figure 3.2 presents exemples of an original image and processed results. The initial version of application contains the following filters:

1. Blur – the idea is to blur an image by averaging values of neighboring pixels (to each pixel).
2. Multi-pass blur – similarly to the standard blur but the value of a considered pixel is also considered in the average. Additionally, several passes through an image are executed.
3. Sobel – in this case, application of the filter relies on conversion of each pixel to grayscale (using a luminosity approach) and application of a 3x3 operator on each pixel. This allows to compute minimum and maximum values across a domain and then normalize final values based on these minimum and maximum values. It should be noted that these minimum and maximum values need to be propagated across all processes (realized using `MPI_Allreduce()`).

4. Experiments. The main goal of experiments was not only to show that the application processes images in reasonable time, but also to present a comparison of an architecture with and without the byte-addressable NVRAM distributed cache. As parameters of expected NVRAM devices are not yet published, the last three experiments were dedicated to different settings of the simulation platform.

4.1. Testbed environment. The extension was tested on cluster named Lap06, its technical specifications are included in Table 4.1 and Table 4.2. As the actual NVRAM devices are not available on the market yet, we used a hardware simulation platform. The platform internally uses RAM but increases its access latency and modifies the bandwidth. Unless otherwise noted, the platform was set according to Table 4.3.

4.2. Results of NVRAM extension vs regular MPI I/O.

4.2.1. Various image sizes. The first set of experiments verified the possibility of processing large images efficiently. In this scenario we processed a single image using 6 computing nodes, 7 processes per each. As presented in Fig. 4.1 and 4.2, in one minute the application was able to apply blur filter on an 800 megapixel image and blur multi-pass filter (10 passes) on a 500 megapixel image. As expected, processing time increases linearly with increasing the size of an image. Comparison of unmodified MPI I/O and the one supported by NVRAM cache clearly shows that extended version performed much better. For the blur filter execution time was about 30% lower for small images (100 megapixels) up to more than 40% lower for images larger that 500

(a) Original image

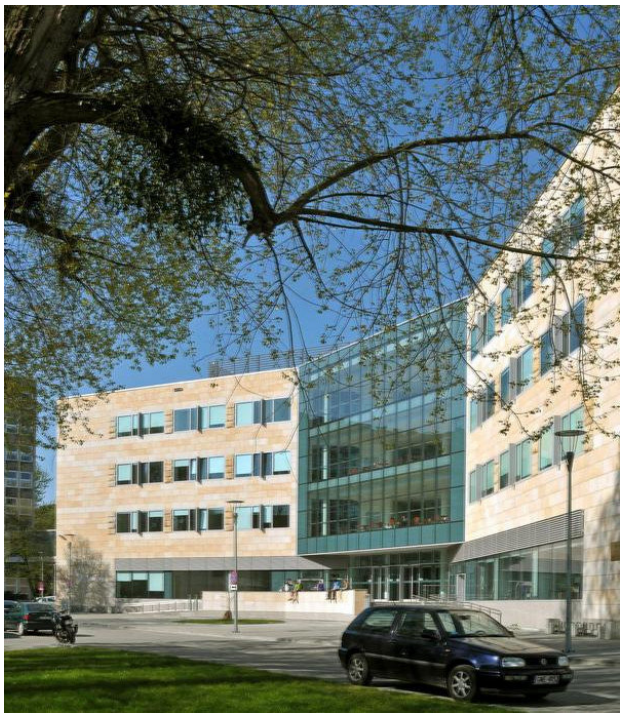

(b) Blur filter

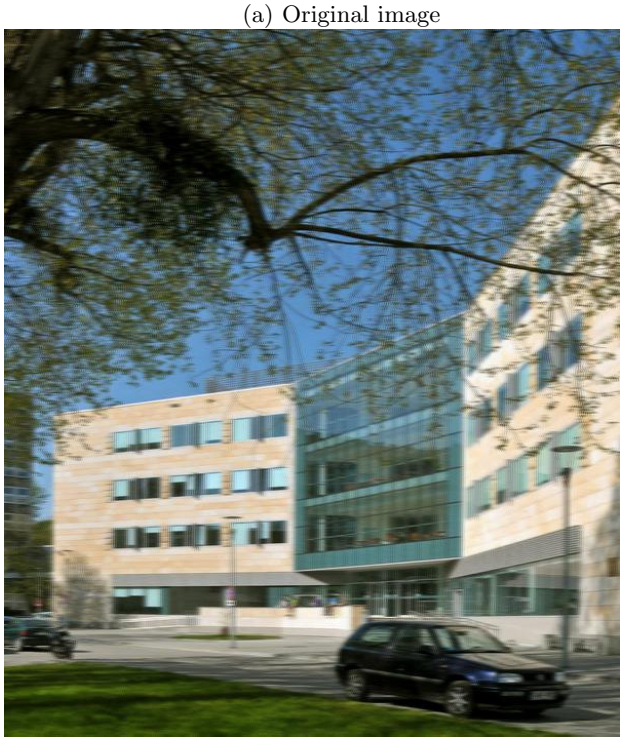

(c) Blur-multipass filter

(d) Sobel filter

FIG. 3.2. *Original image and images processed using three different filters (fragment of a photo of Gdansk University of Technology, author: Krzysztof Krzempek)*

TABLE 4.1
Hardware used in performance tests

Number of computing nodes	6
Number of PFS nodes	2
CPU	2 x Intel® Xeon® E5-4620
RAM	15GB
Network	40Gb/s Infiniband, 10Gb/s Ethernet
Storage	SSD
NVRAM simulation	17GB, hardware simulation

TABLE 4.2
Clusters' software configuration

Operating system	CentOS release 6.5
MPI implementation	MPICH 3.2
PFS	Orange-FS 2.9.6

TABLE 4.3
NVRAM simulation platform parameters

additional latency before accessing the data	2000ns
additional latency before flushing the data on device	600ns
memory bandwidth divider	4

megapixels. According to previous expectations, less demanding algorithms like blur suffer from overhead for opening and closing a file. This issue does not occur with blur multi-pass – for this scenario we were able to observe more than 90% reduction of the execution time.

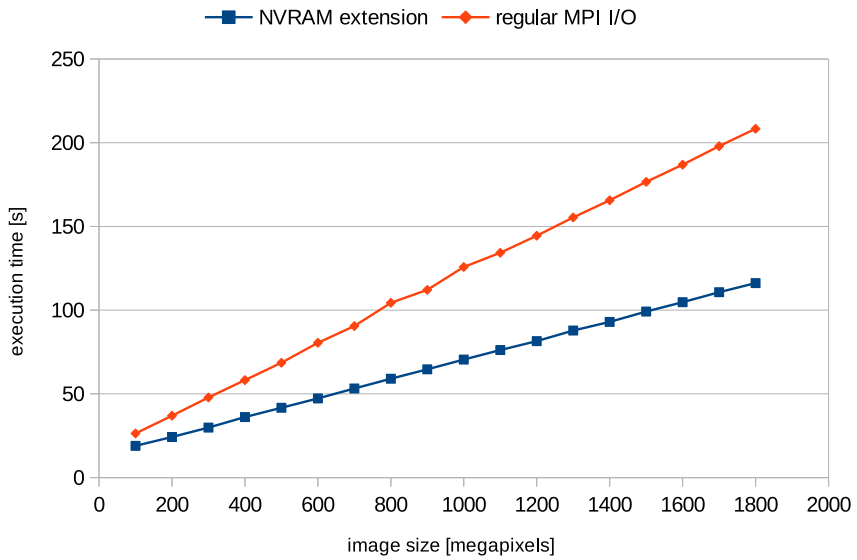

FIG. 4.1. *Image processing results, blur filter, 6 nodes, 42 processes, 512kB application buffers*

4.2.2. Various number of images. The next set of tests was focused on testing effectiveness of overlapping image processing with opening/closing a file. In order to verify the approach we compared the proposed application running with multiple files and the same application, but executed for each single image sequentially. Results presented in Fig. 4.3 and 4.4 demonstrate reduced execution times for application with overlapping.

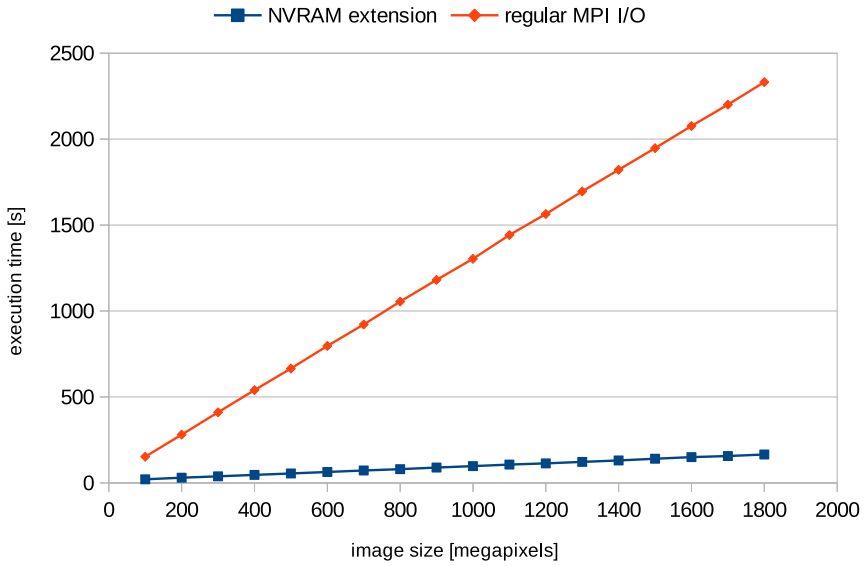

FIG. 4.2. *Image processing results, blur multi-pass filter, 6 nodes, 42 processes, 512kB application buffers*

Unfortunately, the gain from implementation of overlapping was lower that expected. For a relatively simple filter – Sobel – we observed reduction of execution time at the level of 5%. More complicated algorithms like blur multi-pass allow for saving more time – for test scenario illustrated in Fig. 4.4 it was about 10%.

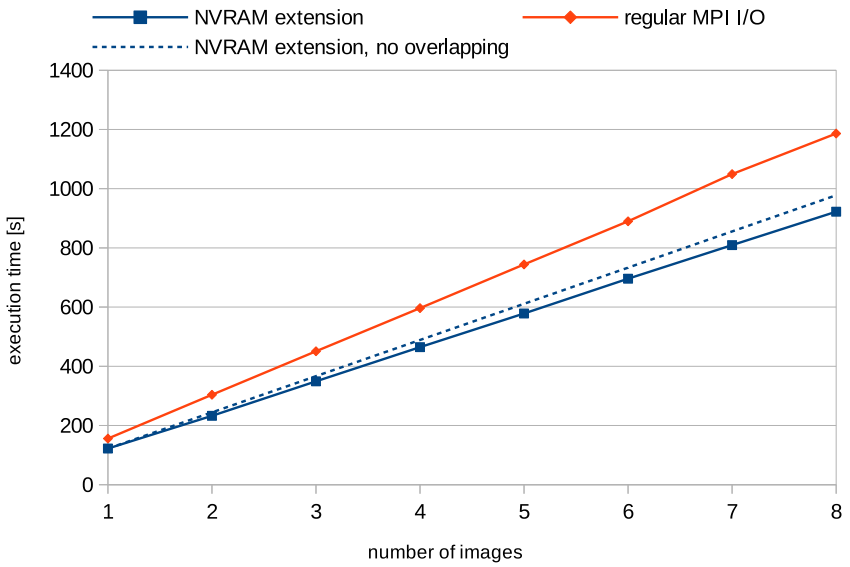

FIG. 4.3. *Image processing results, Sobel filter, 6 nodes, 42 processes, 512kB application buffer, each image of 1 gigapixel*

4.2.3. Various buffer sizes. Although our NVRAM distributed cache is designed to work well with small data chunks (even with access to single bytes), the proposed application uses internal buffers. Two buffers located in RAM, one for read and one for write operations, prevent from too frequent file requests. Results presented in Fig. 4.5 and 4.6 prove that the NVRAM cache is prepared for serving even small data chunks.

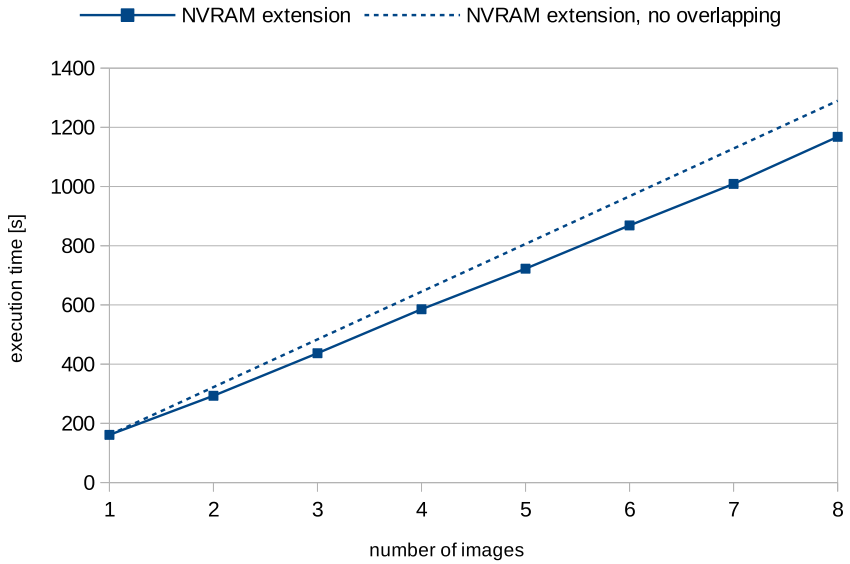

FIG. 4.4. *Image processing results, blur multi-pass filter, 6 nodes, 42 processes, 512kB application buffer, each image of 1 gigapixel*

Results were similar both for simple and more demanding processing algorithms. With unmodified MPI I/O and requests lower than 128kB the application is extremely slow, because the PFS is flooded with a large number of requests incoming frequently. In our opinion, such a result is another argument for applying the proposed architecture – implementing buffers is an additional overhead for developers, especially for more complicated, non-linear image processing algorithms. The proposed solution allows to focus more on implementing algorithms themselves, rather than on difficult I/O optimization.

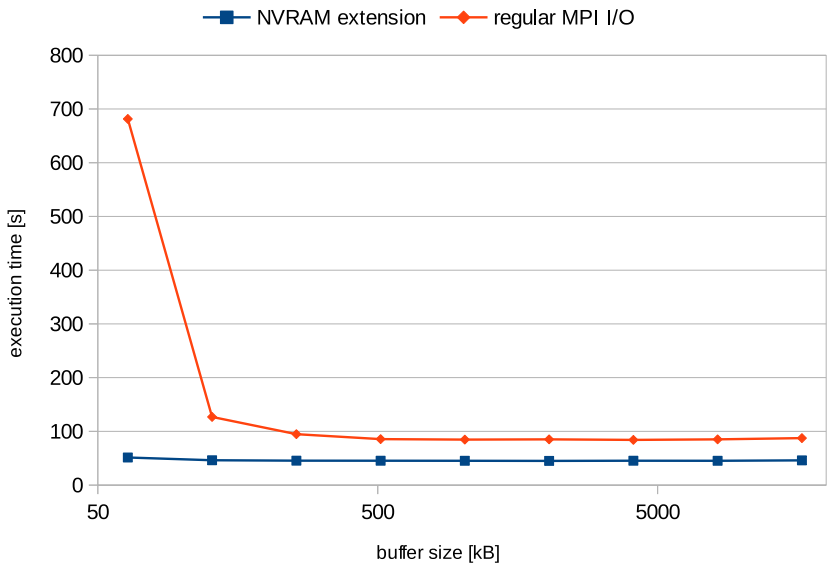

FIG. 4.5. *Image processing results, Sobel filter, 6 nodes, 42 processes, image of 0.5 gigapixel*

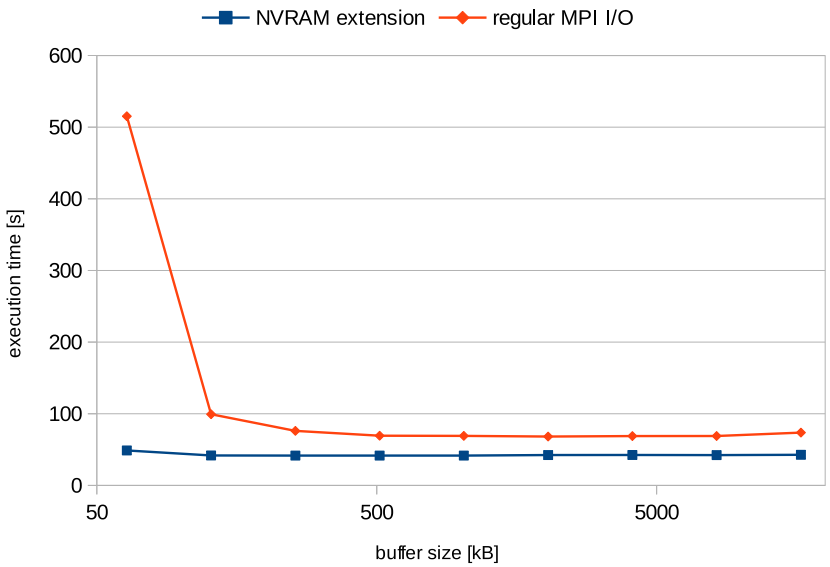

FIG. 4.6. *Image processing results, blur filter, 6 nodes, 42 processes, image of 0.5 gigapixel*

4.2.4. Scalability. One of the most important parameters of HPC applications is scalability regarded as the potential of reducing execution time with increasing hardware resources, today most often the number of a cluster nodes and consequently the number of CPUs and cores. It may seem that with processing multiple images, the application does not require good scalability because it could be executed multiple times for each image independently. In practice, when the I/O is the bottleneck of the system, running many instances of a data intensive application may result in overloading of PFS.

Figure 4.7 shows application speedup while increasing the number of nodes. Unmodified MPI I/O does not scale well because the gain from higher computational power of greater number of nodes is insignificant when PFS is more and more overloaded. The speedup of execution with NVRAM cache is also far from linear, but still significant. Scalability is of the features of the distributed architecture of NVRAM cache. The solution is designed in such way that each node participates in serving read/write requests. With an increasing number of a file accesses from a higher number of processes, the extension has more nodes to process it, so the average number of requests per node is constant. Furthermore, better scalability results are expected for more demanding algorithms with a higher ratio of computations to I/O.

4.2.5. Various NVRAM simulation parameters. As we do not have NVRAM based devices yet, we used a hardware simulation platform. Unknown properties of final devices result in necessity for testing solutions for many different configurations in the range of expected parameter values. Although NVRAM devices should outperform today's SSDs, we assumed pessimistic values at the level similar to announced SSD specifications (i.e. Intel® Optane® P4800X with typical latency of less than 10μs, up to 2400/2000MB/s read/write speed and 500k IOPS for random requests [3]). The following three tests were performed using the blur multi-pass filter.

Figure 4.8 presents comparison of execution times according to the memory bandwidth. Our nodes were equipped with DDR3 1600Mhz memory units, the simulator allowed to divide the bandwidth by a certain factor. In the plot we can observe that this parameter does not have a significant impact on the proposed application – average growth of the execution time after reducing the bandwidth was less than 2.6%. With frequent, low size requests our application depends more on the access latency rather than bandwidth.

Results shown in Fig. 4.9 concern an additional delay required to flush the cached data onto the device to make it persistent. The plot is quite similar to the previous one – even when the additional latency before flushing the data was doubled, average execution time of the application grew up about 2%. This latency is

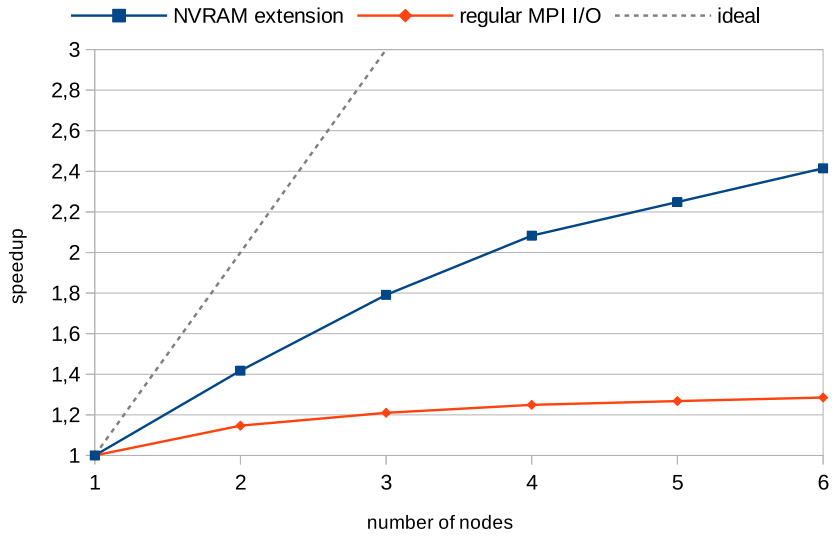

FIG. 4.7. *Image processing results, blur multi-pass filter, 512kB application buffers, image of 1.5 gigapixel*

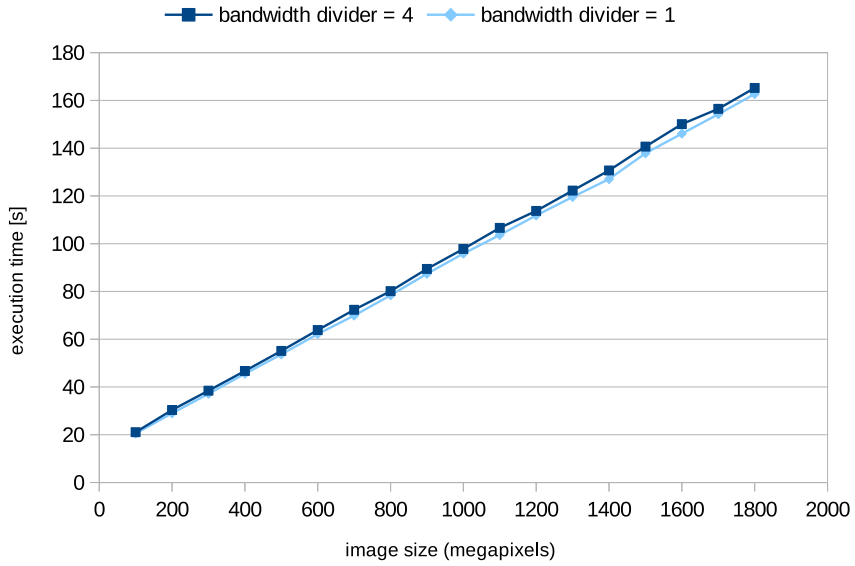

FIG. 4.8. *Image processing results, blur multi-pass filter, 6 nodes, 42 processes, 128kB application buffer*

added only for write accesses and in our application write operations are less common than reads.

A much more visible impact on execution time is shown in Fig. 4.10. In this scenario we increased the additional latency added for each memory request. Obtained results resulted in about 7% growth of processing time.

Those three experiments proved that the impact of NVRAM parameters is significant in terms of execution time, but insignificant when comparing the application with NVRAM cache and the one without. This leads to the conclusion that if only NVRAM devices provide performance at the level of SSD devices or better, the proposed architecture will be more efficient using the proposed distributed cache.

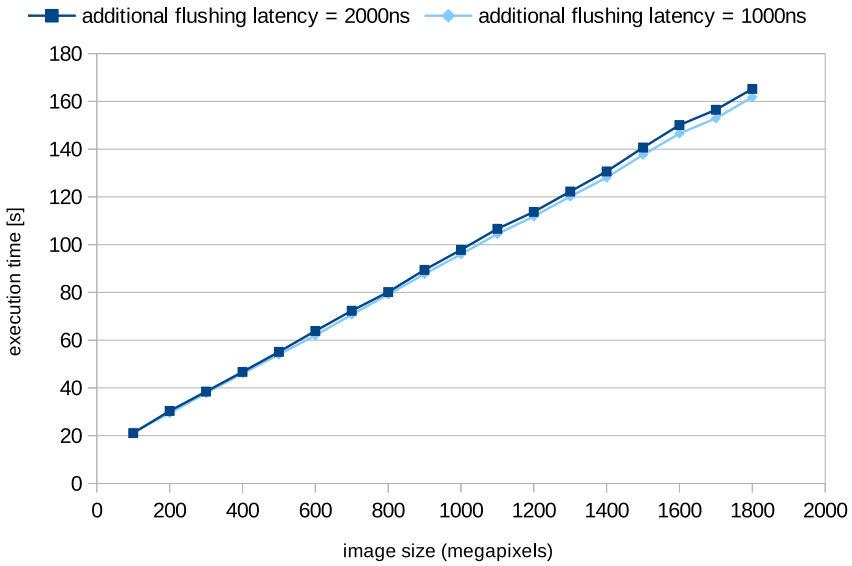

FIG. 4.9. *Image processing results, blur multi-pass filter, 6 nodes, 42 processes, 128kB application buffer*

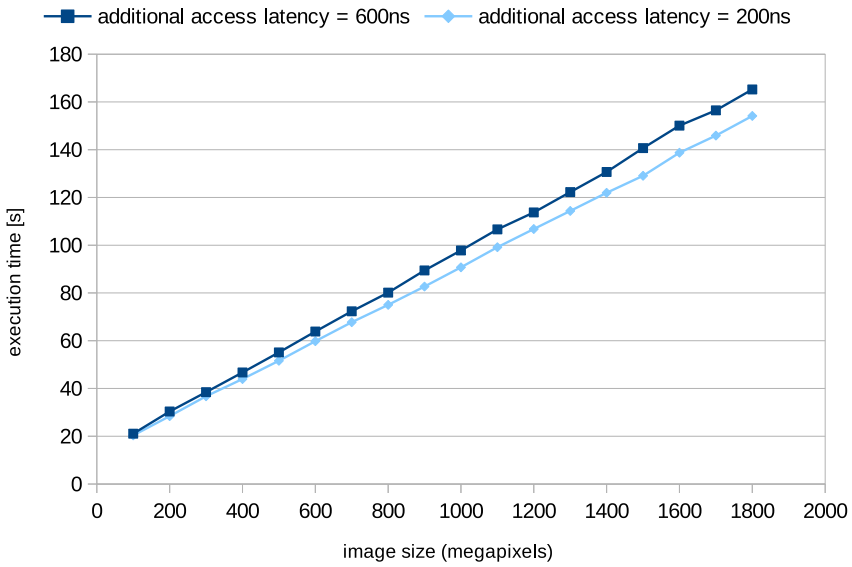

FIG. 4.10. *Image processing results, blur multi-pass filter, 6 nodes, 42 processes, 128kB application buffer*

5. Conclusions and future work. In this paper we proposed an architecture and software/hardware components for large image processing application. Motivations included observation of increasing images sizes and wide interest of efficient image processing architectures collected in the related work. In the exemplary implementation we included three image processing filters: blur, Sobel and multi-pass version of blur. The application is able to process a single image, as well as multiple images using additional optimization that involves overlapping file opening and processing for subsequent images. The most distinguishing feature of the proposed solution is application of byte-addressable NVRAM distributed cache. Emerging memory technology combined with cache design allows for reducing PFS load, making the application development more convenient

by using small data chunks efficiently and easily obtain better scalability with data intensive applications. The presented experimental results show, among others:

1. efficiency of large (more than gigapixel) image processing,
2. better performance of NVRAM cache extension compared to unmodified MPI I/O,
3. performance gain obtained for processing multiple images using overlapping file opening and processing,
4. visible scalability of the solution,
5. impact of NVRAM parameters on the application execution time.

In the future we plan to improve performance of the NVRAM cache, which should also impact efficiency of image processing with proposed architecture. Our idea involves a hybrid approach – using both plain PFS performance and cache by balancing the load at runtime. Another interesting issue is connected with moving the solution into a cloud – combining HPC and cloud processing becomes more and more popular nowadays.

Acknowledgments. The research in the paper was supported by a grant from Intel Technology Poland and afterwards partially elaborated within statutory activities of Dept. of Computer Architecture, Faculty of Electronics, Telecommunications and Informatics, Gdansk University of Technology, Poland.

REFERENCES

[1] Y. Allusse, P. Horain, A. Agarwal, and C. Saipriyadarshan, *GpuCV: A GPU-Accelerated Framework for Image Processing and Computer Vision*, Springer Berlin Heidelberg, Berlin, Heidelberg, 2008, pp. 430–439.

[2] J. Barbosa, J. Tavares, and A. J. Padilha, *Parallel Image Processing System on a Cluster of Personal Computers*, Springer Berlin Heidelberg, Berlin, Heidelberg, 2001, pp. 439–452.

[3] P. Bright, *Specs for first Intel 3D XPoint SSD: so-so transfer speed, awesome random I/O*, 2017. `https://arstechnica.com/?post_type=post&p=1040631`.

[4] M. Cavus, H. D. Sumerkan, O. S. Simsek, H. Hassan, A. G. Yaglikci, and O. Ergin, *Gpu based parallel image processing library for embedded systems*, 2014 International Conference on Computer Vision Theory and Applications (VISAPP), 1 (2014), pp. 234–241.

[5] S.-D. Cosmin, *Mpi-image-processor*, March 2012. https://github.com/cosminstefanxp/MPI-Image-Processor.

[6] P. Czarnul, A. Ciereszko, and M. Fraczak, *Towards Efficient Parallel Image Processing on Cluster Grids Using GIMP*, Springer Berlin Heidelberg, Berlin, Heidelberg, 2004, pp. 451–458.

[7] P. Dorozynski, P. Czarnul, A. Malinowski, K. Czurylo, L. Dorau, M. Maciejewski, and P. Skowron, *Checkpointing of parallel mpi applications using mpi one-sided api with support for byte-addressable non-volatile ram*, Procedia Computer Science, 80 (2016), pp. 30 – 40.

[8] B. V. Essen, R. Pearce, S. Ames, and M. Gokhale, *On the role of nvram in data-intensive architectures: An evaluation*, in 2012 IEEE 26th International Parallel and Distributed Processing Symposium, May 2012, pp. 703–714.

[9] P. Fernando, S. Kannan, A. Gavrilovska, and K. Schwan, *Phoenix: Memory speed hpc i/o with nvm*, in 2016 IEEE 23rd International Conference on High Performance Computing (HiPC), Dec 2016, pp. 121–131.

[10] A. Georgantzoglou, J. d. Silva, and R. Jena, *Image processing with matlab and gpu*, in MATLAB Applications for the Practical Engineer, K. Bennett, ed., InTech, Rijeka, 2014, ch. 22.

[11] Hasselblad Press Release, *Hasselblad introduces the H6D-400c MS*, 2018. `https://www.hasselblad.com/press/press-releases/hasselblad-introduces-the-h6d-400c-ms/`.

[12] J. Huang, K. Schwan, and M. K. Qureshi, *Nvram-aware logging in transaction systems*, Proc. VLDB Endow., 8 (2014), pp. 389–400.

[13] N. Kaiser, W. Burgett, K. Chambers, L. Denneau, J. Heasley, R. Jedicke, E. Magnier, J. Morgan, P. Onaka, and J. Tonry, *The Pan-STARRS wide-field optical/NIR imaging survey*, Proc. SPIE, 7733 (2010), pp. 77330E–77330E–14.

[14] S. Kannan, A. Gavrilovska, K. Schwan, and D. Milojicic, *Optimizing checkpoints using nvm as virtual memory*, in 2013 IEEE 27th International Symposium on Parallel and Distributed Processing, May 2013, pp. 29–40.

[15] S. Kannan, D. Milojicic, A. Gavrilovska, and K. Schwan, *Using active nvram for i/o staging*, 2011. HP Laboratories, HPL-2011-131, http://www.hpl.hp.com/techreports/2011/HPL-2011-131.pdf.

[16] P. Karlsson, *A gpu-based framework for efficient image processing*, September 2014. LiU-ITN-TEK-A-14/043-SE, Department of Science and Technology, Linkping University, Sweden.

[17] W.-H. Kim, J. Kim, W. Baek, B. Nam, and Y. Won, *Nvwal: Exploiting nvram in write-ahead logging*, SIGOPS Oper. Syst. Rev., 50 (2016), pp. 385–398.

[18] K. Kyusik, C. Yongwoon, K. Seongmin, and K. Taeseok, *Reducing the user-perceived latency of browsers with nvram*, JSTS:Journal of Semiconductor Technology and Science, 17 (2017), pp. 23–28. DOI: 10.5573/JSTS.2017.17.1.023.

[19] J. Layton, *How persistent memory will change computing.* Admin Magazine, accessed on 26th April 2017. http://www.admin-magazine.com/HPC/Articles/Persistent-Memory, Linux New Media USA, LLC.

[20] P. Li and D. R. Chakrabarti, *Adaptive Software Caching for Efficient NVRAM Data Persistence*, Springer International Publishing, Cham, 2017, pp. 93–97.

[21] A. Malinowski and P. Czarnul, *Distributed NVRAM Cache – Optimization and Evaluation with Power of Adjacency Matrix*, Springer International Publishing, Cham, 2017, pp. 15–26.

[22] A. Malinowski, P. Czarnul, K. Czuryło, M. Maciejewski, and P. Skowron, *Multi-agent large-scale parallel crowd simulation*, Procedia Computer Science, 108 (2017), pp. 917 – 926. International Conference on Computational Science, ICCS 2017, 12-14 June 2017, Zurich, Switzerland.

[23] A. Malinowski, P. Czarnul, P. Dorożynski, K. Czuryło, Ł. Dorau, M. Maciejewski, and P. Skowron, *A Parallel MPI I/O Solution Supported by Byte-addressable Non-volatile RAM Distributed Cache*, in Position Papers of the 2016 Federated Conference on Computer Science and Information Systems, vol. 9 of Annals of Computer Science and Information Systems, PTI, 2016, pp. 133–140.

[24] A. Malinowski, P. Czarnul, M. Maciejewski, and P. Skowron, *A Fail-Safe NVRAM Based Mechanism for Efficient Creation and Recovery of Data Copies in Parallel MPI Applications*, in Information Systems Architecture and Technology: Proceedings of 37th International Conference on Information Systems Architecture and Technology – ISAT 2016 – Part II, Springer International Publishing, 2017, pp. 137–147.

[25] A. Mochizuki, N. Yube, and T. Hanyu, *Design of a computational nonvolatile ram for a greedy energy-efficient vlsi processor*, in IECON 2015 - 41st Annual Conference of the IEEE Industrial Electronics Society, Nov 2015, pp. 003283–003288.

[26] NASA, *Space Shuttle Mission STS-48 Press Kit*, 1991. `https://science.ksc.nasa.gov/shuttle/missions/sts-48/sts-48-press-kit.txt`.

[27] NASA/ESA, *Hubbles High-Definition Panoramic View of the Andromeda Galaxy*, 2015. `http://www.spacetelescope.org/images/heic1502a/`.

[28] C. Nicolescu and P. Jonker, *Parallel low-level image processing on a distributed-memory system*, Springer Berlin Heidelberg, Berlin, Heidelberg, 2000, pp. 226–233.

[29] C. Nicolescu and P. Jonker, *A data and task parallel image processing environment*, Parallel Computing, 28 (2002), pp. 945 – 965.

[30] A. Ozdemir and T. Altilar, *Gpu based parallel image processing for plant growth analysis*, in 2014 The Third International Conference on Agro-Geoinformatics, Aug 2014, pp. 1–6.

[31] A. Remnyi, S. Sznsi, I. Bndi, Z. Vmossy, G. Valcz, P. Bogdanov, S. Sergyn, and M. Kozlovszky, *Parallel biomedical image processing with gpgpus in cancer research*, in 3rd IEEE International Symposium on Logistics and Industrial Informatics, Aug 2011, pp. 245–248.

[32] W. Ruyten and W. E. Sisson, *Message passing for parallel processing of pressure-sensitive paint images*, in Users Group Conference (DOD UGC'04), 2004, June 2004, pp. 308–312.

[33] J. M. Squyres, A. Lumsdaine, and R. L. Stevenson, *A toolkit for parallel image processing*, in SPIE Annual Meeting, San Diego, 1998.

[34] R. Thakur, W. Gropp, and E. Lusk, *Data sieving and collective I/O in romio*, Frontiers '99 - Seventh Symposium On Frontiers Massively Parallel Computation, Proc., (1999), pp. 182–189.

[35] K. Vincent, D. Nguyen, B. Walker, T. Lu, and T.-H. Chao, *Gpu processing for parallel image processing and real-time object recognition*, 2014.

[36] M. Wasi-ur Rahman, N. S. Islam, X. Lu, and D. K. D. Panda, *Can non-volatile memory benefit mapreduce applications on hpc clusters?*, in Proceedings of the 1st Joint International Workshop on Parallel Data Storage & Data Intensive Scalable Computing Systems, PDSW-DISCS '16, Piscataway, NJ, USA, 2016, IEEE Press, pp. 19–24.

[37] H. Yu, Y. Wang, S. Chen, W. Fei, C. Weng, J. Zhao, and Z. Wei, *Energy efficient in-memory machine learning for data intensive image-processing by non-volatile domain-wall memory*, in 2014 19th Asia and South Pacific Design Automation Conference (ASP-DAC), Jan 2014, pp. 191–196.

[38] M. Zhang, *Bentley Used NASA Tech to Create This 53-Gigapixel Car Photo*, 2016. PetaPixel, `https://petapixel.com/2016/06/23/bentley-used-nasa-tech-create-53-gigapixel-photo-car/`.

[39] Y. Zhang, J. Yang, A. Memaripour, and S. Swanson, *Mojim: A reliable and highly-available non-volatile memory system*, in Proceedings of the Twentieth International Conference on Architectural Support for Programming Languages and Operating Systems, ASPLOS '15, New York, NY, USA, 2015, ACM, pp. 3–18.

Edited by: Dana Petcu
Received: Nov 6, 2017
Accepted: Dec 23, 2017

DOI 10.12694/scpe.v19i1.1390
Scalable Computing: Practice and Experience ISSN 1895-1767
Volume 19, Number 1, pp. 15–29. http://www.scpe.org

SCALE-EA: A SCALABILITY AWARE PERFORMANCE TUNING FRAMEWORK FOR OPENMP APPLICATIONS

SHAJULIN BENEDICT*

Abstract. HPC application developers, including OpenMP-based application developers, have stepped forward to endeavor the future design trends of exa-scale machines, such as, increased number of threads/cores, heterogeneous architectures, multiple levels of memories, and so forth; and, they have initiated procedures to address application level challenges, such as, data-driven scalability issues, energy consumption requirements, data availability needs, and so forth. Despite the existence of manual performance tuning solutions, users still deem it to be an intricate process. This paper proposes a scalability aware autotuning framework (SCALE-EA) that automatically identifies an efficient number of threads for OpenMP parallel regions using a Firefly Algorithm (FA) and a newly designed Modeling Assisted Firefly Algorithm (MAFA). MAFA of SCALE-EA was implemented in two approaches: Modeling Assisted Firefly Algorithm with Random Forest Modeling support (MAFA-RFM) and Modeling Assisted Firefly Algorithm with Linear Regression Modeling support (MAFA-LRM). The modeling and prediction algorithms of the proposed MAFA of SCALE-EA were based on the execution time and the hardware performance events of code regions of OpenMP applications. Experiments were conducted on two machines, namely, a Haswell based machine and an AMD Opteron based 48 core machine. The experimental results of the MAFA of SCALE-EA manifested the energy efficiencies of 31.21 to 77.3 percentage and the search time efficiencies of 5.53 to 32.56 percentage for candidate OpenMP applications such as CoMD, Arraybench, Taskbench, and Syncbench.

Key words: Auto Tuning, OpenMP Applications, Modeling and Scalability

AMS subject classifications. 68M20, 68W10

1. Introduction.

High Performance Computing (HPC) application developments are invariably cropping up among various scientific domains, such as, High Energy Physics (HEP), bioinformatics, eyewear computing, visualizations, electronic automation, graph-based machine learning, and so forth. OpenMP based programming model is indeed reaching out to become a prominent programming model among a sector of HPC application developers owing to the adequate doctrine of standards (OpenMP 4.0 and 4.5), ease of use, controlled programming support, smooth applicability to programmers belonging to various scientific disciplines, and due to the notion of having millions of cores in future exascale machines.

However, the realization of efficiently utilizing HPC applications in its present form for future large scale machines requires innovative approaches to mitigate the following possible risky scenarios:

1. the performance of applications becomes more sensitive to data movement, data availability, data provenance, data management policies, and so forth – a future software-cum-hardware computing system must consider the massive storage options of machines, resiliency nature of applications, dynamic computing behavior of applications, and the dynamic nature of the data access patterns of applications (big data).
2. the current implementations of OpenMP applications might not have considered the design aspects of emerging memory models (including data persistence of modern memory architectures), infrastructural improvements, future parallel data structures, and so forth.
3. the scalability of applications might get an impoverished lead as applications are usually not ported and tested for scalable machines.
4. the energy efficiency of applications could exhibit a daunting scenario when executed on machines with varying degrees of parallelism – smaller or larger.
5. the current OpenMP application developers might not have quantified the possible uncertainties that might evolve due to the underlying future parallel software frameworks.

In short, to mitigate these challenges, programmers or developers have to diligently write scalable and energy efficient parallel algorithms by employing the apt scalability features of programming languages and by considering the underlying requirements of machines. Vividly, OpenMP based application programmers have to gain sophisticated knowledge on handling the newer OpenMP constructs in order to attain higher scalability, portability, and energy efficiency – for instances, the synchronization points of OpenMP applications, such as,

*Indian Institute of Information Technology Kottayam, Kerala, India - 695016. (shajulin@iiitkottayam.ac.in) – Formerly the Guest Professor of Technical University Munich, Germany.

OpenMP barrier constructs should be limited or enriched; the granularity of OpenMP parallel regions should be optimized to achieve higher scalability; and, the programmers should efficiently utilize the OpenMP private data clauses in an application.

In general, the non-scalable and the energy/performance inefficient code regions of an application can be identified and manually tuned. However, the manual tuning processes might laid down hefty responsibilities to users – an intricate process. One solution that makes sense and intends to work in large scale HPC scenarios is to establish an autotuning tool or a framework that automatically finds the non-scalable or energy inefficient parts of the code regions of applications and tunes them accordingly. Historically, a notion of framing autonomic computing systems was highly appreciated by researchers for decades [11, 29]. Moreover, researchers had shown their keen interest in counteracting the scalability and the energy consumption issues of applications [2, 4, 15, 31] at various levels of computing systems so that the existing applications could be executed on future machines at ease.

Auto tuning, although a promising solution for tuning HPC applications, easily leads to voluminous combinations of optimization options which might impede the search time of the tuning process. In addition, the autotuning process could inundate the search space with an immense volume of performance data, as autotuning systems are, in general, self-aware, self-configurable [42], context-aware, and self-optimizable systems. In most cases, the autotuning systems are guided in a single-objective or in a multi-objective modes of operations based on pre-defined objectives, such as, minimizing energy consumption of code regions of applications, maximizing the utilization of machines, minimizing the data movement to Dynamic Random Access Memory (DRAM), and so forth. Thus, there is an increasing need for autotuning solutions or frameworks that intelligently minimizes the search time of the tuning processes.

This paper proposes the SCALE-EA framework, a Scalability-Aware performance tuning framework using EnergyAnalyzer (EA), for OpenMP applications – EnergyAnalyzer tool is an online based energy consumption analysis tool for HPC applications. SCALE-EA automatically identifies the efficient number of threads for individual parallel regions of OpenMP applications using FA and MAFA. The proposed FA and MAFA of SCALE-EA improved the search time of the tuning process and enhanced the energy efficiency of applications. The proposed method was evaluated using several OpenMP applications / benchmarks, such as, CoMD from the co-design center of LLNL, USA [14], and OpenMP benchmarks from EPCC [17], on a Haswell processor based HP-Zbook-15G machine and a 48 core HPProliant machine.

In succinct, the paper has the following contributions:

1. an SCALE-EA framework for automatically finding an efficient number of threads for the parallel regions of OpenMP applications was proposed.
2. FA and modeling assisted heuristic algorithms were implemented in SCALE-EA in order to reduce the search time of the tuning process. The modeling assisted heuristic algorithms were implemented in two flavors: a) Modeling Assisted Firefly Algorithm using Linear Regression Modeling (MAFA-LRM) and b) Modeling Assisted Firefly Algorithm using Random Forest Modeling (MAFA-RFM). MAFA algorithms are the modified versions of FA.
3. Experimental evaluations of the proposed SCALE-EA and its associated algorithms were carried out using OpenMP applications, such as, Arraybench, Syncbench, Taskbench, and CoMD applications.

The rest of the paper is organized as follows. Section 2 presents existing autotuning frameworks and their solutions. Section 3 explains the proposed scalability-aware performance tuning framework for OpenMP applications and Section 4 discusses the modified firefly algorithm which adds modeling support towards the search process. Section 5 manifests the proposed mechanism called the SCALE-EA framework. And, finally, Section 6 presents conclusions.

2. Related Works. HPC applications, specifically data-driven applications, are increasing in the scientific market from various scientific disciplines, such as, massive graphs, HEP, bioinformatics, healthcare, distributed manufacturing, electronic automation, visualization applications (social networks), multi-physics simulations, and so forth. In the meantime, technological advances in hardware architectures are nearing exascale speed through co-design architectural designs, abundant General Purpose Graphical Processing Units (GPGPUs), hierarchical clustering of heterogeneous machines, and so forth. Despite the growth seen in the application sector and in the hardware architectural design sector of HPC, the performances of applications, including the

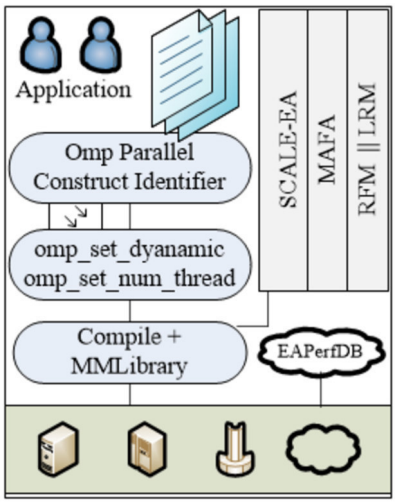

FIG. 3.1. *SCALE-EA: Scalability Aware Performance AutoTuning Framework for OpenMP Applications*

scalability and the energy efficiency of applications, should be concerned about by the researchers.

The HPC community, therefore, oriented their mindset to mitigate the effects of known performance issues of large scale systems such as the dynamic nature of big data in applications (data sizes), heterogeneous hardware architectures [7], energy consumption issues, scalability issues [22, 39], uncertainty of resources (including data resources), and so forth [18].

In fact, the energy consumption issues of HPC applications should be addressed due to the scarcity of power sources (especially in the developing countries, such as, India), owing to the emission of carbon footprints [10] which lead to environmental hazards, and, due to the emerging power wall problem of dark silicons [31].

There exists a few standalone energy reduction mechanisms for HPC applications [28, 36, 21]. The most of the existing approaches are either manual [34] or application-centric.

Researchers have proposed autotuning frameworks/solutions [16, 23, 24, 25, 13] in order to achieve performance/energy improvements. Studies have also led a subset of researchers to frame autotuning solutions at compile time [2, 9, 12, 27, 32] and a few others at run time of applications [37, 3, 40, 8]. In addition, a few autotuning solutions with more emphasis to IOs were designed in [5]. To improve the performance of heterogeneous systems and applications, the authors of [6] have designed an autotuning solution. Additionally, tool developers are constantly finding mechanisms to assist application developers in terms of automatically improving the performance efficiency of HPC applications.

To avoid the burdens caused due to the search time and the emergence of abundant performance data, a few researchers have utilized modeling mechanisms [26, 1] to forecast the performance issues of applications and to tune applications. In addition, modeling assisted automated systems have been successful in cloud and distributed environments [30]. Recently, researchers have adopted autotuning using Domain Specific Languages for autotuning applications in ANTAREX project [13].

This paper proposed a combination of heuristics and modeling approach for the tuning process of OpenMP based HPC applications. To do so, Firefly Algorithm (FA), a heuristic method, is modified with modeling algorithms, such as, RFM and LRM, in this paper. A detailed description about the proposed SCALE-EA framework based on FA and MAFA algorithms is discussed in Section 3.

3. Scalability Aware AutoTuning using EnergyAnalyzer (SCALE-EA). SCALE-EA framework does scalability aware performance autotuning of OpenMP applications. The framework is built based on EnergyAnalyzer tool, an online based energy consumption analysis tool. This section explains the SCALE-EA framework and the entities involved in pursuing the performance aware autotuning mechanism for OpenMP applications.

3.1. SCALE-EA Framework Functionalities. The functionalities of the proposed SCALE-EA framework, the extensions made towards EnergyAnalyzer tool, are described as follows:

SSTranslator and its Extension. SSTranslator, an entity of EnergyAnalyzer tool, is extended to support the proposed SCALE-EA framework. It is a source-to-source translator which includes program statements, such as,

```
#pragma start_user_region
---
#pragma end_user_region
```

These statements notify the Monitoring Manager entity of EnergyAnalyzer about the user-specified code regions of applications. The performance / energy consumption values of these user-specified regions are measured using the Monitoring Manager entity of EnergyAnalyzer at the runtime of applications.

The extended version of SSTranslator additionally identifies each parallel regions of OpenMP based applications. These parallel regions are marked with two additional statements, such as,

```
omp_set_dynamic(0);
omp_set_num_threads(SCALEEA_NUM_THREADS_filename_n);
```

where n resembles the unique number for each *omp parallel* regions in an application and $filename$ is the filename representation of applications.

The line `omp_set_dynamic(0)` is automatically added before the *omp parallel* regions of OpenMP-based applications using the extended version of SSTranslator. This statement instructs compilers to disable dynamic allocation of threads. The variable `SCALEEA_NUM_THREADS_filename_n` is automatically defined at the initial stage of the file using $\#ifdef$ conditions of C/C++ definitions. This is mandatory for the proposed SCALE-EA framework as the framework would later assign the number of threads for each *omp parallel* regions. The heuristics of SCALE-EA are responsible for assigning the values to these variables.

In addition, the line numbers for *omp parallel* regions and the file names of applications where the regions belong to are noticed in a separate *.sst* file (static source-to-source file) of the SCALE-EA framework.

Performance/Energy Measurements. After inserting the required statements for SCALE-EA, (for instances, the statements which would disable the dynamic allocation of threads to OpenMP applications and enable performance measurements), the application is compiled with the MMLibrary of EnergyAnalyzer. The MMLibrary of EnergyAnalyzer measures the performance values of the user-specified code regions of applications and stores the performance values in EAPerfDB, a no-sql (Mongodb) based performance database of EnergyAnalyzer tool.

Heuristic Support. Selecting efficient numbers of threads for each *omp parallel* regions of OpenMP application is a time consuming task. Thus, SCALE-EA framework depends on heuristics which suggest efficient numbers of threads for each *omp parallel* regions.

In this paper, Firefly Algorithm (FA) is applied in the SCALE-EA framework in order to find the efficient number of threads for OpenMP applications. In addition, the time spent for finding the efficient number of threads (the search time) is further reduced using the modified versions of FA – MAFA-RFM and MAFA-LRM. Detailed discussions on the Firefly Algorithm (FA) and MAFA can be found in Section 4.

4. FA and MAFA of SCALE-EA. In this paper, FA and a modified version of FA, namely, Modeling Assisted Firefly Algorithm (MAFA) are proposed for identifying an efficient number of threads for OpenMP applications. MAFA is implemented in two approaches, namely, MAFA-RFM and MAFA-LRM. This section describes the FA and MAFA in detail.

4.1. Firefly Algorithm (FA). Firefly Algorithm (FA) is a meta-heuristic algorithm which is actively utilized by a few researchers [41, 19, 35] in order to solve their real-world combinatorial optimizations problems. FA was developed in 2007 by Xin-She Yang at Cambridge University [41]. In fact, the idea of meta-heuristics intrigued the real world problem solvers when compared to the classical optimization techniques for decades owing to the algorithms' problem independent nature – the classical optimization techniques find solutions based on analytical models (continuous or differentiable functions).

FA, an iterative based heuristic technique or a population based meta-heuristics, was introduced in several flavors, such as, adaptive, multi-objective, hybrid, DiscreteFA, and so forth. A wide survey of FA and its

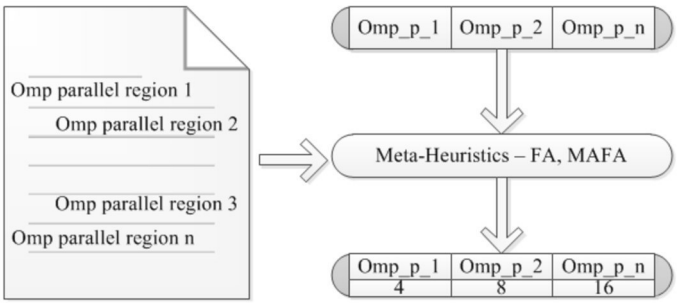

FIG. 4.1. *Realization of FA in SCALE-EA – Thread String Formation*

derivatives was elaborated in [20].

FA was named after fireflies which exist in tropical geographical locations. In general, FA depends on the flashing and mating communication behavior of fireflies. In succinct, the male fireflies lit a specific flashing behavior and the females subsequently respond to the flash with unique characteristics. The bonding between the male and the female fireflies heavily rely upon the distance between them. FA assumes the following:

1. Fireflies of FA are unisex. This ensures that each firefly would be attracted to the other available fireflies irrespective of what sex they belong to.
2. The attractiveness of fireflies is dependent on the brightness of the fireflies, which is the the objective function of FA.

4.2. Realization of FA in SCALE-EA – Problem Definition. SCALE-EA based on FA identifies efficient number of threads for each *omp parallel* regions of OpenMP applications. To do so, the following steps are carried out in the SCALE-EA framework:

SCALE-EA Preparatory Phase. As mentioned earlier, SSTranslator of EnergyAnalyzer includes statements, such as, `omp_set_num_threads(SCALEEA_NUM_ THREADS_filename_n)` for each OpenMP parallel regions of applications. Later, in the SCALE-EA preparatory phase, SCALE-EA represents those statements in a string form so that the heuristics could literally assign the number of threads for applications at the initialization and the iterative phases of SCALE-EA. The string form representation of the parallel regions of OpenMP applications is given as shown below:

```
ompP_1 ompP_2 ompP_3 ... ompP_n
```

where n represents the number of parallel regions in an application. For instance, Figure 4.1 shows the assignment of threads 4, 8, and 16 for three parallel regions `ompP_1 ompP_2 and ompP_n`.

The string form based on the parallel regions of applications are uniquely represented irrespective of the files of applications. For instance, the eleven *omp parallel* regions from 3 files, namely, eam.c, initAtoms.c, and ljForce.c, of the CoMD application are represented as `ompP_1 ompP_2 ompP_3 ompP_4 ompP_5 ompP_6 ompP_7 ompP_8 ompP_9 ompP_10 ompP_11` based on parallel regions `SCALEEA_NUM_THREADS_eam_1` (for `ompP_1`) to `SCALEEA_NUM_THREADS_ljForce_2` (for `ompP_11`).

FA Initialization Phase. During the initialization phase, the initial values of FA parameters are set. The FA paramters include the number of initial population of sequences (fireflies), the objective functions, the number of generations applied in FA, and epsilon, alpha, beta, and gamma values. In the experiments, the impacts of six combinations of FA parameter variations are studied as shown in Table 5.3.

In addition, during this initialization phase of SCALE-EA, the initial population of sequences (F_n) is generated. The pictorial representation of the sequences in the initialization phase of the SCALE-EA mechanism for an application is shown in Figure 4.2.

Based on the initialization phase values, SCALE-EA assigns the number of threads for each *omp parallel* regions and execute them on the underlying HPC machine. Meantime, the performance values for the user-specified code regions of applications are recorded in the EAPerfDB of SCALE-EA. Subsequently, the objective function values of these sequences are noticed for the next phase of FA.

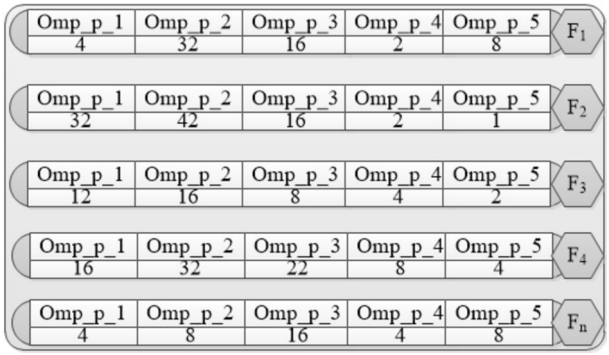

FIG. 4.2. *Initialization Phase of FA at SCALE-EA*

FA Iteration Phase. During this phase, FA iteratively evaluates the light intensities of the two series of sequences ($F_{i=1\ to\ n} and F_{j=1\ to\ n}$) based on the objective functions. In fact, the objective functions of sequences decrease with respect to the distance between them. The objective functions applied in SCALE-EA is a Combined Simultaneous Objective (CSO) function with weight functions as shown in equation 4.1. The weight functions are mandatorily devised for CSO – 50 percentage weights were given to the scalability parameter and the other 50 percentage weights were splitted into 20, 20, and 10 for execution time, energy and performance parameters of equation 4.1:

$$CSO = 0.5 * (\frac{ET}{ET_{p=1}}) + 0.2 * ET + 0.2 * EY + 0.1 * gistPerf \tag{4.1}$$

where: ET is the execution time of F_n in seconds; EY is the energy consumption of F_n in Joules; $gistPerf$ is represented using formula 4.2, where the performance values are converted to a two-decimal rounded off values:

$$gistPerf = \sum_{i=1...pf} Perf_i \tag{4.2}$$

where pf is the number of performance counters, and $Perf_i$ is the performance value for each performance counters such as Level 1 cache misses, Level 3 cache misses, unconditional branches, and so forth. For example, if the total number of instructions, level1 data cache misses, unconditional branches, and level3 total cache misses for an application are measured as 11960995473, 5486, 869583951, and 3801, the $gistPerf$ value would be rounded off as 1.28 (actual value = $1.28 * 10^{10}$).

If the light intensity IF_j of F_j is better than IF_i, then FA moves F_i to F_j. In SCALE-EA, the movement of firefly F_i to an attractive firefly F_j is determined using the formula given in equation 4.3:

$$Movement\ F_i^{t+1} = F_i^t + \beta_0 e^{-\gamma r_{ij}^2}(F_j^t - F_i^t) + \alpha_t \epsilon_i^t \tag{4.3}$$

where the first component represents the previous F_i sequence (thread sequence); the second component represents the essence of attraction parameter. This component relates to the distance between two fireflies – β_0 represents attractiveness at distance 0 and r relates to the distance between them at a constant value γ; and the third component represents the randomization parameter – α_t is a scalable value specified at time t and ϵ is a random number for each iteration of FA.

The second component of equation 4.3 moves the sequences in a discrete manner instead of pursuing a bare continuous calculation.

FA Ranking Phase. In this phase, the sequences are ordered and the local best sequence LB_F_g for that particular generation of sequences are noticed. FA continues the ranking process for each generations until the final iteration are complete. And, finally, FA searches for the global best sequence GB_F_g for the OpenMP application from the list of available LB_F_g and their corresponding light intensity values.

Thus, identifying the efficient number of threads for the parallel regions of OpenMP applications is based on the global best sequence which is derived from the pre-defined objectives (minimizing execution time, minimizing energy consumption and increasing speedup) calculated using the CSO formula (see equation 4.1).

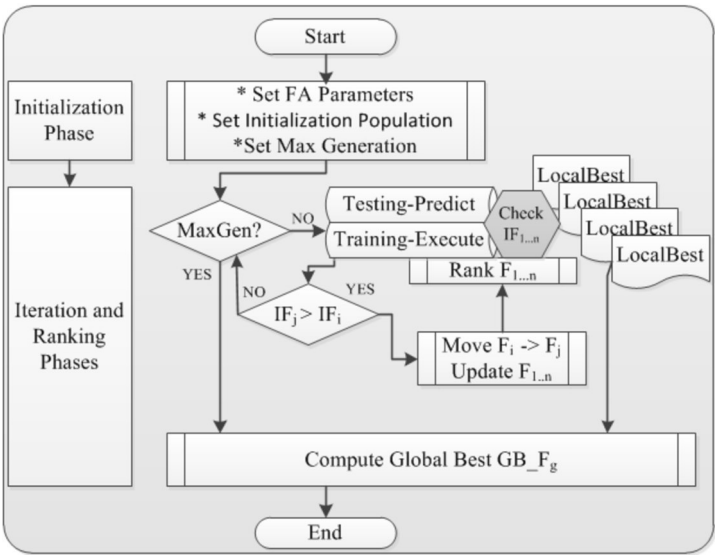

FIG. 4.3. *Modeling Assisted Firefly Algorithm (MAFA)*

4.3. Modeling Assisted Firefly Algorithm (MAFA) – a modified FA. Although classical FA would reduce the time for searching the efficient number of threads in OpenMP applications, the search time of the SCALE-EA tuning process can further be improved using prediction models. Reducing the search time of tuning process is crucial while pursuing autotuning in large scale machines. For instance, an application with 9 OpenMP parallel regions might have 134217728 number of combinations of thread sequences when experimented with 8 threads. This could deliberately issue hefty number of performance data for each combinations of thread sequences. SCALE-EA, thus, proposed a Modeling Assisted Firefly Algorithm (MAFA) in order to further reduce the search time of the SCALE-EA tuning process.

In MAFA, a few iterative portions of FA are executed and the other remaining iterative portions of FA are predicted using prediction algorithms, such as, Random Forest Modeling (RFM) and Linear Regression Models (LRM). In the previous works, prediction algorithms were applied for predicting the efficient problem sizes [38] of applications at compile time. In this paper, these prediction algorithms are applied for the first time for assisting the search process of FA based meta-heuristics – i.e., a modified implementation of firefly algorithm. Based on the utility of RFM or LRM, MAFA is represented as MAFA-RFM and MAFA-LRM.

The working principle of MAFA is pictorially represented in flow chart (see Figure 4.3). In general, MAFA assumes the four phases as similar to FA – Preparatory, Initialization, Iteration, and Ranking phases. During the initialization phase of MAFA, the initial parameters of FA are set; initialization population is defined; and, the maximum number of generations for the tests is initialized. Later, MAFA iteratively evaluates sequences and their corresponding intensities (objective functions) for the pre-assigned number of generations as discussed in Section 3.

The modification adopted to FA resides in the iterative phase of MAFA. During the iteration phase of MAFA, all of the combinations of thread sequences that are suggested by FA are not executed. Thus, instead of executing and evaluating all of the combinations of sequences (the thread sequences of OpenMP applications), some of the combinations of thread sequences are executed and the others are predicted using prediction algorithms. To do so, initially, the sequences are enrolled in the Training-Execute list (see Figure 4.3). This list ensures that SCALE-EA executes the OpenMP application during the evaluation step of FA. After a few iterations, there are sufficient number of entries in the Training-Execute list (for instance, 100 entries in the Training-Execute list of SCALE-EA), the next 30 percentage of the population in the FA generation is enrolled in the Testing-Predict list of SCALE-EA.

If the sequence is listed in the Testing-Predict list of SCALE-EA, the OpenMP application with the corresponding thread sequence would not be compiled or executed in the underlying machine. Rather, the modeling-

cum-prediction component of MAFA is invoked by SCALE-EA. During this step, the RFM/LRM prediction algorithms model (and predict) the outcomes of sequences based on the performance counter values (based on the experimental results) available in the EAPerfDB of SCALE-EA.

A detailed insights on the RFM and LRM algorithms are explained in the following paragraphs:

Random Forest Modeling. RFM applies tree based technique for modeling the independent variables and for predicting the dependent variables. It gains knowledge using ensemble learning methods; it predicts the unknown variables after a creation of the high variance of de-correlated trees was done. Thus, RFM has modeling and prediction phases for predicting the dependent variables in a regression form or in a classification form.

RFM undergoes two processes in the modeling phase, namely, the bagging and ensembling processes. During the bagging process, random forest trees (RFTrees) are grown with high variances and they are grouped in separate bags. The ensembling process of RFM ensures that there is enough information from the created trees to generate models. At the end of this phase, a model is created using RFM.

RFM, at the prediction phase, tries to reduce the noises of the generated trees of the modeling phase of RFM. Testing data is utilized at this phase of RFM for the prediction process.

Linear Regression Modeling. LRM predicts the dependent variables based on the linear predictor functions. LRM suits well if the dependent function is mostly linear in nature as it attempts to find the best fitting line. In both the prediction cases (RFM and LRM), a squared error based calculation is utilized in order to find the error.

5. Experimental Results. This section demonstrates the proposed mechanism, SCALE-EA, the scalability aware performance tuning of OpenMP applications framework using EnergyAnalyzer (EA) tool by: i) conducting a study on the impact of variants of FA parameters, ii) understanding the energy efficiencies of FA and MAFA in SCALE-EA, and iii) analyzing the search time efficiencies of MAFA-LRM and MAFA-RFM based tuning processes.

5.1. Experimental Setup. Experiments were conducted on two machines, namely, a HP-Zbook-15G machine – a Haswell processor based workstation – and a 48 core HPProliant machine. In all experiments, the EnergyAnalyzer tool was utilized to measure the energy / performance values for the code regions of applications.

The following OpenMP applications / benchmarks are considered to demonstrate the proposed SCALE-EA mechanism:

1. *Arraybench*: This benchmark suite of EPCC [17] is written in OpenMP-C and it consists of ten benchmarks which reflect the performance of shared memory architectures in terms of the impact due to array operations of OpenMP applications. The array operations of OpenMP benchmarks are considered based on the private clauses of OpenMP, such as, copyin, threadprivate, and so forth, within loop blocks. The thread private data that are operated within the functional blocks of Arraybench are in the range of 3, 9, 27, 81, 243, 729, 2187, 6561, 19683, and 59049. The Arraybench application of the benchmark suite consists of four OpenMP parallel regions.
2. *Syncbench*: This benchmark consists of nine OpenMP parallel regions which are responsible for studying the impact of utilizing synchronization points in OpenMP. In general, OpenMP applications can enter into synchronization points at nine OpenMP constructs, such as, *parallel* regions, *parallel for* regions, *barriers*, *single* regions, *critical* regions, *ordered* sections, *atomic* regions, reduction states, and OpenMP locks. The impacts of these synchronization points of OpenMP constructs could be analyzed using Syncbench application.
3. *Taskbench*: Taskbench studies the effects of task creation and scheduling aspects of OpenMP 3.0. For instances, parallel task generation, master task generation, master task generation with busy slaves, conditional task generation, and so forth, are analyzed in Taskbench application. This benchmark consists of ten OpenMP parallel regions which could be tuned when executed on machines.
4. *CoMD application*: CoMD application [14] is an algorithmic representation of molecular dynamics simulations. It was developed at the co-design center of LLNL, USA. For the tests, OpenMP version of CoMD v.1.1 was utilized. This version of CoMD has eleven OpenMP parallel regions that are spread across the files, such as, eam.c (4 regions), initAtoms.c (5 regions), and ljForce.c (2 regions).

In experiments, SCALE-EA identified an efficient number of threads for the OpenMP parallel regions of the above mentioned applications based on the energy / performance values of user-specified regions of applica-

TABLE 5.1
OpenMP Applications and Parallel Regions

Application	No.of Parallel regions	Parallel region files	User region (lineNo)	User region file	No.of Perf. Measurements
ArrayBench-3 to ArrayBench-59049	4	arraybench.c	lineNo: 46-88	arraybench.c	6
SynchBench	9	syncbench.c	lineNo: 45-101	syncbench.c	6
TaskBench	10	taskbench.c	lineNo: 44-97	taskbench.c	6
CoMD	4	eam.c	lineNo: 119-136	CoMD.c	6
	5	initAtoms.c			
	2	ljForce.c			

TABLE 5.2
Energy and Performance Values of OpenMP Applications

Application	Energy (Joules)	ExecutionTime (secs)	TOT_INS	L1_DCM	BR_UCN	L3_TCM	EA Time (secs)
ArrayBench-3	16.04	0.395	1.05E+09	1.01E+07	2.80E+07	206	0.547
ArrayBench-9	13.43	0.37	9.70E+08	7.19E+06	2.70E+07	181	0.541
ArrayBench-27	15.27	0.363	8.60E+08	9.50E+06	2.70E+07	229	0.535
ArrayBench-81	11.58	0.279	7.20E+08	7.60E+06	2.50E+07	201	0.448
ArrayBench-243	14.29	0.349	9.20E+08	1.00E+07	2.40E+07	202	0.51
ArrayBench-729	12.15	0.284	7.40E+08	8.30E+06	2.60E+07	254	0.43
ArrayBench-2187	17.54	0.399	1.21E+09	4.60E+07	2.10E+07	279	0.56
ArrayBench-6561	16.71	0.35	1.04E+09	7.30E+07	1.59E+07	246	0.68
ArrayBench-19683	17.15	0.35	1.03E+09	6.79E+07	1.19E+07	373	0.537
ArrayBench-59049	13.75	0.277	7.40E+08	5.08E+07	9.70E+06	533	0.44
SynchBench	32.75	0.867	2.01E+09	1.30E+07	3.30E+07	262	1.02
TaskBench	25.42	0.69	2.14E+09	9.60E+06	3.50E+07	247	0.846
CoMD	285.99	7.845	5.41E+10	6.4E+07	9.8E+07	1.39E+07	8.23

tions. The number of parallel regions, the user-specified regions, and the number of performance measurements undergone for OpenMP applications are listed in Table 5.1. The six performance measurements comprise of four hardware performance events (mentioned in the following section), the execution time in seconds, and the energy consumption of the code regions of applications in Joules.

5.2. Performance and Energy Consumption Values. In order to study the efficiency of SCALE-EA, at first, applications were experimented without SCALE-EA and the performance / energy consumption values of user-regions were recorded using EnergyAnalyzer tool. Table 5.2 shows the values obtained using the EnergyAnalyzer tool when the applications were experimented using eight threads for all parallel regions of OpenMP applications. The EnergyAnalyzer tool measured energy consumption values in Joules and four hardware performance events, such as, total number of instructions (TOT_INS), data cache misses in level 1 (L1_DCM), unconditional branches (BR_UCN), and total cache misses in level 3 (L3_TCM).

From Table 5.2, it could be observed that CoMD application had the highest energy consumption value when experimented with 8 threads (285.99 Joules). In this application, the total cache misses were in the order of 10^7. The other applications had energy consumption values in the range of 11 to 32 Joules.

5.3. Impact of FA Parameters. In previous experiments, OpenMP applications were executed without FA or MAFA. In this subsection, experiments were conducted using the FA algorithm of SCALE-EA for studying the impacts of the variants of FA parameters.

In general, FA consists of seven parameters which control the performance of FA in terms of the convergence speed of the algorithm. These seven parameters are named as number of generations, population size of

TABLE 5.3
FA Parameters and their Variants

FA-Variant	No.of Generations	Population Size	Initial Randomness	Epsilon	Alpha	Beta	Gamma
FA-Variant-1	10	10	0.1	0.009	0.5	0.5	0.0001
FA-Variant-2	10	10	0.0001	0.009	1	1	0.0001
FA-Variant-3	10	10	0.0001	0.009	0.5	0.5	0.0001
FA-Variant-4	10	10	0.001	0.09	1	1	0.009
FA-Variant-5	10	10	0.5	0.009	0.5	0.5	0.005
FA-Variant-6	50	10	0.5	0.009	0.5	0.5	0.005

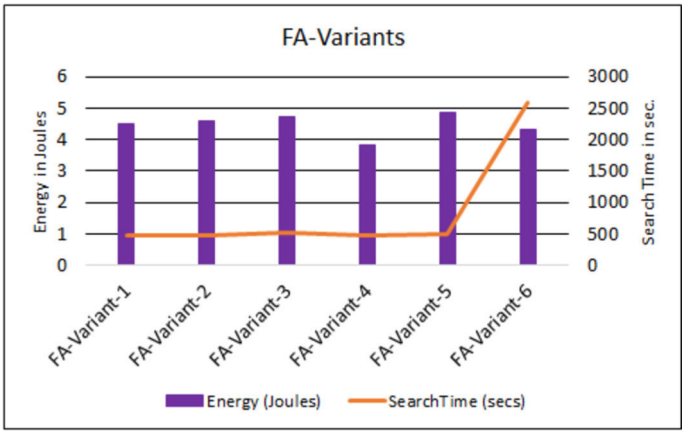

FIG. 5.1. *FA Parameter variants and their Impacts on Energy / Search Time Efficiency on the Haswell Machine.*

sequences, initial randomness, epsilon value, alpha value, beta value, and gamma value. The equations involved to describe two fireflies (sequences) mate each other are discussed in the algorithmic section of this paper (see 4.1).

It is crucial to understand the impact of these FA parameters during the process of identifying the efficient number of threads for parallel regions of OpenMP applications. Thus, experiments were conducted using Arraybench_19683 benchmark with seven varying combinations of FA parameters as shown in Table 5.3 on two machines in order to observe the impact of these parameters on the quality of observations.

It could be observed from Figure 5.1 that FA-Variant-4 achieved better energy consumption values at the reasonable amount of search time (3.841 Joules and 467.03 sec.) when compared to the others in the Haswell machine. FA-Variant-6, which was experimented with 50 number of generations, recorded the highest search time. Similar was the case when execution time efficiency was considered for the 48-core machine (see Figure 5.2). FA-Variant-4 achieved only 2275.8 seconds of search time (represented as line in Figure 5.2) when compared to FA-Variant-5 and FA-Variant-6 (2490.5 and 11969.5 seconds). The efficient number of threads identified by SCALE-EA when FA-Variant-4 was utilized in SCALE-EA was listed as 7, 10, 12, and 11 for the parallel regions of Arraybench-19683 benchmark. It should be noticed that the energy measurements could not be performed for the 48-core machine owing to the lack of RAPL counters in it.

In subsections 5.4 and 5.5, FA and MAFA based SCALE-EA were, therefore, experimented based on the FA-Variant-4 based parameter setting.

5.4. Energy Efficiency of OpenMP Applications – FA and MAFA. Fixing FA-Variant-4, SCALE-EA was executed for OpenMP applications using FA on the Haswell machine. SCALE-EA identified the efficient number of threads for parallel regions of applications as shown in Table 5.4. In addition, the energy consumption values for the user-specified regions of OpenMP applications as identified by FA and MAFA are given in Figure 5.3. As seen in Figure 5.3, all the applications showed better energy improvements when FA

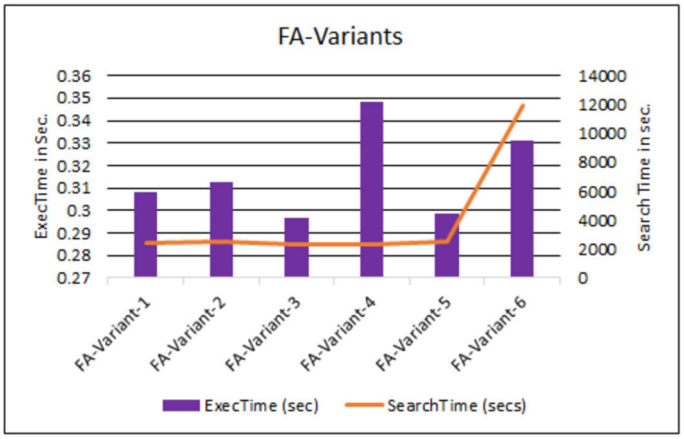

FIG. 5.2. *FA Parameter variants and their Impacts on Exec.Time / Search Time Efficiency on 48core Machine.*

TABLE 5.4
Optimal Number of Thread Sequence Identified using FA of SCALE-EA

Application	Optimal Thread Sequence
ArrayBench-3	2 3 2 3
ArrayBench-9	4 4 2 3
ArrayBench-27	4 2 3 5
ArrayBench-81	4 2 2 6
ArrayBench-243	2 1 4 5
ArrayBench-729	3 2 2 3
ArrayBench-2187	5 2 2 5
ArrayBench-6561	3 2 2 3
ArrayBench-19683	3 2 2 3
ArrayBench-59049	3 4 2 1
SynchBench	6 3 4 2 4 5 2 5 5 2
TaskBench	7 5 2 4 6 2 5 3 4 4
CoMD	1 3 1 7 2 4 1 5 2 3 2

and MAFA were applied. For instance, CoMD observed better energy consumption value when the eleven OpenMP parallel regions of three files were automatically executed with 1 3 1 7 2 4 1 5 2 3 2 thread numbers – i.e., the parallel regions of eam.c were executed with 1, 3, 1, and 7 threads; the parallel regions of initAtoms.c were executed with 2, 4, 1, 5, and 2 threads; and, the parallel regions of ljForce.c were executed with 3 and 2 threads. Similarly, the other applications, such as, Arraybench-2187 and Syncbench showed improved energy consumption values when experimented with SCALE-EA.

Figure 5.4 reveals the energy efficiencies of applications due to FA, MAFA-LRM and MAFA-RFM. The energy efficiencies of applications due to FA and MAFA were compared with the normal executions of applications constituting eight threads throughout the OpenMP parallel regions of applications. For instance, the energy efficiencies of ArrayBench-3 while experimenting with FA, MAFA-LRM and MAFA-RFM were identified as 69.01, 77.30, and 74.05 – i.e., Energy=16.04J for normal execution (all parallel regions with 8 threads), Energy=4.97J for FA, Energy=3.64J for MAFA-LRM, and Energy=4.161J for MAFA-RFM. Similarly, the experiments were carried out for all test applications (see Figure 5.4).

As seen in Figure 5.4, the following points could be inferred:

1. FA and MAFA, in general, performed well while identifying the efficient number of threads for OpenMP applications. In all experiments, the energy efficiencies achieved for the applications were from 31.21 percentage (MAFA-LRM for CoMD application) to 78.51 percentage (MAFA-LRM for Arraybench-

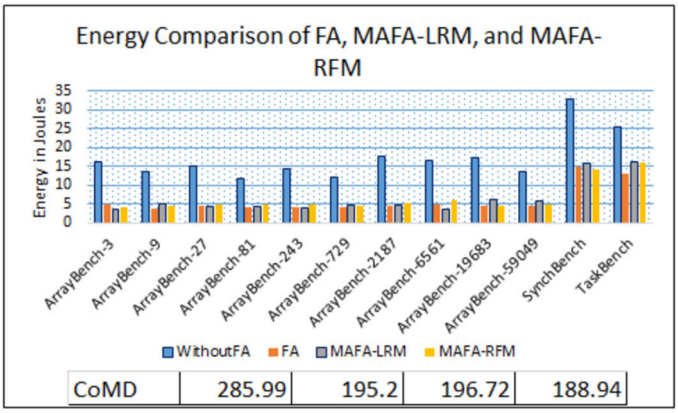

FIG. 5.3. *Comparison of Energy Consumption Values – FA, MAFA-LRM, and MAFA-RFM*

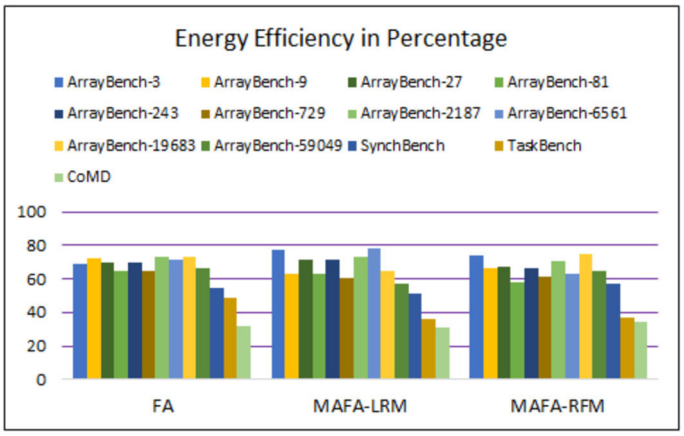

FIG. 5.4. *Energy Efficiency of MAFA-LRM and MAFA-RFM based on FA*

6561).

2. MAFA-LRM could achieve better energy efficiency in applications, such as, Arraybench-3,27,243, and Arraybench-6561. In some cases, FA produced better energy efficiency than the other two MAFA based algorithms – see the results of Arraybench-9,81,729, 2187,59049, and Taskbench application in Figure 5.4.

5.5. Search Time Efficiency of MAFA. Although FA achieved better energy efficiencies in six OpenMP applications (see the previous subsection), it resulted from challenging the search time of the tuning process. Figure 5.5 shows the search time efficiency of MAFA algorithms (MAFA-RFM and MAFA-LRM) with respect to FA. The points represented in the graph clearly manifests the inability of FA when compared to MAFA based algorithms – i.e., MAFA-RFM and MAFA-LRM outperformed traditional FA in terms of search time efficiency: MAFA-RFM reached up to 32.56 percentage of search time improvement for Arraybench-2187 when compared to FA. It is also important to notice the improved energy consumption values achieved for Arraybench-2187 application based on these algorithms (without-FA–16.71 (J); FA–4.72 (J); MAFA-LRM–3.59 (J); and MAFA-RFM–6.192 (J)). Vividly, MAFA based algorithms outperformed FA and without-FA in terms of energy efficiency and search time efficiency when compared to the other approaches.

In addition, the efficiency chart of MAFA-RFM and MAFA-LRM with respect to FA is represented as a 100 percentage stacked column chart (see Figure 5.5). As seen, the search time efficiency values of MAFA-RFM and MAFA-LRM for ArrayBench_3 had higher variations, while the values for CoMD had lower variations.

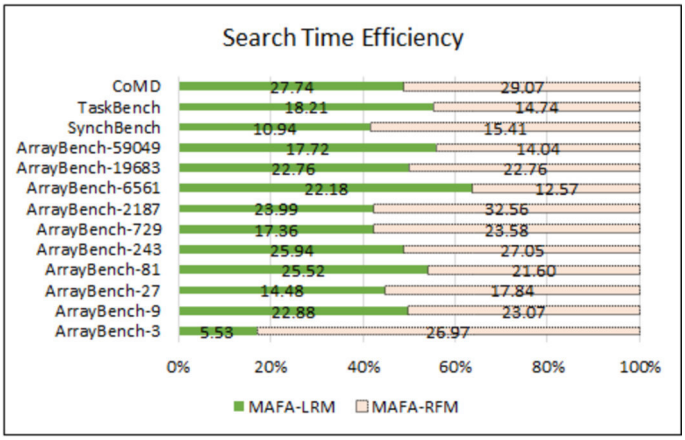

FIG. 5.5. *Search Time Efficiency of MAFA-LRM and MAFA-RFM based on FA*

6. Conclusion and Outlooks. Scalability and energy consumption issues must be considered for future HPC applications. These issues are dependent on the underlying HPC machines and the software frameworks. Autotuning is one of the solution that supports application developers in these contexts. However, autotuning solutions suffer from hefty search time for obtaining better solutions. This paper proposed a scalability-aware performance tuning framework (SCALE-EA) using the Firefly Algorithm and using Modeling Assisted Firefly Algorithm (MAFA) for OpenMP applications. SCALE-EA identified an efficient number of threads for each OpenMP parallel regions of applications at reduced search time. The results when experimented on the machines manifested that SCALE-EA achieved energy efficiencies of of 31.21 to 77.3 percentage and search time efficiencies of 5.53 to 32.56 percentage for candidate applications, such as, Arraybench, Syncbench, Taskbench, and CoMD applications.

Acknowledgements. The author thanks Rejitha R.S who has jointly worked for the paper when she was affiliated to St. Xaviers Catholic College of Engineering, India.

REFERENCES

[1] ABDUL WAHID MEMON AND GRIGORI FURSIN, *Crowdtuning: systematizing auto-tuning using predictive modeling and crowd-sourcing*, in PARCO mini-symposium on Application Autotuning for HPC (Architectures), 2013.

[2] ANANTA TIWARI, CHUN CHEN, JACQUELINE CHAME, MARY W. HALL, JEFFREY K. HOLLINGSWORTH, *A scalable auto-tuning framework for compiler optimization*, IPDPS, Italy, pp. 1-12, 2009.

[3] ANNA SIKORA, EDUARDO CÉSAR, ISAAS COMPRÉS, AND MICHAEL GERNDT, *Autotuning of MPI Applications Using PTF*, In Proceedings of the ACM Workshop on Software Engineering Methods for Parallel and High Performance Applications (SEM4HPC '16), pp. 31-38, 2016.

[4] ANANTA TIWARI, MICHAEL A. LAURENZANO, LAURA CARRINGTON, AND ALLAN SNAVELY, *Auto-tuning for energy usage in scientific applications*, in Euro-Par'11, pp. 178–187, 2012.

[5] BABAK BEHZAD, HUONG VU THANH LUU, JOSEPH HUCHETTE, SURENDRA BYNA, PRABHAT, RUTH AYDT, QUINCEY KOZIOL, MARC SNIR, *Taming parallel I/O complexity with auto-tuning*, in SC13, Vol. 28, doi:10.1145/2503210.2503278, 2013.

[6] SIEGFRIED BENKNER, SABRI PLLANA, JESPER LARSSON TRÄF, PHILIPPAS TSIGAS, ANDREW RICHARDS, RAYMOND NAMYST D., BEVERLY BACHMAYER E., CHRISTOPH KESSLER F., DAVID MOLONEY G., PETER SANDERS H., *The PEPPHER Approach to Programmability and Performance Portability for Heterogeneous many-core Architectures*, in ParCo, Belgium, pp.1-8, Aug. 2011.

[7] BRIAN J. N. WYLIE AND WOLFGANG FRINGS, *Scalasca support for MPI+OpenMP parallel applications on large-scale HPC systems based on Intel Xeon Phi*, In Proc. of the Conf. on Extreme Science and Engineering Discovery Environment: Gateway to Discovery (XSEDE '13), New York, NY, USA, Vol. 37, pp. 1-8, 2013.

[8] BUSE YILMAZ, BARI AKTEMUR, MARÍA J. GARZARÁN, SAM KAMIN, AND FURKAN KIRAÇ, *Autotuning Runtime Specialization for Sparse Matrix-Vector Multiplication*, ACM Trans. Archit. Code Optim., Vol. 13, No.1, pp. 1-26, 2016.

[9] CAVAZOS, JOHN AND FURSIN, GRIGORI AND AGAKOV, FELIX AND BONILLA, EDWIN AND O'BOYLE, MICHAEL F. P. AND TEMAM, OLIVIER, *Rapidly Selecting Good Compiler Optimizations Using Performance Counters*, doi:10.1109/CGO.2007.32, pp. 185-197, 2007.

[10] CarbonFootprint, in `CarbonFootprint_and_Energy_Efficiency_Rev_1.0_2.pdf`, accessed in 2016.

[11] Cesar E., A. Moreno, J. Sorribes, E. Luque, *Modeling Master/Worker applications for automatic performance tuning*, in Parallel Computing, Vol. 32, No. 78, pp. 568-589, 2006.
[12] Cheng Y., and Zeng Y., *Automatic Energy Status Controlling with Dynamic Voltage Scaling in Power-Aware High Performance Computing Cluster*, in proc. of 12th Int. Conf. on PDCAT, pp. 412 - 416, 2011.
[13] Cristina Silvano, Giovanni Agosta, Stefano Cherubin, Davide Gadioli, Gianluca Palermo, Andrea Bartolini, Luca Benini, Jan Martinovic, Martin Palkovic, Katerina Slaninova, Joao Bispo, Joao M. P. Cardoso, Rui Abreu, Pedro Pinto, Carlo Cavazzoni, Nico Sanna, Andrea R. Beccari, Radim Cmar, Erven Rohou, *The ANTAREX approach to autotuning and adaptivity for energy efficient HPC systems*, in ACM International Conference on Computing Frontiers, 2016.
[14] CoMD Application, from LLNL, USA, in `http://www.exmatex.org/comd.html`, accessed in Sep.2016.
[15] Daniel A. Ellsworth, Allen D. Malony, Barry Rountree, Martin Schulz, *POW: System-wide Dynamic Reallocation of Limited Power in HPC*, in Proc. of HPDC 2015, pp. 145-148, 2015.
[16] Enes Bajrovic, Siegfried Benkner, Jir Dokulil, Martin Sandrieser, *Autotuning of Pattern Runtimes for Accelerated Parallel Systems*, in Proc. of PARCO 2013, pp. 636-645, 2013.
[17] EPCC OpenMP Benchmark suite, in `https://www.epcc.ed.ac.uk/research/computing/performance-characterisation-and-benchmarking/epcc-openmp-micro-benchmark-suite`, accessed in Sep 2016.
[18] Erika Abraham, Costas Bekas, Ivona Brandic, Samir Genaim, Einar Broch Johnsen, Ivan Kondov, Sabri Pllana, and Achim Streit, *Preparing HPC Applications for Exascale: Challenges and Recommendations*, in ADPNA at NBiS, pp. 1-6, 2015.
[19] Fister, I., Yang, X.S., Brest, J. and Fister Jr, I., *Memetic self-adaptive firefly algorithm*, in Swarm intelligence and bio-inspired computation: theory and applications, pp.73-102, 2013.
[20] Fister I., Yang X. S., Brest J., *A comprehensive review of firefly algorithms*, in Swarm and Evolutionary Computation, Vol. 13, pp. 34-46, 2013.
[21] Giorgio Luigi Valentini, Walter Lassonde, Samee Ullah Khan, Nasro Min-Allah, Sajjad A. Madani, Juan Li, Limin Zhang, Lizhe Wang, Nasir Ghani, Joanna Kolodziej, Hongxiang Li, Albert Y. Zomaya, Cheng-Zhong Xu, Pavan Balaji, Abhinav Vishnu, Fredric Pinel, Johnatan E. Pecero, Dzmitry Kliazovich, Pascal Bouvry, *An overview of energy efficiency techniques in cluster computing systems*, in Cluster Computing, Vol. No. 1, pp 315, 2013.
[22] Greg Faanes, Abdulla Bataineh, Duncan Roweth, Tom Court, Edwin Froese, Bob Alverson, Tim Johnson, Joe Kopnick, Mike Higgins, and James Reinhard, *Cray cascade: a scalable HPC system based on a Dragonfly network*, In Proceedings of the International Conference on High Performance Computing, Networking, Storage and Analysis (SC '12), Los Alamitos, CA, USA, 9 pages, 2012.
[23] Guojing Cong, I-Hsin Chung, Hui-Fang Wen, David J. Klepacki, Hiroki Murata, Yasushi Negishi, Takao Moriyama: *A Systematic Approach toward Automated Performance Analysis and Tuning*, in IEEE Trans. Parallel Distrib. Syst., Vol. 23, No. 3, pp. 426-435, 2012.
[24] Haihang You., Q. Liu, Z. Li, and S. Moore, *The Design of an Auto-tuning I/O Framework on Cray XT5 System*, in Proc. of Cray Users Group Conference (CUG'11) Alaska, May 2011.
[25] Jason Ansel, Shoaib Kamil, Kalyan Veeramachaneni, Jonathan Ragan-Kelley, Jeffrey Bosboom, Una-May O'Reilly, and Saman Amarasinghe, *OpenTuner: an extensible framework for program autotuning*, In Proceedings of the 23rd international conference on Parallel architectures and compilation (PACT '14), USA, pp. 303-316, 2014.
[26] Jee W. Choi, Amik Singh, and Richard W. Vuduc, *Model-driven autotuning of sparse matrix-vector multiply on GPUs*, In Proceedings of the 15th ACM SIGPLAN Symposium on Principles and Practice of Parallel Programming (PPoPP '10), USA, pp. 115-126, 2010.
[27] Jordan, Herbert and Thoman, Peter and Durillo, Juan J. and Pellegrini, Simone and Gschwandtner, Philipp and Fahringer, Thomas and Moritsch, Hans, *A Multi-objective Auto-tuning Framework for Parallel Codes*, Proc. of the Int. Conf. on HPC, Networking, Storage and Analysis, SC12, pp. 10:1-10:12, 2012.
[28] Knobloch M., Mohr B., and Minartz T., *Determine energy-saving potential in wait-states of large-scale parallel programs*, in Computer Sci. - Res. and Dev. pp. 1-9, 2011.
[29] Manish Parashar, Salim Hariri, *Autonomic Computing: An Overview*, in Unconventional Programming Paradigms, Vol. 3566, LNCS, Springer, pp 257-269, 2005.
[30] Matthieu Doriera, Orcun Yildizc, Shadi Ibrahimc, Anne-Cécile Orgerieb, Gabriel Antoniuc, *On the energy footprint of I/O management in Exascale HPC systems*, in FGCS, Vol. 62, pp. 17-28, 2016.
[31] Dark Silicon, in `https://www.dagstuhl.de/en/program/calendar/semhp/?semnr=16052`, 2016.
[32] Pan Z. and Eigenmann R., *Fast and effective orchestration of compiler optimizations for automatic performance tuning*. In Proc. of the Int. Symp. on Code Generation and Optimization, pages 319?332, 2006.
[33] Prasanna Balaprakash, Stefan M. Wild, Boyanna Norris, *SPAPT: Search Problems in Automatic Performance Tuning*, in Procedia Computer Science, Vol 9, pp. 1959 - 1968, 2012.
[34] Robert Schöne, Daniel Molka, and Michael Wern, *Wake-up latencies for processor idle states on current x86 processors*, in Comput. Sci. Res. Dev. Vol. 30, pp. 219227, 2015.
[35] Senthilnath J., Omkar S. N., Mani V., *Clustering using firefly algorithm: performance study*, in Swarm and Evolutionary Computation, Vol. 1, No. 3, pp. 164-171, 2011.
[36] Shajulin Benedict, *Application of Energy Reduction Techniques using Niched Pareto GA of EnergyAnalzyer for HPC Applications'*, in 7th IEEE IC3 2014, http://dx.doi.org/10.1109/IC3.2014.6897234, 2014.
[37] Shajulin Benedict, *Threshold Acceptance Algorithm based Energy Tuning of Scientific Applications using EnergyAnalyzer*, ISEC2014, ACM publishers, 2014.
[38] Shajulin Benedict, Rejitha R.S., Phillip G., Radu Prodan, Thomas Fahringer, *Energy Prediction of OpenMP Ap-*

plications using Random Forest Modeling Approach, in iWAPT2015 @ IPDPS 2015 DOI 10.1109/IPDPSW.2015.12, pp. 1251-1260, 2015.

[39] Sukhyun Song and Jeffrey K. Hollingsworth, *Computationcommunication overlap and parameter auto-tuning for scalable parallel 3-D FFT*, in Journal of Computational Science, Vol. 14, pp. 3850, 2016.

[40] Weifeng Liu, Michael Gerndt, Bin Gong, *Model-based MPI-IO tuning with Periscope tuning framework*, Concurrency and Comp.: Prac. and Exp., Vol. 28, No.1, pp: 3-20, 2016.

[41] Xin-She Yang, *Firefly algorithm, stochastic test functions and design optimisation*, in Int. Journal of Bioinspired Computation, Vol. 2, No. 2, pp. 78-84, 2010.

[42] Yury Oleynik, Michael Gerndt, Joseph Schuchart, Per Gunnar Kjeldsberg, and Wolfgang E. Nagel, *Run-Time Exploitation of Application Dynamism for Energy-Efficient Exascale Computing (READEX)*, CSE 2015, pp:347-350, 2015.

Edited by: Dana Petcu
Received: Oct 17, 2017
Accepted: Dec 23, 2017

DOI 10.12694/scpe.v19i1.1391
Scalable Computing: Practice and Experience ISSN 1895-1767
Volume 19, Number 1, pp. 31–38. http://www.scpe.org

GPU-BASED ACCELERATION OF METHODS BASED ON CLOCK MATCHING METRIC FOR LARGE SCALE 3D SHAPE RETRIEVAL

MOHAMMED BENJELLOUN*, EL WARDANI DADI† AND EL MOSTAFA DAOUDI ‡

Abstract. In this paper, we exploit the potential of the GPU in order to accelerate the process of 3D shape retrieval in large databases. Indeed, the massive parallelism of the GPU offers a huge performance in much high-performance computing (HPC) applications. Our solution consists to accelerate the shape matching process of methods that use a specific similarity metric called Clock Matching (CM). This CM measure is used by view-based methods as an efficient solution to compare two 3D models even if they are not presented in same pose and orientation by taking into account all possible poses in the matching phase. However, the increase in the number of comparisons has a strong influence on the execution time. Our challenge is to exploit the maximum benefit of GPU computing resource by considering the difficulty of implementing the CM metric on GPU. Indeed, the descriptor of a given 3D object is organized using a specific data structure (hash table), where only the information whose values are not equal to zero appears in the feature vector, which makes the parallelization on GPU to be not trivial. Experiment results show a reasonable benefit from the GPU approach.

Key words: GPU, 3D Shape retrieval, Clock Matching, CM-BOF, CM-VGG, 3D object.

AMS subject classifications. 68W10, 68P05

1. Introduction.

Thanks to the current digitizing and modeling technologies, the number of accessible and available 3D models on the web is increasing, which yielded large databases of 3D models. This has led to the development of 3D shape retrieval systems [1, 7, 6, 9, 10, 12, 14, 15, 16] that, given a query object, retrieve similar 3D models. These systems work into two essentials phases which are shape indexing and shape matching. The first one consists to compute the descriptor of a given 3D object while the second one, consists to compare the query object with the 3D models in the database. For most of 3D shape retrieval method, the k objects similar to the query are returned until the shape matching is done with the whole 3D objects in the database. When the dataset size gets very large, the shape matching process becomes very challenging. The challenges come especially from the augmentation of computational time.

In order to accelerate the retrieval process, various content-based retrieval methods and approaches have been proposed in the literature [1, 2, 3, 4, 8, 14, 16]. Including sequential solutions [1, 4] and those based on high-performance computing, like multi-core [3]and GPU[2, 8], ... Despite the high-efficiency of HPC solutions, the problem is that there are a few works in the literature that implement the 3D shape retrieval under GPU environment, most of them are partial since they only concern the shape indexing phase [8].

To accelerate the shape matching phase we have already proposed a GPU-based implementation [2], of a given 3D shape retrieval method called BF-SIFT [11]. The solution proposed in [2] is general and it can be applied to several methods based on the same similarity metric which is KLD (Kullback-Leibler divergence), such as Euclidean distance.

In this paper, we propose a GPU-based implementation of a specific similarity metric called Clock Matching (CM). This similarity measure is used by two view-based methods which are CM-BOF proposed by [10], and CM-VGG presented in [14]. The only difference between the two methods is in the way they do shape indexing, the first one uses Bag-Of-Feature [5, 10, 11] while the second one uses the deep learning approach [14]. The CM metric is the common point between them, its basic idea is to compare two 3D objects even if they are presented in different poses and directions by doing a set of comparison according to 24 different poses still exist for a normalized model. This technique permits to overcome the problem of the alignment and the reflexion. However, the increase in the number of comparisons is a very critical point with a strong influence on the execution time.

*Department of Computer Science, Faculty of Engineering University of Mons, BELGIUM. (mohammed.benjelloun@umons.ac.be).

†National School of Applied Sciences, LaRi Laboratory, University of Mohammed First, MOROCCO.(e.dadi@ump.ma). Questions, comments, or corrections to this document may be directed to that email address.

‡Faculty of Sciences, LaRi Laboratory, University of Mohammed First, MOROCCO.(m.daoudi@fso.ump.ma).

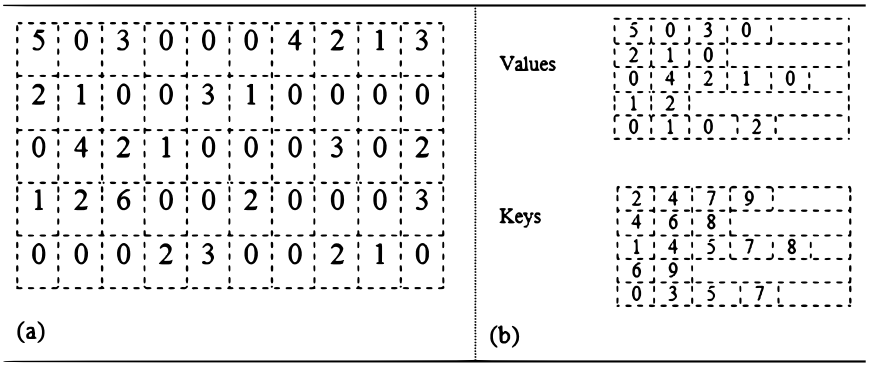

FIG. 1.1. *An example of the used two types of data,(a) Indexed structure,(b) Specific structure*

Our challenge is to adapt the CM metric to be performed on GPU. Indeed, the difficulty of this implementation is that the feature vector of a given 3D object is organized using a specific data structure cf. Figure 1.1.b, which makes the parallelization GPU to be not trivial. Note that as our contribution concerns not only the CM approach but it resolves the problem of how performing a metric between specific data-structure as a hash table on the GPU.

The rest of the paper is organized as follows. Sect. 2 is devoted to the related works. In Sect. 3 we give a brief description of the Clock matching technique. Our proposed implementation is presented in Sect. 4. Sect. 5 is devoted to the experimental results. We conclude the paper in Sect. 6.

2. Related works. 3D shape content-based retrieval in large datasets is an active research topic related to different fields such as computer vision and pattern recognition,... Indeed, large databases of multimedia data have become available on the web. However, when the dataset size gets very large, the retrieving process becomes very challenging. The challenges come from storage, computation speed, and features representation. Various methods and techniques have been proposed in the literature to accelerate the process of retrieving [1, 2, 3, 4, 8, 14, 16]. The different solutions proposed can be classified into two categories:

- Solutions based on sequential approaches: as an example of these solutions, our proposed work [4], the idea is, for a classified database, we represent each class by a representative in order to orient the process of matching only in the classes of which its representative is the most similar to query. In other work [1], we have proposed an approach that can reduce the number of comparisons of the query in the database.
- Solutions based on high-performance computing(HPC), for multi-core architecture, the idea presented in [3] is to compare the query object simultaneously with P objects, where P is the number of processors. For GPU solutions, Wu [8] have proposed an implementation of SIFT algorithm, this solution is partial because it concerns only a step of shape indexing process and not the shape matching process. To our knowledge, the only work that dealt with the shape matching process on GPU is [2], in which we have proposed a GPU-based implementation of an existing method called BF-SIFT [11]. This solution is general it can be applied to different well-known dissimilarity measurements such as Euclidean L2, Minkowski.

3. Description of the Clock Matching metric. The Clock matching is a specific similarity metric employed for the first time by the CM-BOF [10] method to compare descriptors of two 3D objects. Recently, it's used in SHREC'17 Track by the CM-VGG method [14]. The CM-BOF and CM-VGG are both view-based methods and the only difference between them is in the way that's used to characterize the shape of a given 3D object. The first one uses the Bag-Of-Features approach [5, 10, 11] while the second one uses the deep learning approach [14].

To characterize a given 3D object, these view-based methods capture a set of 2D view around its 3D shape using a virtual camera. Each 2D view is described as a feature vector of one dimension. Fortunately, for the two case, in CM-BOF and in CM-VGG, the feature vector produced is a very sparsely populated histogram,

in which most of the bins have population zero, and the remaining non-zero elements are small (e.g., < 200) positive integers. Thus, the descriptor can be replaced by a lookup into a small table in order to minimize the spatial storage and then the execution time. In this case, a 3D object is described by a matrix of a set of lines, corresponding to each 2D view; while the number of columns differs from one view to another. Each line represents the data structure, it contains the following information: number of non-zero elements, the non-zero elements and its index in the original form cf. Figure 1.1.b.

To compare two 3D objects, the two methods uses the Clock Matching metric. The basic idea of this approach is that, after getting the major axes of an object, instead of completely solving the problem of fixing the exact positions and directions of these three axes to the canonical coordinate frame, all possible poses are taken into account during the shape matching stage. For this, 24 different poses still exist for a normalized model.

When comparing two 3D objects, one is fixed in the original orientation while the second one may appear in 24 different poses. The dissimilarity between two 3D objects is measured by the minimum distance of their all (24) possible matching pairs. The dissimilarity measurement used is:

$$\boldsymbol{D\,(O_1, O_2) = \min_{0 \le i \le 23} \sum_{k=0}^{N_v - 1} Dist(\, dV_{o_1},\, dV_{o_2}^{P^i});} \tag{3.1}$$

where $\boldsymbol{O_1, O_2}$ are the two objects to be compared, N_v is the number of 2D views of a given 3D object. Dist is the distance between the descriptors of two 2D views and it's defined as follows:

$$\boldsymbol{Dist\,(dV_{o_1}, dV_{o_2}) = 1 - \frac{\sum_{j=0}^{N_w - 1} min(dV_{o_1}\,(j)\,, dV_{o_2}\,(j)\,)}{max(\,\sum_{j=0}^{N_w - 1} dV_{o_1}\,(j), \sum_{j=0}^{N_w - 1} dV_{o_2}\,(j))};} \tag{3.2}$$

where N_w is the number of features in each 2D view. Note that this number differs from one view to another.

4. The proposed implementation. Our solution is to adapt Clock Matching dissimilarity measurements used by CM-BOF and CM-VGG to be performed in the GPU by parallelizing the two functions cf. Eq(3.1) and cf. Eq(3.2) presented in previous section.

In order to maximize the benefits power of GPU computing, by launching the maximum of threads, our general idea is to compare the query object simultaneously with the whole database of 3D models instead of comparing one by one such as the sequential solution.

Launching the maximum of threads using Clock Matching metric is very challenging because this similarity function contains several loops, and it's necessary to take into account several permutations. The matter is further complicated by the fact that, the data of the descriptors are organized using a specific data structure (cf. Figure 1.1.b) which makes the parallelization GPU to be difficult and not trivial. For example, to compute the following function

$$\sum_{j=0}^{N_w - 1} min(dV_{o_1}\,(j)\,, dV_{o_2}\,(j)),$$

we need to compute the minimum between elements of two vectors for the same indices, which is not the case because the two vectors are data structured.

To achieve the aim of comparing the query object at the same time as the entire database by launching the maximum of threads, we need a good preparation of the data and an efficient adaptation of the treatment.

Assume that we have a database of m 3D models, and we want to retrieve similar objects for a given query on the GPU. The first step is to prepare the data to be transferred to the GPU. For m 3D objects in the database, the descriptor of each 3D object is represented by a matrix of $N_v * N_w(j)$, while and $N_w(j)$ is the size of the jth line; this size is different from one view to another cf. Fig 1.1. All this data will be converted to a one-row vector of size equal $m * N_v * N_w(j)$ and we transfer it to the GPU. We denote this vector by $dataDB = [O_1, O_2, ..., O_m]$

Regrouping all the data of m 3D objects as one vector will raise the problem of how to determinate the size of each jth line corresponding to each 2D view. To overcome this problem, our idea is to keep the data of the query object in the original form without structuring it. In this case, the query object is represented by a matrix of size $N_w * N_v$ while N_w is the size of the descriptor of each 2D view. Since the indexing process of the object query is performed online, our solution that consists of keeping the initial form permits to reduce the execution time allowed to the structuring process.

So, after transferring the *dataDB* to GPU, we transfer the data of query object as one vector of $N_w * N_v$ which we denote *dataQuery*.

To perform the shape matching on the GPU, by taking into account the exploiting of the maximum of GPU computing power, our solution consists to separate the treatment of the two functions cf. Eq(3.1) and cf. Eq(3.2) as follows:

- **Step 1**: we calculate the function $\sum_{j=0}^{N_w-1} min(dV_{o_1}(j), dV_{o_2}(j))$
- **Step 2**: we calculate the function $max(\sum_{j=0}^{N_w-1} dV_{o_1}(j), \sum_{j=0}^{N_w-1} dV_{o_2}(j))$
- **Step 3**: we calculate the distance: $Dist(dV_{o_1}, dV_{o_2})$
- **Step 4**: we calculate the distance: $D(O_1, O_2)$
- **Step 5**: we sort the obtained distance D.

Several kernels are used to calculate the different functions on GPU such as:

1. Kernel 1 is used to compute the minimum between pair of elements of two vectors
2. Kernel 2 is used to compute the maximum between pair of elements of two vectors
3. Kernel 3 is used to compute the sum of elements of a given vector.
4. Kernel 4 is used to compute the division between pair of elements of two vectors

Each step of the five steps has its special adaptation on GPU. To clarify this, we will explain step by step.

4.1. Step 1. For the first step which is $\sum_{j=0}^{N_w-1} min(dV_{o_1}(j), dV_{o_2}(j))$, we use two kernels (kernel 1 and kernel 2). The first one is to compute the minimum function and the second one to calculate the summation of results obtained by the first kernel.

4.1.1. The minimum function. Instead of computing the minimum between two descriptors one by one and sequentially, our solution is to compute this minimum function simultaneously and in the same time between query and all objects in the database. Our idea is to launch a m*N_v*N_w(j)*24 threads on GPU each one will execute following instruction:

```
if(dataQuery[]<dataDB[])
        Result[]=dataQuery[ ]
else
        Result[]=dataDB[]
```

The problem with launching these numbers of threads simultaneously is how to control access index to vector elements because the size of each row in the database is different from one line to another cf. Figure 1.1. For example, assume we have launched 18 threads to compute the minimum between the two vectors presented in cf. Figure 1.1, for the first four threads there is no problem, each one will execute its instruction as follows:

Thread 1	**Thread 2**
dataQuery[0]<dataDB[0])	dataQuery[1]<dataDB[1]
Thread 3	**Thread 4**
dataQuery[2]<dataDB[2])	dataQuery[3]<dataDB[3]

The problem start with the second line of the matrix, it consists of determining the index that permits the access to the second line of query matrix. To overcome this problem our solution is to generate two vectors :

- The first one is to control the acces to information in dataDB, its size is equal to the size of the database data ($m * N_v * N_w(j)$); we call it *TableSize*. Note that as this operation is performed offline. This vector is generated as follows:

```
For i=0 to m Do
    For j=0 to N_v Do
        For k=0 to N_w(j) Do
            TableSize[]=j
        EndFor
    EndFor
EndFor
```

- The second one is to control the access to the information in *dataQuery*, its size is equal to the size of the data query $N_v * N_w$. We call it $IndexDB$.

The two tables are used as follows :

```
if(dataQuery[ indexDB[j]+N_w*tableSize[i]<dataDB[j])
        Result[j]=dataQuery[ indexDB[j] +N_w*tableSize[i]]
else
        Result[j]=dataDB[j]
```

where $0 \leq i < m*N_v*N_w(j)*24$ and $0 \leq j < m*N_v*N_w(j)$.
It remains to take into account the 24 permutations possible, to do this our kernel is presented as follows:

```
__global__ void MinGPU(const int *dataQuery ,const int *indexDB, const int *
tableSize, const int *dataDB, const int *Permute, int *ResultMin, int num, int
numElements)
{
int i = blockDim.x * blockIdx.x + threadIdx.x;
if (i < numElements)
{
 int j=i%num;
 if( dataQuery[indexDB[j] + N_w * Permute[tableSize[i]]] < dataDB[j] )
    ResultMin[i] = dataQuery[indexDB[j] + N_w * Permute[tableSize[i]]];
 else
    ResultMin[i] = dataDB[j];
}
}
```

The kernel represented above is not very optimized. To optimize it, we calculate the treatment $indexDB[j] + N_w * tableSize[i]$ on CPU since it's an offline operation. To optimize the memory, we transfer the result of this treatment using the vector allowed to return the result; this vector is called $ResultMin$.
The final kernel is given as follows:

```
__global__ void MinGPU(const int *dataQuery, const int *dataDB, int *ResultMin,
int num, int numElements)
{
int tmp,j;
int i = blockDim.x * blockIdx.x + threadIdx.x;
if (i < numElements)
{
    j=i%num;
    tmp= dataQuery[ResultMin[i]];
    if(tmp < dataDB[j] )
        ResultMin[i] = tmp ;
    else
        ResultMin[i] = dataDB[j];
}
}
```

This kernel is used to execute $m*N_v*N_w(j)*24$ threads simultaneously. The data transferred to GPU memory for this kernel is as follows:

- The vector *dataQuery* is of size equal to $N_w * N_v$
- The vector *dataDB* is of size equal to $m * N_v * N_w(j)$
- The vector *ResultMin* is of size equal to $24 * m * N_v * N_w(j)$

4.1.2. Calculate the sum of the obtained result. In this step we calculate the sum of the sub-vectors of size $N_w(j)$ of the obtained result (*ResultMin*). To compute this sum we have used the kernel 'reduce_by_key' of Thrust library by exploiting *tableSize* vector used previously.

4.2. Step 2. For this step, we proceed as follows:

- We transfer to the GPU the vector that contain the sum of lines of dataDB ($\sum_{j=0}^{N_w-1} dV\,(j)$). Note that as this sum is calculated offline on the CPU (cf. Figure 4.1). This vector of size $m * N_v$ is denoted by *SumDB*.
- We calculate on GPU of the sum $\sum_{j=0}^{N_w-1} dV\,(j)$ of the dataQuery. We obtain by this a vector of size N_v. We call this vector by *SumQuery*. Note that as the data of the query is previously transferred to the GPU memory.
- We calculate the max function simultaneously between the two vectors *SumQuery* and *SumDB*. To do this we proceed as follows : we launch $24 * m * N_v$ threads on the GPU, each one will execute the operation:
  $tabMax[i] = max(SumQuery[j], SumDB[Permute[k] + N_v * t])$, where $0 \leq i < 24 * m * N_v$, $j = i\%N_v$, $k = i\%(24 * N_v)$ and $t = i/(24 * N_v)$.

To optimize the treatment and the memory by avoiding multiple transferring of data and by avoiding the using of modulo function, The operation $Permute[k] + Nv * t$ is performed on the CPU, since it's an offline operation. The corresponding kernel in this case is given as follows:

```
__global__ void MaxGPU(const int *SumQuery, const int *SumDB,const int
*Permute, int *ResultMax, int numElements)
{

int i = blockDim.x * blockIdx.x + threadIdx.x;
int j,tmp;
if (i < numElements)
{
    j=i%66;
    tmp= SumDB[ ResultMax[i] ];
    if(SumQuery[j]>tmp)
        ResultMax[i] = SumQuery[j];
    else
        ResultMax[i] = tmp;
}
}
```

4.3. Step 3. In this step we use the kernel4 and we launch $24 * m * N_v$ threads in order to calculate the operation : $Dist[i] = 66 - (ResultMin[i]/ResultMax[i])$

4.4. Step 4. In this step :

- Firstly, we calculate the sum of sub-vector of size N_v of the obtained $Dist$ vector. This step is performed on GPU using the kernel 3. We obtain by this a vector of size $24 * m$. We call it by *SumDist*.
- Then, we calculate the minimum of 24 elements of the obtained vector (*SumDist)*. This step is performed on GPU using reduce kernel but instead of calculating the sum we calculate the min between two elements. The obtained vector *(D)* is the distance of the object query and m objects in the database.

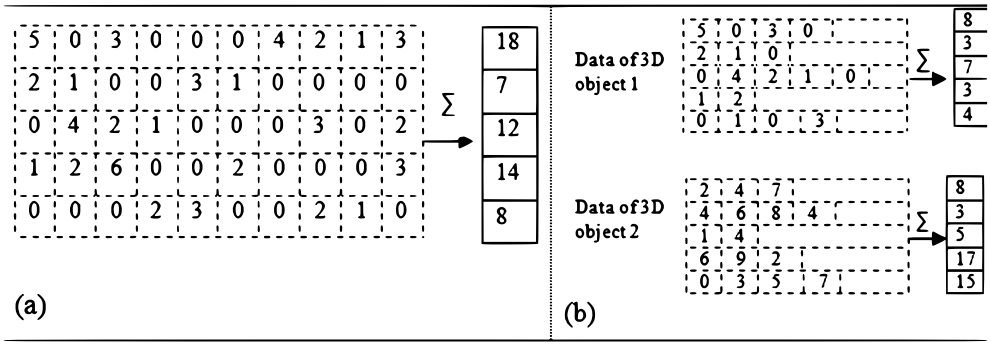

FIG. 4.1. *calculate the sum of each line of matrices.*

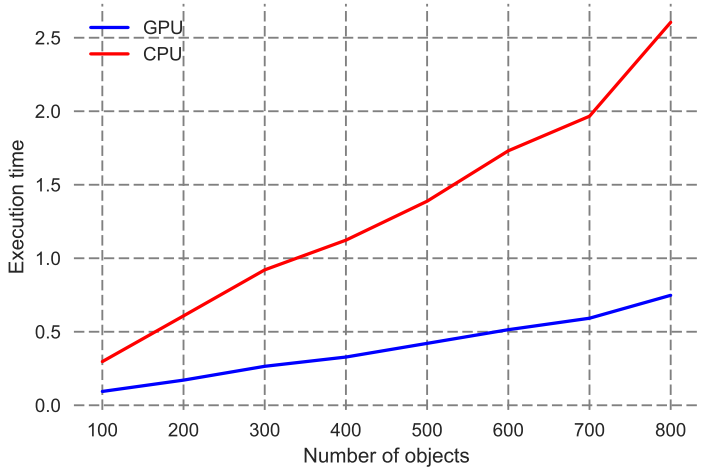

FIG. 5.1. *The obtained execution time for different sizes of the database.*

4.5. Step 5. In order to return the result, the last step is to sort the obtained vector of distance. This step is performed also on GPU.

5. Experimental results. Tests are performed on a machine with a GPU of type GeForce GT610 of 2048 MB global memory. For the GPU programming, we have used CUDA.

For the 3D object database, we have used Princeton 3D Shape Benchmark database [13]. We have compared between CPU and GPU for the sizes of the database (100, 200, 300, 400, 500, 600, 700, 800).
Figure 5.1, shows the evolution of the execution time of the shape matching process with different sizes of the database and for both implementations on the CPU and on the GPU. The obtained results show that the execution time is significantly reduced for the case of GPU based implementation which means that's interesting to use this new resource of high-performance computing. On the other hand and always for the case of GPU, the Fig Figure 5.1 shows that the evolution of the execution time when increasing the size of the database is almost linear; if we consider T_m as the GPU time obtained for m 3D objects, the obtained results show as $T_m \approx (2 * T_{m/2})$, which means that the large scale can be achieved using GPU. For multi-GPU, the database of m 3D objects can be divided on the number k of GPUs. Each one performs the matching of m/k 3D models independently.

6. Conclusion. In this paper, we are interested in the computational efficiency of 3D shape retrieval process. We have proposed a GPU-based implementation in order to accelerate the shape matching of methods

that use Clock Matching metric. This implementation exploits the maximum of the potential of the GPU and it permits to compare simultaneously, the query object with a large number of 3D models. This has the advantages of obtaining the retrieval results in a very short time, the thing that was well justified by the experimental results. Experimental results show that the execution time is significantly reduced compared to the execution on the CPU. Our proposed solution shows that the large-scale retrieval can be achieved using GPU.

REFERENCES

[1] M. Benjelloun, E. W. Dadi, and E. M. Daoudi, *New approach for efficiently retrieving similar 3D models based on reducing the research space*. International Journal of Imaging 01/2014; 13(2), pages 104-111.

[2] E. W. Dadi and E. M. Daoudi, *GPU-Based for accelerating the BF-SIFT method for large-scale 3D shape retrieval*, Multimedia Computing, and Systems (ICMCS), 2014 International Conference on, Marrakech, 2014, pages 38-41.

[3] E. W. Dadi, and E. M. Daoudi. *Large Scale 3D Shape Retrieval Based on Multi-core Architectures*, Lecture Notes in Computer Science 7853, 2013, pages 295-299.

[4] E. W. Dadi, E. M. Daoudi, and C. Tadonki. *Fast 3D shape retrieval method for classified databases*, IEEE International Conference on Complex Systems (ICCS) 2012.

[5] J. Fehr, A. Streicher and H. Burkhardt, *A Bag of Features Approach for 3D Shape Retrieval*, Advances in Visual Computing, Lecture Notes in Computer Science, 2009, pages 34-43.

[6] T. A. Funkhouser, M. Kazhdan, P. Min, P. Shilane, *Shape-based retrieval and analysis of 3D models*, Communications of the ACM - 3d hard copy, Volume 48 Issue 6, June 2005, pages 58-64.

[7] Y. Gao, Q. Dai, M. Wang, N. Zhang, *3D model retrieval using weighted bipartite graph matching*, Signal Processing: Image Communication Journal Volume 26 Issue 1, January, 2011, pages 39-47.

[8] C. Wu, *A GPU Implementation of Scale Invariant Feature Transform (SIFT)*, *http://cs.unc.edu/˜ccwu/siftgpu*

[9] A. Koutsoudis, C. Chamzas, *3D pottery shape matching using depth map images*, Journal of Cultural Heritage, Journal of Cultural Heritage, Volume 12, Issue 2, AprilJune 2011, pages 128-133.

[10] Z. Lian, A. Godil, X. Sun and J. Xiao, *CM-BOF: visual similarity-based 3D shape retrieval using Clock Matching and Bag-of-Features*, Journal of Machine Vision and Applications; Vol. 24 Issue 8, Nov 2013, p1685 ISBN 0932-8092.

[11] R. Ohbuchi, K. Osada, T. Furuya, T. Banno, *Salient Local Visual Features for Shape-Based 3D Model Retrieval*, IEEE International Conference on Shape Modeling and Applications (SMI08), Stony Brook University, June 4-6, 2008.

[12] L. Pengjie, H. Ma, and A. Ming, *Nonrigid 3D model retrieval using multi-scale local features*, Proceedings of the 19th ACM international conference on Multimedia - MM 11, 2011.

[13] P. Shilane, P. Min, M. Kazhdan, and T. A. Funkhouser, *The Princeton shape benchmark*, in Shape Modeling and Applications Conference, SMI2004, Genova, Italy, June 2004, IEEE, pp. 167178.

[14] M. Savva, F. Yu, H. Su, A.Kanezaki, T. Furuya, R. Ohbuchi, Z. Zhou, R. Yu, S. Bai, X. Bai5, M. Aono, A. Tatsuma, S. Thermos, A. Axenopoulos, G. Th. Papadopoulos, P. Daras, X. Deng, Z. Lian, B. Li, H. Johan, and Y. Lu, S. Mk, *SHREC17 Track Large-Scale 3D Shape Retrieval from ShapeNet Core55*, Eurographics Workshop on 3D Object Retrieval 2017.

[15] J.W.H. Tangelder and R.C. Veltkamp, *A survey of content based 3D shape retrieval methods*, Multimedia Tools and Applications, vol. 39, no. 3, pp. 441471, Sept. 2008.

[16] R. C. Veltkamp, G. J. Giezeman, H. Bast, T. Baumbach, T. Furuya, J. Giesen, A. Godil, Z. Lian, R. Ohbuchi, W. Saleem, *SHREC10 Track: Large Scale Retrieval*, Eurographics Workshop on 3D Object Retrieval 2010.

Edited by: Dana Petcu
Received: Oct 10, 2017
Accepted: Feb 16, 2018

DOI 10.12694/scpe.v19i1.1392
Scalable Computing: Practice and Experience ISSN 1895-1767
Volume 19, Number 1, pp. 39–51. http://www.scpe.org

ROUND ROBIN WITH LOAD DEGREE: AN ALGORITHM FOR OPTIMAL CLOUDLET DISCOVERY IN MOBILE CLOUD COMPUTING

RAMASUBBAREDDY SOMULA* AND SASIKALA R†

Abstract. Mobile devices have become essential in our daily lives but it has limited resources such as battery life, storage, and processing capacity. Offloading resource intensive task into the cloud is an efficient approach to improve battery utilization, storage capacity and processing capabilities. Efficiently computing using cloud resources to process offloaded task in order to improve response time and reduce both tasks' waiting time and latency problems is one of the main goals in mobile cloud computing (MCC). In order to improve user satisfaction and performance of the mobile application, a cloudlet framework concept has been developed to reduce latency problems which improve response time. The cloudlet brings the cloud closer to the user to perform a computational task. This article proposes a new balancing model among cloudlets in mobile cloud computing environment to find the required resources and create an impact on performance. The efficient load balancing model makes mobile cloud computing more attractive and improves user satisfaction. This paper introduces a Round Robin with Load degree algorithm for public cloudlets in mobile cloud computing using a switch mechanism to choose different approaches for different situations. This algorithm uses game theory based load balancing approach to improve application response time in public mobile cloud environments.

Key words: public cloud; cloudlet, offloading, mobile cloud computing, load balancing model, game theory

AMS subject classifications. 68M14, 91A80

1. Introduction. Mobile cloud computing (MCC) can be viewed as a resource to fill the gap between limited resources of mobile devices (MD) and computation requirement of MD. According to the definition provided by [9], mobile cloud computing is a task in which both computation and storage will happen outside of smart device. The mobile cloud computing has attracted the attention of industries do to its benefits. It reduces the efforts in developing application and also allows users to use the latest technology on demand basis (or) pay per use model. The MCC has three main components: mobile device, wireless connection, cloud infrastructure where both data storage and processing power will be available. Computation offloading means that a computation part of mobile application is offloaded into remote cloud for execution in order to extend mobile device capabilities. Computation offloading can be sufficient when network connection is good and cloud provides enough resources [31]. The cloud provides resource to MD with the help of network communication in heterogeneous environment [22].

The cloudlet is an emerging technology in mobile cloud computing that brings cloud near to mobile user (being like a data center in the box). The cloudlet is based on a cluster of physical machines which allows nearby mobile users to use available resources [24]. It can be available around mobile users. Figure 1.1 depicts the cloudlet architecture: a cloudlet is a kind of small scale server, associated with specific resources. This can be accessed by mobile devices within specific range. The cloudlet provides cloud resources to users in a short time and with a certain level of throughputs [15].

The cloudlet can be composed of three layers: component layer, node layer and cloudlet layer. The component layer provides resources to higher layer through interface overlooked by execution environment. The node can be formed by running a node agent on one or more execution environments on the top of OS. Multiple nodes can be formed as cloudlet by a cloudlet agent [27].

The cloudlet can be efficient and scalable, but maintaining and processing a large number of incoming jobs consistently is very difficult. Therefore, the researchers are paying attention to the load balancing problem. The behavior of the incoming jobs from mobile users is unpredictable and each cloudlet capabilities cannot be constant (number of physical systems can always be changed). In order to improve the system performance and maintain stability, controlling the workload distributed among cloudlets is very important.

Load balancing mechanisms can be classified into two types: static and dynamic [25]. In case of static, the mechanism is simple and does not consider nodes performance before distributing load into heterogeneous environment and handles nodes showing low load variation while dynamic mechanism uses nodes performance

*School of Computer Science and Engineering (SCOPE), VIT University, Vellore, India (svramasubbareddy1219@gmail.com).
†School of Computer Science and Engineering (SCOPE), VIT University, Vellore, India.(sasikala.ra@vit.ac.in)

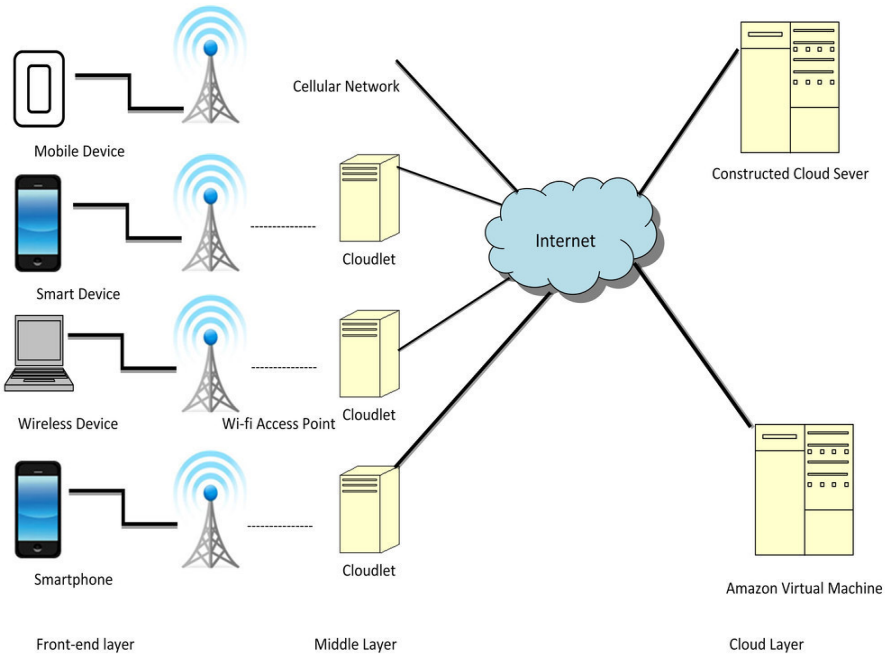

FIG. 1.1. *Cloudlet Architecture*

while distributing work load. Dynamic nature algorithms are more complex than static nature algorithms. The behavior of dynamic scheme is changing according to node status or performance and brings additional cost.

In our model, the proposed method also follows dynamic load balancing as the load is distributed with progression of time. The proposed model contains a cloudlet_ manager cloudlet agents. The cloudlet manager directs the jobs from users to cloudlet. The cloudlet agent collects the information of cloudlet and updates the status in cloudlet manager. The dynamic model is using system status and decides the best balancing strategy. This process will influence other working nodes in cloudlet. The Load balancing model is mainly based on public cloud environment. The cloudlets are distributed in geographical locations. The Cloudlet_manager maintains distributed cloudlets and each cloudlet is assigned to one agent. The Cloudlet_manager will select a cloudlet for incoming jobs and agent decides load balancing strategy. The existing algorithms allocate arriving jobs from mobile users to available cloudlets without knowing the status of the cloudlet. These makes jobs to wait for long time in queue until other jobs get finished. To address this problem a new balancing algorithm is proposed in this paper. The proposed algorithm computes Load_degree of each node in cloudlet to drive the incoming jobs to a particular cloudlet in geographical area.

2. Background. Ofloading mobile application into remote cloud to avoid limitation of mobile devices and increases the performance of application was studied in [4, 23, 20, 19]. There are many mechanisms introduced to find when the task should offload on cloudlet [5, 8, 11, 26]. Usually, the model for offloading mobile application into remote cloud consists of components for both client and server. The client components work on mobile devices at client side whereas server components at remote cloud. The client side components monitor network performance, predicts the computational resources of mobile application and estimating time for local as well as remote execution times. By using this information the client components make decisions on how much portion of the application to offload [7, 8]. The task offloading can be done by migrating VM from one cloudlet to another cloudlet [13]. The recent works ThinkAir [17], cloudclone [7], proposed the concept of offloading mobile application from single-machine execution into distributed execution environment automatically. The study of the efficient model for offloading task solution to improve QoS of user application is done in [14]. The users are able to offload tasks into a cloudlet by selection, in the papers [28, 29], [6]. There are studies which are mainly focused to minimize revenue of service providers in cloud using linear programming model for offloading.

The author of [10] proposed to incorporate QoS requirements and energy consumption.

The problem with offloading task to remote cloud is the latency which disturbs user experience with interactive applications. A cloudlet is a new solution for high-latency problem between mobile user and remote cloud. The cloudlet is a small scale datacenter which is available to nearby users. This provides rich computing resource access and improves the performance of mobile application. Generally, the offloading application can be done by the following VM-based approach [10]. The mobile device continues the process of creating VM instances of applications and they are transferred to cloudlet, then the device remotely executes the offloaded task on cloudlet. Once offloaded task execution is done, its result is sent back to the device. This approach can cause the cloud to become constrained if more number of requests increases from the user. There are studies which have presented novel model to find a task with average response time at cloudlet using queuing theory [16]. When a cloudlet goes overloaded, the task is offloaded into remote cloud from current cloudlet. The author of [27] proposed a new model for offloading tasks which can be distributed to multiple cloudlets by dividing application into multiple independent executable components at runtime. The advantage of this approach is the distribution of the workload into multiple cloudlets allowing parallel processing. However, this approach is not applicable at some conditions especially when network condition is poor.

Load balancing is still a new problem in MCC, but load balancing mechanism is not a new concept, it is a widely adapted mechanism in different fields especially in cloud computing. Load balancing concept has been clearly described in the whitepaper [1] which describes the tools commonly utilized for implementing load balancing in cloud. The load balancing scheme is used in mobile cloud computing among widely distributed cloudlets in geographical environment. This scheme is a new approach in MCC to reduce latency, response time and user satisfaction by balancing arriving jobs with a help of agent and cloudlet manager. The cloud can be well utilized in geographical area by dividing the entire cloud into different regions [30], but it requires new approach to improve the user satisfaction.

We propose a new architecture for representing the distributed different cloudlets in geographical environment. Different load balancing algorithms are there since decades. They are Equally Spread Current Execution, Round Robin, Ant colony [2]. Ant colony algorithm can be used to analyze and compare the performance with different algorithms in terms of time and cost [21]. Some of the widely used algorithms are similar to the operating system method allocations, such as the First Come First Serve (FCFS), Shortest Job First (SJF), Round Robin (RR). In our proposed mechanism Round Robin is used for simplicity.

3. Cloudlet Architecture. MCC has many models; our model is based on public cloud. The user will get many services from the public cloud infrastructure provided by the cloud service provider. The cloudlet is a subarea in the cloud computing. The public cloud is spread on a large area and hosts a certain number of cloudlets and each cloudlet is composed with many number of nodes. The cloudlets are distributed in geographical areas which are managed by the cloudlet_manager. The following architecture depicts the cloudlet in different regional areas. The load balancing strategy follows by selection of cloudlet in public cloud environment. When job arrives from mobile user, then cloudlet_manager will receive and decide cloudlet for processing the arriving job. If the status of cloudlet (nodes) is normal then the job allocated to the local cloudlet otherwise, the job gets forwarded to another cloudlet. Figure 3.1 depicts the complete idea of the proposed model and process.

3.1. Cloudlet_Manager and Agent. The cloudlet_manager maintains information of cloudlets distributed in geographical area. The cloudlet_manager takes the arriving jobs and sends it to the optimized cloudlet. Each cloudlet has an agent which will refresh the system status. Small dataset requires more processing. The information related to the nodes in cloudlet are maintained by the agent. Based on this, the load balancing strategy is decided. Figure 3.3 depicts the association between the agent and cloudlet_manager.

Figure 3.2 describes the flow of cloudlet selection. When jobs arrive at the cloudlet_manager, the first step is to select the resourceful cloudlet. The status of cloudlet can be represented in three models.

1. LCL (low loaded cloudlet): when load of the nodes exceeds to A, turn to LCL status.
2. BCL (Balanced cloudlet): when load of the nodes exceed to B, turns to BCL status.
3. OCL (Overloaded cloudlet): when load of the nodes exceeds to C, turns to OCL status

The parameters A, B, C (threshold values) are set by cloudlet agents. The cloudlet_manager will maintain continuous connection with the agents of different cloudlets. When a job arrives to the cloudlet_manager

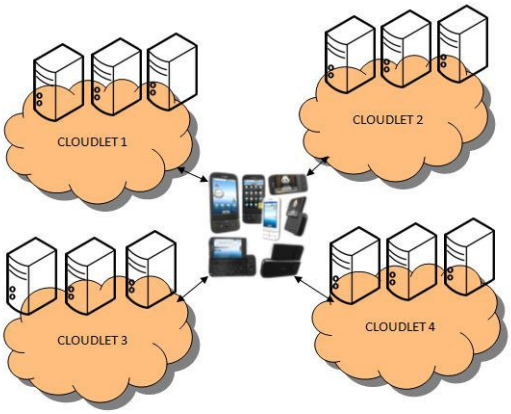

FIG. 3.1. *Cloudlet Selection*

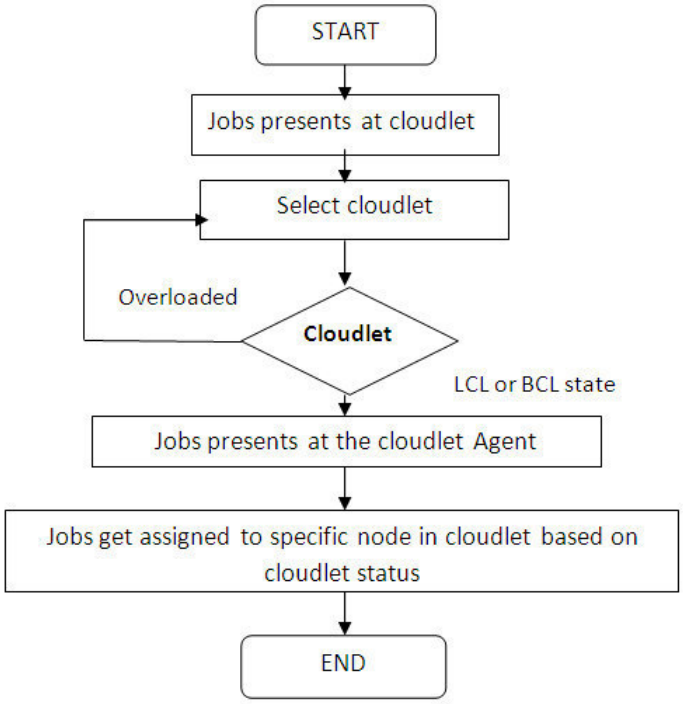

FIG. 3.2. *Flow of Job Scheduling*

questions the cloudlet agent where the job is to be located. If the cloudlet status is LCL or BCL then job is executed locally. Otherwise, another cloudlet is found with status either LCL or BCL. The algorithm is depicted in Algorithm 1.

3.2. Assigning jobs to nodes in the cloudlet. The cloudlet agent gathers information about all nodes in cloudlet to calculate the degree of each node. This is important to evaluate each node status in cloudlet selection process. Based on the status of each cloudlet the job gets assigned to it. The first step is to find the degree of nodes in each cloudlet.

The calculation of degree of each node depends on the dynamic and static parameters. The static parameters contain the number of CPUs, CPU speed, size of the memory, software information, etc. The dynamic

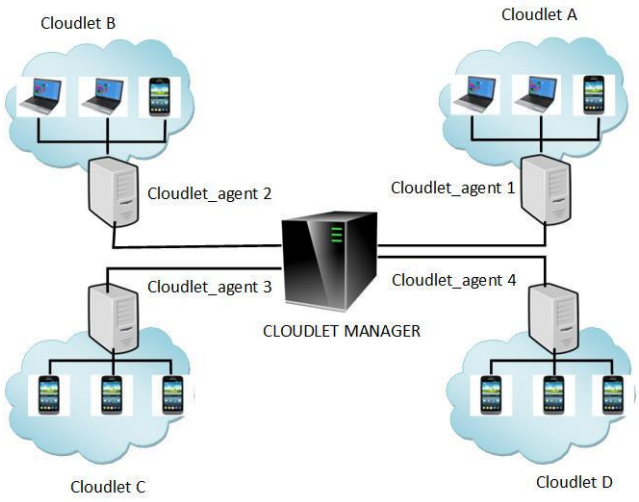

FIG. 3.3. *Cloudlet Management Architecture*

Algorithm 1 Efficient Cloudlet Finding

```
1: begin
2:     while job do
3:         SearchPerfectCloudlet (job)
4:         if cloudlet_State=LCL || Cloudlet_State=BCL then
5:             Send Job to Cloudlet
6:         else
7:             Search for another Cloudlet;
8:         end if
9:     end while
10: end
```

parameters contain data about usage ratios of CPU, memory, speed, network bandwidth, etc. The evaluation of load degree with different parameters is depicted in the following section.

The cloudlet Load_degree values are input to the cloudlet agents for creating tables. Each cloudlet in mobile cloud computing maintains an agent that decides the status of the cloudlet based on values available in the table. The table updating is done at particular periodic time T. When jobs arrives at cloudlet, the cloudlet agent assigns the jobs to a particular node in cloudlet based on cloudlet load status. The cloudlet agent assigns jobs to another cloudlet if cloudlet is not having sufficient resources to handle the incoming jobs.

4. Cloudlet selection with load balancing algorithm. A load balancing mechanism is used to improve the performance of mobile application by selecting resourceful cloudlet. There is no efficient load strategy to satisfy all mobile users problems. Each load strategy has its own advantage in specific area. Multiple load balancing methods have been developed to solve the existing problem and improve existing solutions. In our model, the load strategy method is changed according to the system status information. System information can always be changed based on the load balance method that has been adapted. In this model, simple methods can be used for LCL state with complex method for BCL. This model mainly aims to select resourceful cloudlet to reduce waiting time and improve the performance. An enhanced round robin method is used for LCL while BCL uses game theory based load balancing method.

4.1. Load Balancing for LCL. When the cloudlet load status is LCL, the nodes in cloudlet are resourceful for handling the arriving jobs. Then the cloudlet processes the arriving jobs as fast as possible and also a simple algorithm is used for scheduling different jobs to nodes. There are many simplest algorithms for

Algorithm 2 Calculation of Load Degree

Step 1: Let the load parameter set $B = \{B_1, B_2, B_3, \ldots, B_m\}$ with each $B_i (1 \leq i \leq m, B \in [0,1])$ the parameter inside set can be static (or) dynamic. M denotes number of parameters.
Step 2: Evaluate load degree of node as follows:

$$\text{Load\_degree}(N) = \sum_{i=1}^{m} A_i B_i$$

$A_i (\sum_{i=1}^{N} A_i = 1)$ is representing weights of the jobs, it may differ every time. N represents current cloudlet.
Step 3: Calculate the size of the cloudlet from the node degree statistics with the formula

$$Load\_degree_{avg}(N) = \frac{\sum_{i=1}^{N} Load\_degree(N_i)}{n}$$

The threshold Load_degreehigh is applicable for various situations based on value of step 3. Where N is number of nodes in cloudlet.
Step 4: The Cloudlet can be classified into three states as follows:
LCL (Low loaded cloudlet): when there is no job to be processed then cloudlet turns to be LCL state.

$$\text{Load\_degree}(N) = 0$$

BCL (Balanced cloudlet): when a cloudlet is neither LCL nor OCL, then cloudlet turns to be BCL state.

$$0 < \text{Load\_degree}(N) = 0 \leq Load\_degree_{high}$$

OCL (Overloaded cloudlet): when cloudlet nodes are busy and unable to process incoming jobs then cloudlet turns to be OCL state

$$Load\_degree_{high} < Load\_degree(N)$$

scheduling arriving jobs such as round robin algorithm, weighted round robin algorithm, dynamic round robin algorithm [18]. The Round robin (RR) scheduling strategy is the simplest algorithm for allocating jobs to the servers. RR will send all incoming jobs to queue inside the server but not the main status of each connection. RR scheduling methods consider every node in cloudlet equally so that equal chance is given for every node in cloudlet to be chosen. However, in a cloudlet each node differs with respect to configuration and performance. RR can be improved by assigning arriving jobs based on load degree of each node. The incoming jobs get stored into the circular queue. The system goes through the queue over and over. Each cloudlet in public cloud maintains a table for the load status of the nodes, based on which the nodes get placed in the table from low load to high load. The order of the nodes in table will be changed based on status of the load status table. However, the inconsistency problem has been taken between read and write at refresh interval T. The jobs keep on arriving at cloudlet manger when load balancing table is being refreshed. This makes wrong cloudlet selection and wrong order of cloudlets in the table. Since the table will have old data after getting refreshed, inconsistency problem will lead the arriving jobs to get assigned to wrong node in cloudlet. To address this problem, the cloudlet manager should maintain two load refresh tables: Table 1 and Table 2. A label called read or write can be assigned to each table through flag. The read table contains information of load of the nodes in cloudlet which can be used by improved round robin based on load degree evolution. The write table will be updated with new load information. One table provides exact location of the node in the queue and other table is getting written with new information of the nodes. Both read and write labels will be exchanged to avoid inconsistency problem. Figure 4.1 sketches the inconsistency problem to be addressed by read and write tables.

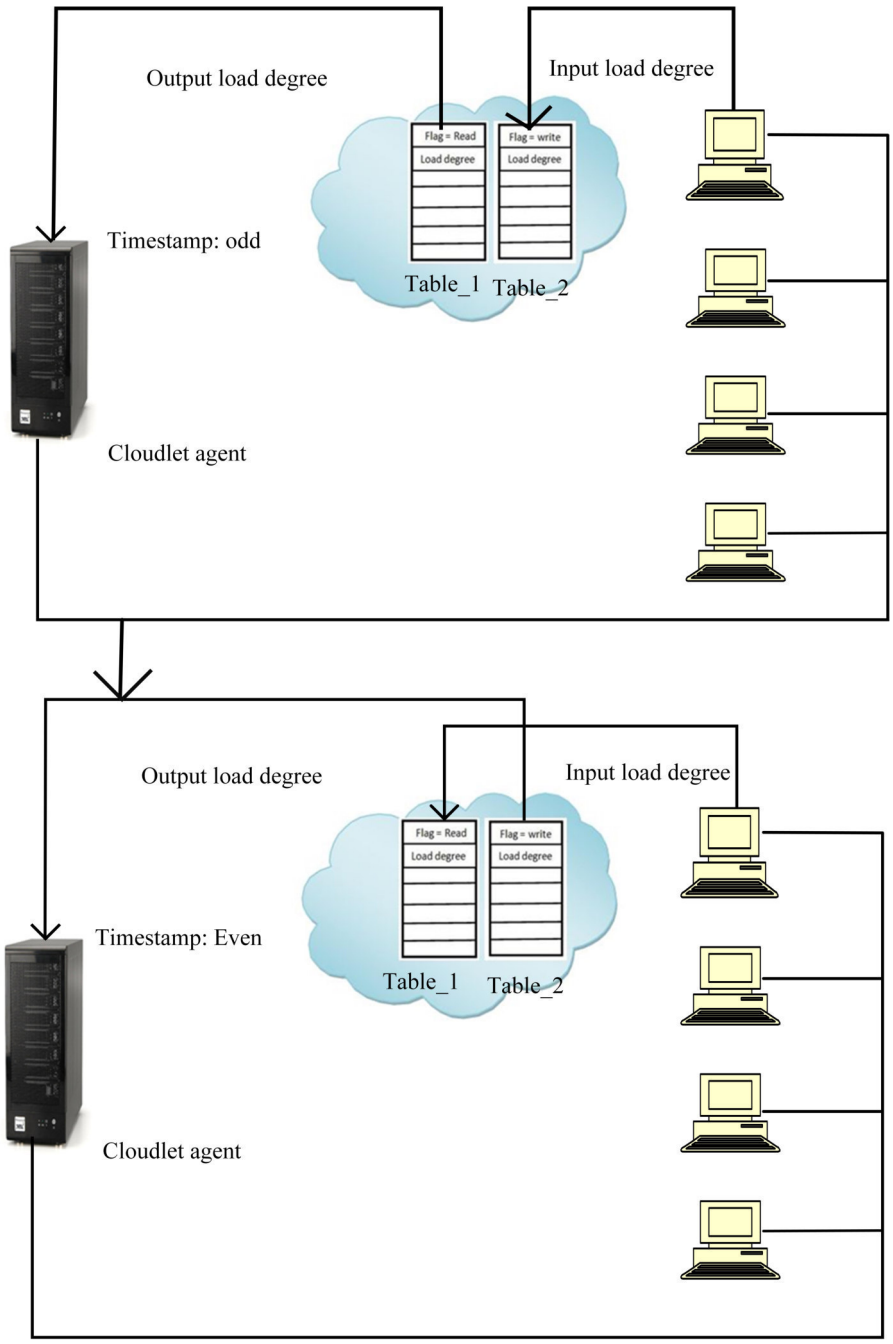

FIG. 4.1. *Efficient model for inconsistency problem*

4.2. Load Balancing for BCL. When a cloudlet status is BCL, then all jobs arrives to BCL than LCL, every user wants to finish their work as early as possible. A cloudlet needs a special method to finish all the incoming requests from mobile users. So different strategies are used for improving response time. Static load balancing based on game theory is proposed by chronopulos [20]. This gives us a new idea of cloudlet in mobile cloud computing: the load balancing in mobile cloud computing can be viewed as a game. In the game theory there are cooperative games and non- cooperative games. In a cooperative game, the decision maker will take

decision by discussing with other player or comparing each node with each other. In a non- cooperative game the decision is taken for his own benefit and the other players in the game will take their own decision. The system will reach to Nash equilibrium where each player will make his/her own optimized decision and no player gets benefited by changing his or her own plan, while remaining players decisions are unchanged.

The game theory has been proposed by many studies to solve various problems and was adapted by different areas. It is mainly introduced for distributed computing and later it has been popular in cloud computing too. A dynamic load balancing based on game theory is proposed by Aote and Khara [3]. In this method, users being decision makers in non-cooperative game. Mobile cloud computing is integrated with multiple technologies, networking, mobile computing and cloud computing. Mobile cloud computing is also viewed as distributed computing because this MCC technology is integrated with cloud computing. So the load balancing algorithm can be viewed as a non-cooperative game. The players in the game are nodes and jobs. For instance there are 'n' nodes in current cloudlet with 'm' arriving jobs. The following define this process:

β_i: Each node processing ability, $i= 1, 2, \ldots, n$

φ_j: Each job execution time

$\varphi : \sum_{j=1}^{N} \varphi_j$: total time of the entire cloudlet for processing $\varphi < \sum_{i=1}^{n} \beta_i$

F_{ji}: Job j get assigned to node $(\sum_{i=1}^{n} F_{ji})$ and $0 \leq F_{ji} \leq 1$

Finding appropriate value F_{ji} is an important step. Grosu et al. [12] has proposed a model called best reply by using this model to evaluate F_{ji} for each node with a greedy algorithm. The procedure will produce a Nash equilibrium to reduce response time of each job. The balancing mechanism changes according to the system status information. Figure 4.2 depicts the proposed model.

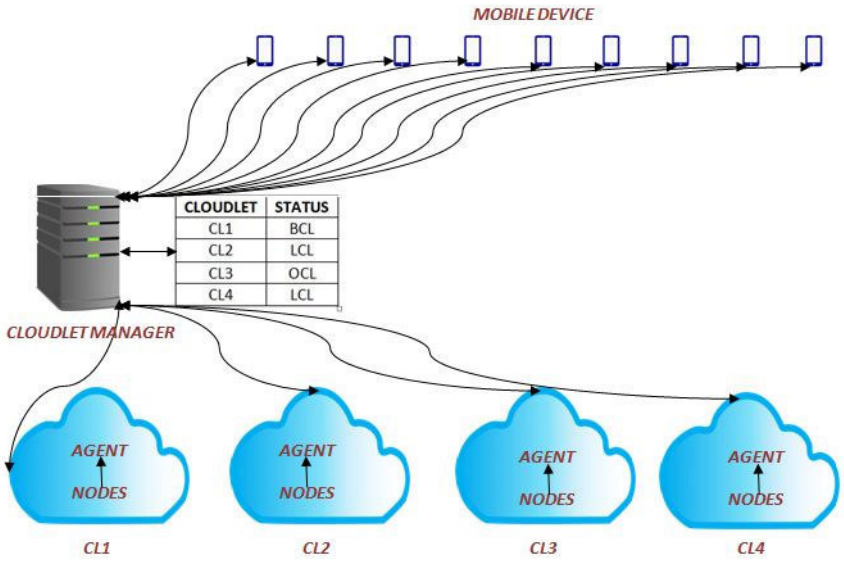

FIG. 4.2. *Proposed cloudlet selection model*

4.3. Extended Round Robin Algorithm. We use the Algorithm 3 to find optimal cloudlet to process tasks coming from mobile users in MCC environment.

5. Performance Evaluation. In this section we describe how the proposed algorithm performs in various work loaded environments using cloudlets. The computing performance of proposed algorithm is compared with

Algorithm 3 Extended Round Robin Algorithm

Step 1: Calculate load degree of current node based on following equation:

$$\text{Load\_degree}(N) = \sum_{i=1}^{m} A_i B_i$$

Step 2: Calculate average load of the cloudlet from each node statistics:

$$Load\_degree_{avg}(N) = \frac{\sum_{i=1}^{N} Load\_degree(N_i)}{n}$$

Step 3:Classify the states of cloudlet based on following statistics:
LCL: Load_degree$(N) = 0$
BCL: $0 <$ Load_degree$(N) \leq Load_degree_{high}$
OCL: $Load\_degree_{high} < Load\_degree(N)$
Step 4: The job from user will get placed based on load such as LCL,BCL,OCL.

```
1: begin
2:     while job do
3:         SearchPerfectCloudlet (job)
4:         if cloudlet_State=LCL || Cloudlet_State=BCL then
5:             Send Job to Cloudlet
6:         else
7:             Search for another Cloudlet;
8:         end if
9:     end while
10: end
```

TABLE 5.1
Simulation environment

Symbol	Definition	Predefined
N	Number of cloudlets	30
μ_i	Response rate	20
λ_i	Arrival rate at cloudlet	5
K	Number of servers at cloudlet	4
A	Number of cloudlet agents	30
M	Cloudlet Manager	1

an existing algorithm.

5.1. Experimental results. We have conducted an experiment by sending a number of requests to different cloudlets. We observed the cloudlet selection process based on load_degree of different cloudlets. If the number of tasks at one cloudlet is more than the cloudlet capacity then the tasks are automatically leaded to another cloudlet by considering cloudlet status without wasting time for cloudlet response.

We use MATLAB environment to generate a random number of cloudlets and requests. Each cloudlet load status evaluated by considering capacity of each node involved in particular cloudlet. Furthermore, the information of load of each cloudlet will be updated with cloudlet_manager. We simulate a cloudlet environment in MATLAB by assuming number of cloudlet (1 to N) and response rate for each cloudlet μ_i by sampling normal distribution $(6, 3) > 0$, the number of nodes setup in cloudlet is mean of 3 (Table 5.1). In this model, we assumed that the system should not exceed μ_i.

Figure 5.1 shows the comparison between the proposed and the existing algorithm: the proposed algorithm decreases the response time of the cloudlet from 0.5 to 0.9 and the probability of processing a certain number

of requests of the users is higher than for the conventional algorithm.

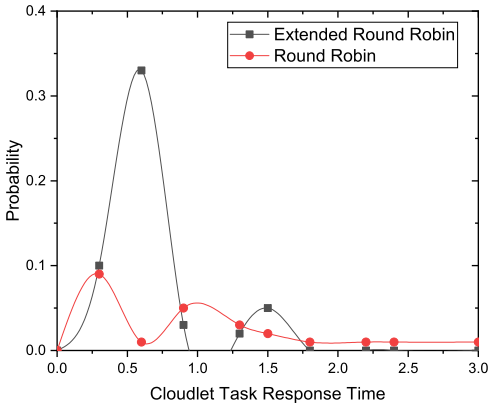

FIG. 5.1. *Probability of Response Time*

Figure 5.2 shows the minimum and maximum task response time of the cloudlets. When the average response time is higher, say R=1.5, the outgoing task demands in the overloaded cloudlets are lesser than the underloaded cloudlets. Also the data flow among the cloudlets and the response time decreases. Similarly, when the average task response time is set low, say R=0.6, the outgoing task demands in the overloaded cloudlets are higher than underloaded cloudlets. The dataflow increases in the cloudlets, thus the response time increases. When the average response time is set to zero, all the cloudlets are fully loaded.

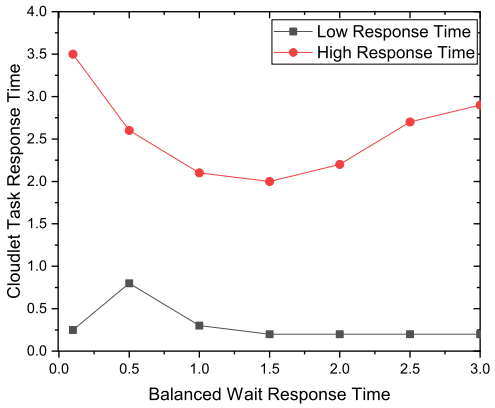

FIG. 5.2. *Low and High Response Time for Average Number of Tasks*

Figure 5.3 states that the proposed algorithm is not affected even though the number of cloudlets increases respectively. Examine the response time of proposed algorithm when there are no requests coming from users as well as requests from users with increasing number of cloudlet. When the count of overloaded cloudlet increases, the task response time also increases.

Figure 5.4 shows the running time of proposed algorithm and existing algorithms (SJF, FCFS, Round Robin) when the number of cloudlets is increased. The time was changed according to the number of cloudlets, system configuration, network status. The graph represents the running time captured from 2.40 GHz Intel Core i5 with 16GB RAM; the number of incoming requested to be processed in system over 0.4 seconds with 400

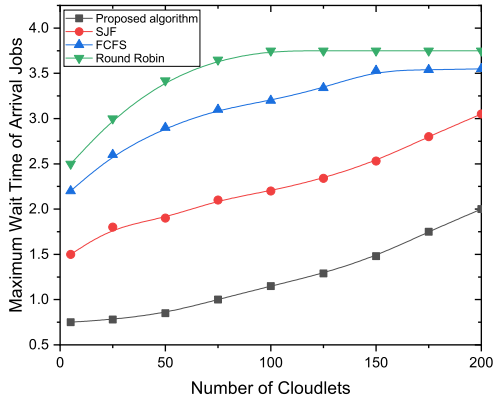

FIG. 5.3. *Delay for Arrival Jobs with Different Cloudlets*

cloudlets. The table updating is done at particular periodic time T when jobs arrives at cloudlet: the cloudlet agent assigns jobs to particular nodes in cloudlet based on cloudlet load status.

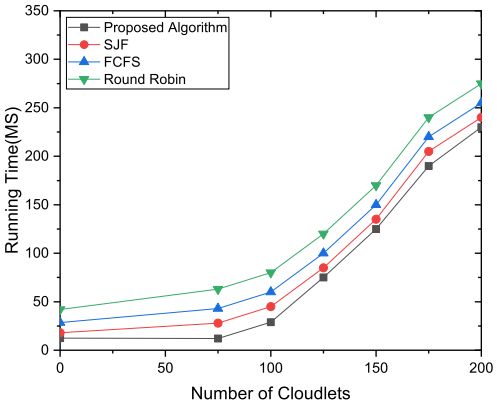

FIG. 5.4. *Running time of proposed algorithm on number of cloudlets*

Figure 5.5 shows the cloudlet task response time with and without the proposed algorithm in a static network. As graph shows, the number of incoming jobs increases, while the task response time also increases under normal distribution. As can be seen, the cloudlet response time can be different from the existing algorithm. The execution time includes transferring time and processing time. If the number of requests comming from the users increases then the performance of existing algorithms is decreasing.

Figure 5.6 shows the cloudlet task response time for proposed method, SJF, FCFS and RR algorithms in a static network. The X-axis represents the cloudlet response time and the y-axis represents the cloudlet arrival rate. As graph shows, the Proposed Method is efficient in comparison with the other three existing algorithms.

6. Conclusion and Future work. This paper proposed a novel conceptual framework which is mainly focusing on selection of distributed resourceful cloudlet in a public cloud with the help of a load balancing algorithm. The Cloudlet_manager and Cloudlet_agent are responsible for scheduling the arriving jobs in the

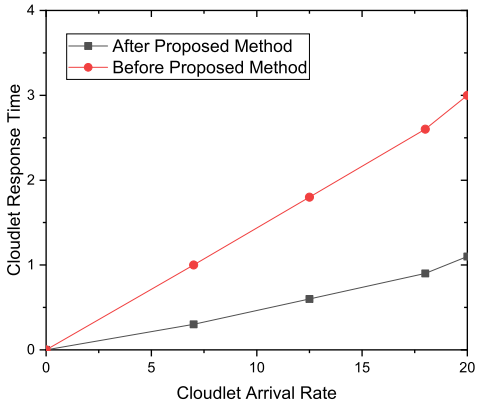

FIG. 5.5. *cloudlet response time for cloudlet arrival rate*

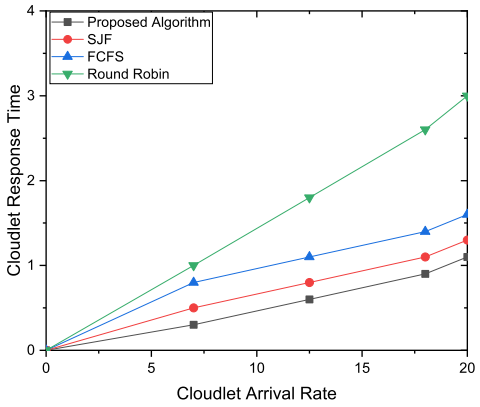

FIG. 5.6. *The response time of cloudlet arrival rate for SJF, FCFS and RR*

cluster of cloudlets. The job scheduling strategy is changed according to the status of the cloudlet of load degree. The proposed algorithm is compared with SJF, FCFS and Round Robin. The results are showing that the response time and the execution time are better than the ones of existing algorithms. Future work need to focus on different aspects, as a Cloudlet selection process is not a simple task: the framework need to be enhanced to represent cloudlet selection process in details, for instance, the number of hosts in cloudlet and how far each host is away from other host, host may be away from other hosts in same cloudlet. The Cloudlet_agent refreshes system information at particular time period.

REFERENCES

[1] B. ADLER AND S. ARCHITECT, *Load balancing in the cloud: Tools, tips and techniques*, 2012.
[2] M. H. AGHDAM, N. GHASEM-AGHAEE, AND M. E. BASIRI, *Text feature selection using ant colony optimization*, Expert systems with applications, 36 (2009), pp. 6843–6853.
[3] S. S. AOTE AND M. KHARAT, *A game-theoretic model for dynamic load balancing in distributed systems*, in Proceedings of the International Conference on Advances in Computing, Communication and Control, ACM, 2009, pp. 235–238.
[4] R. BALAN, J. FLINN, M. SATYANARAYANAN, S. SINNAMOHIDEEN, AND H.-I. YANG, *The case for cyber foraging*, in Proceedings of the 10th workshop on ACM SIGOPS European workshop, ACM, 2002, pp. 87–92.

[5] N. Bobroff, A. Kochut, and K. Beaty, *Dynamic placement of virtual machines for managing sla violations*, in Integrated Network Management, 2007. IM'07. 10th IFIP/IEEE International Symposium on, IEEE, 2007, pp. 119–128.
[6] V. Cardellini, V. D. N. Personé, V. Di Valerio, F. Facchinei, V. Grassi, F. L. Presti, and V. Piccialli, *A game-theoretic approach to computation offloading in mobile cloud computing*, Mathematical Programming, 157 (2016), pp. 421–449.
[7] B.-G. Chun, S. Ihm, P. Maniatis, M. Naik, and A. Patti, *Clonecloud: elastic execution between mobile device and cloud*, in Proceedings of the sixth conference on Computer systems, ACM, 2011, pp. 301–314.
[8] E. Cuervo, A. Balasubramanian, D.-k. Cho, A. Wolman, S. Saroiu, R. Chandra, and P. Bahl, *Maui: making smartphones last longer with code offload*, in Proceedings of the 8th international conference on Mobile systems, applications, and services, ACM, 2010, pp. 49–62.
[9] H. T. Dinh, C. Lee, D. Niyato, and P. Wang, *A survey of mobile cloud computing: architecture, applications, and approaches*, Wireless communications and mobile computing, 13 (2013), pp. 1587–1611.
[10] E. Gelenbe, R. Lent, and M. Douratsos, *Choosing a local or remote cloud*, in Network Cloud Computing and Applications (NCCA), 2012 Second Symposium on, IEEE, 2012, pp. 25–30.
[11] L. Gkatzikis and I. Koutsopoulos, *Migrate or not? exploiting dynamic task migration in mobile cloud computing systems*, IEEE Wireless Communications, 20 (2013), pp. 24–32.
[12] D. Grosu, A. T. Chronopoulos, and M.-Y. Leung, *Load balancing in distributed systems: An approach using cooperative games*, in Parallel and Distributed Processing Symposium., Proceedings International, IPDPS 2002, Abstracts and CD-ROM, IEEE, 2001, pp. 10–pp.
[13] J. Heo, K. Terada, M. Toyama, S. Kurumatani, and E. Y. Chen, *User demand prediction from application usage pattern in virtual smartphone*, in Cloud Computing Technology and Science (CloudCom), 2010 IEEE Second International Conference on, IEEE, 2010, pp. 449–455.
[14] D. T. Hoang, D. Niyato, and P. Wang, *Optimal admission control policy for mobile cloud computing hotspot with cloudlet*, in Wireless Communications and Networking Conference (WCNC), 2012 IEEE, IEEE, 2012, pp. 3145–3149.
[15] Y. Jararweh, F. Ababneh, A. Khreishah, F. Dosari, et al., *Scalable cloudlet-based mobile computing model*, Procedia Computer Science, 34 (2014), pp. 434–441.
[16] L. Kleinrock, *Queueing systems, volume 2: Computer applications*, vol. 66, wiley New York, 1976.
[17] S. Kosta, A. Aucinas, P. Hui, R. Mortier, and X. Zhang, *Thinkair: Dynamic resource allocation and parallel execution in the cloud for mobile code offloading*, in Infocom, 2012 Proceedings IEEE, IEEE, 2012, pp. 945–953.
[18] D. MacVittie, *Intro to load balancing for developersthe algorithms*, 2012.
[19] N. Palaniappan and S. Ramasamy, *A survey on procedures dealing with mobile offloading schemes*, 7 (2017), p. 178.
[20] S. Penmatsa and A. T. Chronopoulos, *Game-theoretic static load balancing for distributed systems*, Journal of Parallel and Distributed Computing, 71 (2011), pp. 537–555.
[21] M. Randles, D. Lamb, and A. Taleb-Bendiab, *A comparative study into distributed load balancing algorithms for cloud computing*, in Advanced Information Networking and Applications Workshops (WAINA), 2010 IEEE 24th International Conference on, IEEE, 2010, pp. 551–556.
[22] Z. Sanaei, S. Abolfazli, A. Gani, and R. Buyya, *Heterogeneity in mobile cloud computing: taxonomy and open challenges*, IEEE Communications Surveys & Tutorials, 16 (2014), pp. 369–392.
[23] M. Satyanarayanan, *Pervasive computing: Vision and challenges*, IEEE Personal communications, 8 (2001), pp. 10–17.
[24] M. Satyanarayanan, P. Bahl, R. Caceres, and N. Davies, *The case for vm-based cloudlets in mobile computing*, IEEE pervasive Computing, 8 (2009).
[25] N. G. Shivaratri, P. Krueger, and M. Singhal, *Load distributing for locally distributed systems*, Computer, 25 (1992), pp. 33–44.
[26] H. N. Van, F. D. Tran, and J.-M. Menaud, *Sla-aware virtual resource management for cloud infrastructures*, in Computer and Information Technology, 2009. CIT'09. Ninth IEEE International Conference on, vol. 1, IEEE, 2009, pp. 357–362.
[27] T. Verbelen, P. Simoens, F. De Turck, and B. Dhoedt, *Cloudlets: Bringing the cloud to the mobile user*, in Proceedings of the third ACM workshop on Mobile cloud computing and services, ACM, 2012, pp. 29–36.
[28] Q. Xia, W. Liang, and W. Xu, *Throughput maximization for online request admissions in mobile cloudlets*, in Local Computer Networks (LCN), 2013 IEEE 38th Conference on, IEEE, 2013, pp. 589–596.
[29] Q. Xia, W. Liang, Z. Xu, and B. Zhou, *Online algorithms for location-aware task offloading in two-tiered mobile cloud environments*, in Utility and Cloud Computing (UCC), 2014 IEEE/ACM 7th International Conference on, IEEE, 2014, pp. 109–116.
[30] G. Xu, J. Pang, and X. Fu, *A load balancing model based on cloud partitioning for the public cloud*, Tsinghua Science and Technology, 18 (2013), pp. 34–39.
[31] K. Yang, S. Ou, and H.-H. Chen, *On effective offloading services for resource-constrained mobile devices running heavier mobile internet applications*, IEEE communications magazine, 46 (2008).

Edited by: Dana Petcu
Received: Sep 23, 2017
Accepted: Feb 16, 2018

DOI 10.12694/scpe.v19i1.1393
Scalable Computing: Practice and Experience ISSN 1895-1767
Volume 19, Number 1, pp. 53–67. http://www.scpe.org

AUTOADMIN: AUTOMATIC AND DYNAMIC RESOURCE RESERVATION ADMISSION CONTROL IN HADOOP YARN CLUSTERS

ZHENGYU YANG, JANKI BHIMANI, YI YAO, CHO-HSIEN LIN*, JIAYIN WANG†, NINGFANG MI‡ AND BO SHENG§

Abstract. Hadoop YARN is an Apache Software Foundation's open project that provides a resource management framework for large scale parallel data processing, such as MapReduce jobs. Fair scheduler is a dispatcher which has been widely used in YARN to assign resources fairly and equally to applications. However, there exists a problem of the Fair scheduler when the resource requisition of applications is beyond the amount that the cluster can provide. In such a case, the YARN system will be halted if all resources are occupied by ApplicationMasters, a special task of each job that negotiates resources for processing tasks and coordinates job execution. To solve this problem, we propose an automatic and dynamic admission control mechanism to prevent the ceasing situation happened when the requested amount of resources exceeds the cluster's resource capacity, and dynamically reserve resources for processing tasks in order to obtain good performance, e.g., reducing makespans of MapReduce jobs. After collecting resource usage information of each work node, our mechanism dynamically predicts the amount of reserved resources for processing tasks and automatically controls running jobs based on the prediction. We implement the new mechanism in Hadoop YARN and evaluate it with representative MapReduce benchmarks. The experimental results show the effectiveness and robustness of this mechanism under both homogeneous and heterogeneous workloads.

Key words: Cloud Computing, MapReduce, Hadoop, YARN, Scheduling, Resource Management, Admission Control, Big Data, Scalable Computing, Cluster Computing

AMS subject classifications. 68M14, 68P05

1. Introduction.

Large scale data analysis is of great importance in a variety of research and industrial areas during the age of data explosion and cloud computing. MapReduce [11] becomes one of the most popular programing paradigms in recent years. Its open source implementation Hadoop [5] has been widely adopted as the primary platform for parallel data processing [1]. Recently, the Hadoop MapReduce ecosystem is evolving into its next generation, called Hadoop YARN (Yet Another Resource Negotiator) [19], which adopts fine-grained resource management for job scheduling.

The architecture of YARN is shown in Figure 1.1. Similar to the traditional Hadoop, a YARN system often consists of one centralized manager node running the ResourceManager (RM) daemon and multiple work nodes running the NodeManager (NM) daemons. However, there are two major differences between YARN and traditional Hadoop. First, the RM in YARN no longer monitors and coordinates job execution as the JobTracker of traditional Hadoop does. Alternatively, an ApplicationMaster(AM) is generated for each application in YARN to coordinate all processing tasks (e.g., map/reduce tasks) from that application. Therefore, the RM in YARN is more scalable than the JobTracker in traditional Hadoop. Secondly, YARN abandons the previous coarse grained slot configuration used by TaskTrackers in traditional Hadoop. Instead, NMs in YARN consider fine-grained resource management for managing various resources. e.g., CPU and memory, in the cluster.

On the other hand, YARN uses the same scheduling mechanisms as traditional Hadoop and supports the existing scheduling policies (such as FIFO, Fair and Capacity) as the default schedulers. However, we found that a resource (or "container") starvation problem exists in the present YARN scheduling under Fair and Capacity. As mentioned above, for each application in YARN, an ApplicationMaster is first generated to coordinate its processing tasks. Such an ApplicationMaster is indeed a special task in the YARN system, which has a higher priority to get resources (or containers) and stays alive without releasing resources till all processing tasks of that application finish. Consequently, when the amount of concurrently running jobs becomes too high, for example, a burst of jobs arrived, it is highly likely that system resources are fully occupied by ApplicationMasters of

* Department of Electrical & Computer Engineering, Northeastern University, 360 Huntington Ave., Boston, MA, USA, 02115 (yangzy1988@coe.neu.edu, bhimani@ece.neu.edu, yyao@ece.neu.edu, jacks953107@ece.neu.edu).
† Computer Science Department, Montclair State University, 1 Normal Ave, Montclair, NJ, USA, 07043 (wangji@montclair.edu)
‡ Department of Electrical & Computer Engineering, Northeastern University, 360 Huntington Ave., Boston, MA, USA, 02115 (ningfang@ece.neu.edu).
§ Deptartment of Computer Science, University of Massachusetts Boston, 100 Morrissey Boulevard, Boston, MA, USA 02125 (shengbo@cs.umb.edu).

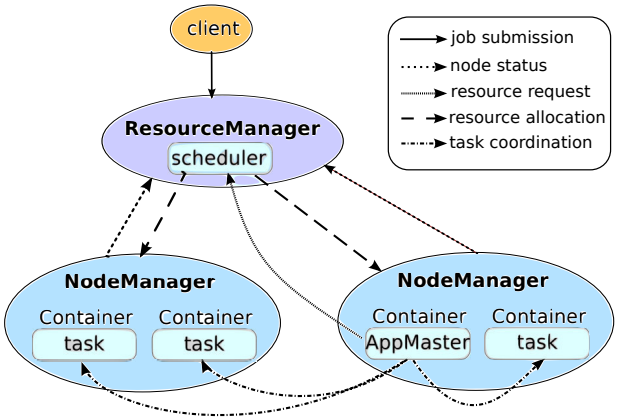

FIG. 1.1. *YARN Architecture. When a client submits a job to the ResourceManager (RM), the RM communicates with a NodeManager (NM) to launch an ApplicationMaster(AM) for running that job. The AM is responsible for submitting resource requests to the RM and negotiating with a set of NMs to launch containers for processing the tasks of the job.*

these running jobs. A *resource deadlock* thus happens such that each ApplicationMaster is waiting for other ApplicationMasters to release resources for running their application tasks.

To solve this problem, one could kill one or multiple jobs and their ApplicationMasters to break the deadlock. A preventative solution is to apply the admission control mechanism to control the number of concurrently running jobs (or ApplicationMasters) in the system and thus reserve resources to run processing tasks. By this way, the previous deadlock of resource waiting can be avoided. However, choosing a good admission control mechanism (e.g., how many jobs admitted in the system?) is difficult when efficiency of the system is also an important consideration. If we reserve too many resources for running processing tasks, then the concurrency of jobs will be sacrificed because the resources for starting ApplicationMasters are limited. In contrast, the running jobs may take too much time to wait for resources for running their tasks and thus be delayed dramatically if we admit too many jobs in the system. Furthermore, MapReduce applications in real systems are often heterogeneous, with job sizes varying from a few tasks to thousands of tasks and different submission rates [7]. A static and fixed admission control mechanism thus cannot work well.

Therefore, the objective of this work is to design a new admission control mechanism which can automatically and dynamically decide the number of concurrently running jobs, with the goal of avoiding the resource waiting deadlock and meanwhile preserving good system performance. The main performance metric we take into consideration is the makespan (i.e., total completion length) of a given set of Mapreduce jobs. There are three main components of our admission control mechanism.

- **Resource Information Collector** (**RIC**): this module periodically records the resource usage information of the running jobs of each worker node.
- **Reserved Resource Predictor** (**RRP**): this is the major component of this mechanism. RRP resides in the RM and uses the information provided by the **RIC** module to decide the amount of resources that need to be reserved for regular tasks.
- **Application Resource Controller** (**ARC**): this module controls the admission of incoming applications based on the current amount of reserved resources determined by the **RRP** module. All applications that are not allowed to enter the system for running will be queued.

We implement these components in a YARM platform (e.g., Hadoop YARN) and evaluate our new admission control mechanism with a suite of representative MapReduce benchmarks. The experimental results demonstrate the effectiveness of the proposed mechanism under both simple and complex workloads.

The remainder of the paper is organized as follows. In Section 2, we introduce the deadlock problem of YARN systems and show our preliminary investigation on static admission control. Our proposed mechanism is proposed in Section 3. Evaluation of this mechanism is presented in Section 4. We describe the related works in Section 5 and conclude in Section 6.

2. Motivation.

2.1. Background. In a YARN system, each application needs to specify the resource requirements of all their tasks, such as ApplicationMasters, map tasks and reduce tasks. The resource requirement is a bundle of physical resources with the format as <2 CPU, 1GB RAM>, for example. Then, a task from that application will only be executed in a container whose resource capacity (e.g., 2 CPU and 1GB RAM) is equal to that task's resource demand. Meanwhile, the NodeManager (NM) keeps monitoring the actual resource usage of that container and could kill that container if the actual usage exceeds the granted resource amount.

The ResourceManager (RM) acts as a central arbitrator, dispatching available containers to various competing applications in light of each application's resource demand and the scheduling policy. NMs residing in the work machines (i.e., slave nodes) associate with the RM to manage the resource; they periodically report the information of resource and containers usage to the RM through the *heartbeat* message in YARN. The scheduler in the RM then schedules the queuing jobs based on the waiting resource requests of applications and the current residual resource amount on each slave node.

When an application is submitted, the RM needs to first allocate resources for launching the ApplicationMaster container on a work node according to the resource requirement specified by the client. The launched AM will then send resource requests for processing remaining tasks of that application to the RM. The RM responses with resource allocations on NMs and the AM then communicate with the NMs for launching containers and executing tasks. The AM is also responsible for monitoring and coordinating the execution of other processing tasks, e.g., re-submitting failed tasks, gradually submitting reduce tasks according to the progress of map tasks, etc.. Therefore, the AM only terminates and releases the resources its container occupies after all the remaining tasks of its application are finished.

Moreover, the AM is the head of a job and it must be launched firstly when processing the job. Since AM needs to harness some resource to running the job's tasks, it will issue requests to RM for allocating the Task Container (TC) to process the tasks. While RM accepts the requests then it will response to AM that which nodes have the available resource. The AM then continuously negotiates with the NMs of those nodes to running the tasks. Finally, while all the tasks are processed the AM can be finished and the RM will release the AMC. In conclusion, the RM and NM starts running when the YARN system is set up; however, the AM launched upon a container is based on the condition that a job is submitted to the RM and the RM accepts to processing it; then, the AM can start its negotiating mission, relative state [17] is as Fig. 2.1.

2.2. The Deadlock Problem of Fair Scheduler in YARN. Since an ApplicationMaster is the first launched task of each job and will not release its resource until the associated job finishes, the number of AM tasks running in a YARN system is always equal to the number of concurrently running jobs. It is not a problem if a small amount of jobs are concurrently running in the system. However, it is possible that these AMs use up most or even all of the resources during a busy period, for example, when a large amount of users submit many ad-hoc MapReduce query jobs. In such a case, the YARN system faces a *deadlock* problem, i.e., none of these AMs could get resources for running their map/reduce tasks. Consequently, overall efficiency of the YARN system is severely degraded because the AMs are occupying most resources yet waiting for others to release resources.

Therefore, our goal in this work is to design a new mechanism that can automatically control the resource reservation in the YARN system such that the deadlock problem can be avoided even under busy conditions when resource demands of AMs exceed the entire cluster capacity. Moreover, this new mechanism can dynamically adjust the strategy for resource reservation according to the present workloads in order to improve the efficiency of the YARN system, e.g., minimizing the makespan (i.e., the overall completion length) of a set of MapReduce jobs.

2.3. Preliminary Investigations. The basic solution of preventing the deadlock situation is to reserve a fixed amount of resources for non-AM processing tasks. However, as we discussed before, the system performance could be degraded if the reservation number is not carefully chosen. We first modify the Fair scheduler to support the static resource reservation and investigate the impact of resource reservation on the performance. Two sets of experiments are conducted to evaluate the performance of resource reservations. For the sake of simplicity, we only consider the cpu resource in these experiments (i.e., all jobs are cpu intensive). The YARN cluster we

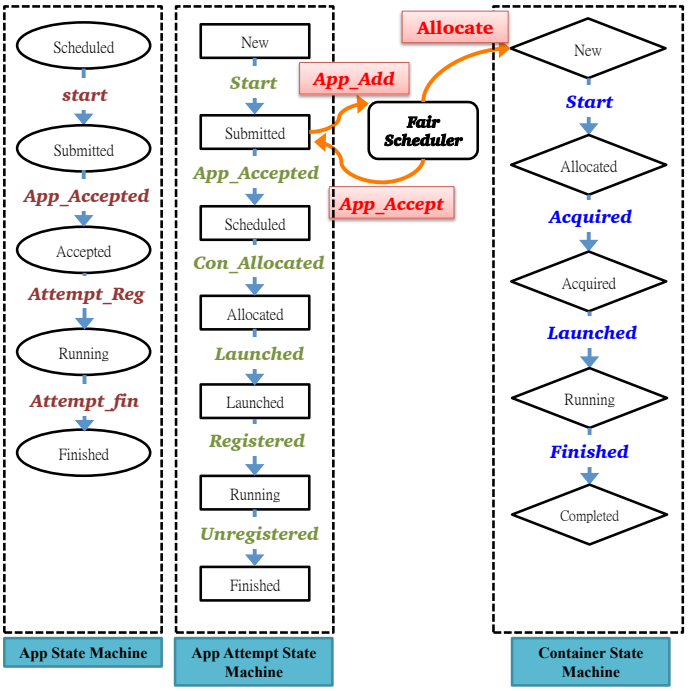

FIG. 2.1. *Job Processing State Graph in YARN. When a job is submitting, the scheduler (in this case is Fair Scheduler) will depend on the resource usage situation to decide to accept the application and allocate the AM container or not.*

used has the resource pool of 64 vcores.

Case 1: We submit a batch of 66 *terasort* jobs to the YARN cluster. Each job will process 100 MB input data generated through *teragen*. In this case, we fix the amount of resource requirement of each job's map and reduce tasks to be equal to 4 vcores in all the experiments. At the same time, we tune the resource requirements of each job's AM from 1 vcore to 4 vcores in different sets of experiments. The makespans of these jobs under different resource requirement settings and different static resource reservations are shown in Figure 2.2. As observed from the figure, the number of reserved resources has great impacts on the makespan of jobs and the optimal configuration of resource reservation is changing as the resource requirement of AMs changes, see the lower plot in Figure 2.2.

Case 2: In this case, we submit the same 66 *terasort* jobs to the cluster. We fix the resource requirement of each job's AM to be equal to 4 vcores and tune the resource-requisition of map and reduce tasks of each job from 1 vcore to 4 vcores in different sets of experiments. The makespans of these jobs under different resource requirement settings and different static resource reservations are shown in Fig. 2.3. Similar to case 1, we can observe that the optimal reservation point (i.e., the number of reserved vcores) is changing as shown in the lower plot.

Based on the above observations, we conclude that the optimal amount of reserved resources is related with the characteristic of workloads. Generally, the best reservation number (R_R) is inversely proportional to the resource requirement of AM (AMC_R), but proportional to the resource demands of other tasks (TC_R), i.e., $R_R \propto \frac{TC_R}{AMC_R}$.

3. Algorithm Design. As shown in Section 2.3, the number of reserved resources has a great impact on system efficiency, and the optimal value could change under different workloads. Therefore, we design a new admission control mechanism for YARN that can dynamically predict the optimal tuning point (i.e., the amount

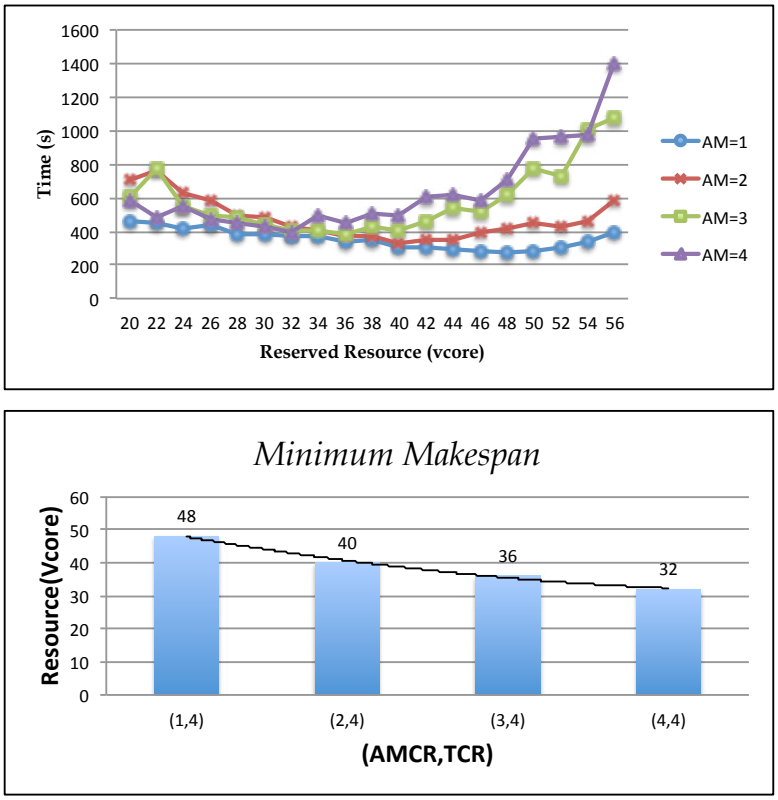

FIG. 2.2. *Makespans of 66* terasort *jobs under different resource requirement settings on AM and different static resource reservations.*

of resources reserved for non-AM tasks) and perform the admission control on incoming YARN jobs. There are three main components in our mechanism:

- RIC (Resource Information Collector): collect the resource and container's information from each node through heartbeat messages.
- RRP (Reserved Resource Predictor): decide how many resources should be reserved based on the information collected by from RIC.
- ARC (Application Resource Controller): leverage the predicted value of RRP to manipulate an application's running.

We will describe the design of these components in details in the following sections.

3.1. Resource Information Collector. The key function of this component is to record the number of currently running ApplicationMasters and normal processing tasks as well as the resources that have been occupied by these two kinds of containers on each worker node. A map data structure is maintained to record the information and will be updated through each heartbeat message between NodeManager and ResourceManager. The algorithm of RIC is shown in Alg. 4.

3.2. Reserved Resource Predictor. The purpose of the RRP component is to find out the amount of reserved resources that can not only preserve high throughput of the system but also prevent the deadlock problem. As shown in Section 2.3, the optimal value of reservation is varying under different workloads. Therefore, the RRP component should be frequently triggered to recalculate the desired reservation level in order to adapt to dynamic workload changes. The overhead of this component thus becomes a primary concern when the workload changes too frequently. In this paper, we propose a simple, heuristic approach to decide an appropriate reservation level according to the information of workload characteristics provided by the RIC component.

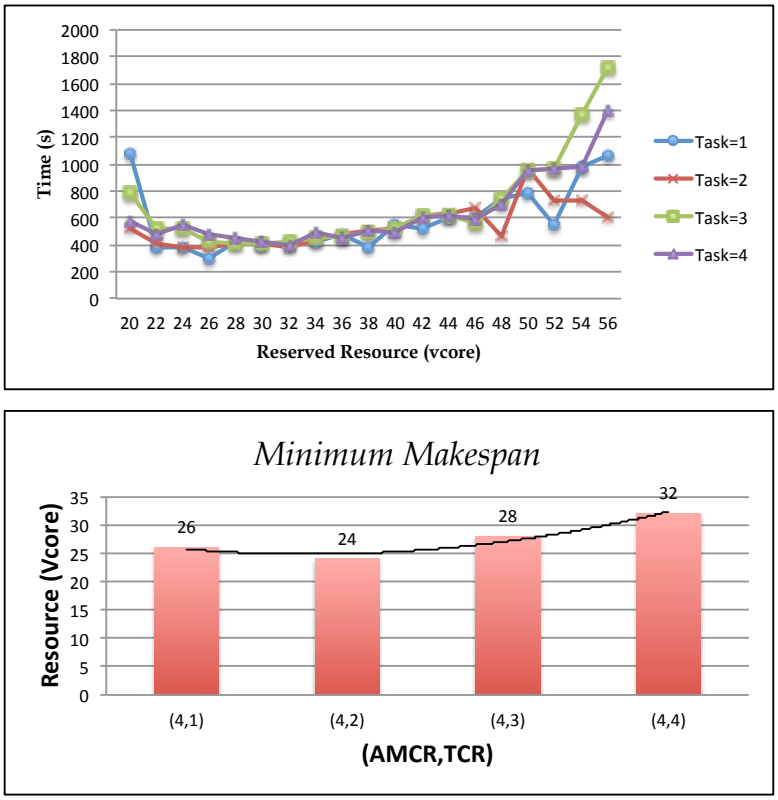

FIG. 2.3. *Makespans of 66* terasort *jobs under different resource requirement settings on map/reduce tasks and different static resource reservations.*

Algorithm 1: Resource Information Collector

Data:
Number of AM containers in node N_i: $N_{AMC_{N_i}}$;
Number of task containers in node N_i: $N_{TC_{N_i}}$;
Total resource of AMC in node N_i: Total_AMC_{N_i};
Total resource of TC in node N_i: Total_TC_{N_i};
HashMap that records each node's AMC information: Map_AMC;
HashMap that records each node's TC information: Map_TC;

1 **while** *each node* N_i *doing NodeUpdate* **do**
2 Record or update N_i: $N_{AMC_{N_i}}$ and Total_AMC_{N_i} into Map_AMC;
3 Record or update N_i: $N_{TC_{N_i}}$ and Total_TC_{N_i} into Map_TC;
4 Update $AvgAMC_R$ and $AvgTC_R$;

In Section 2.3, we also find that the optimal amount of reserved resources (R_R) seems to be proportional and inversely proportional to the resource requisition of non-AM task's (TC_R) and AM task's (AMC_R) containers, i.e., $R_R \propto \frac{TC_R}{AMC_R}$, under static workloads. To get a more clear understanding of this relationship, we conduct 16 sets of experiments. In each set of experiments, we run a batch of jobs with the same resource requirements, i.e., static workloads, repeatedly under different static resource reservations. The optimal resource reservation amounts in terms of makespan are shown in Figure 3.1. We can observe a linear relationship between the optimal reservation and the resource requirements of AM and tasks of jobs. Thus, we have the function:

$$R_R = C_R \cdot \frac{TC_R}{AMC_R + TC_R}, \tag{3.1}$$

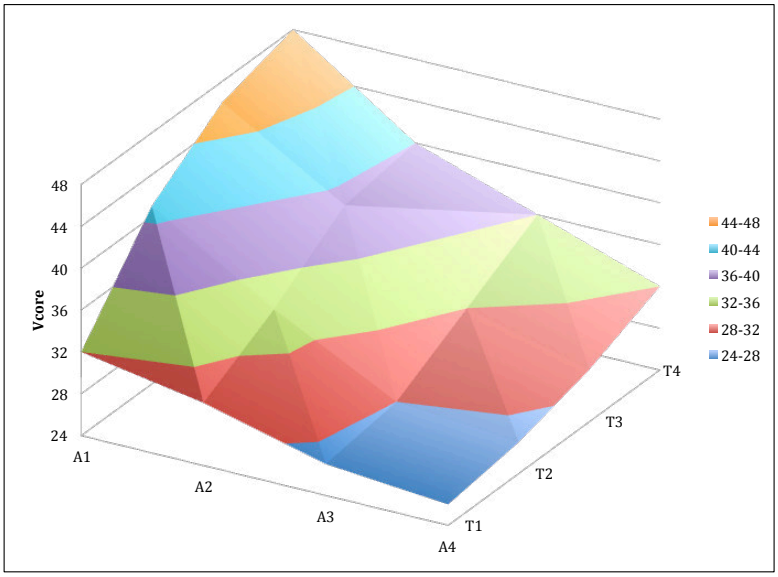

FIG. 3.1. *3D diagram of 16 sets of experiments under static workloads, where x-axis shows the resource requirements of an AM task (from 1 vcore to 4 vcores), y-axis shows the resource requirements of a regular task (from 1 vcore to 4 vcores), and z-axis gives the amount of reserved resources (i.e., number of vcores). Different colors in 3D surface indicate different makespans of the given set of jobs.*

TABLE 3.1
Optimal and predicted resource reservation, i.e., the number of reserved vcores. Predicted values are shown in the parenthesis.

	AMC=1 EXP(PDI)	AMC=2 EXP(PDI)	AMC=3 EXP(PDI)	AMC=4 EXP(PDI)
TC=1	32(32)	30(22)	27(16)	26(13)
TC=2	41(43)	34(32)	28(26)	27(22)
TC=3	46(48)	39(39)	32(32)	29(31)
TC=4	48(52)	40(43)	36(37)	32(32)

that fits such a linear relationship shown in the figure. The intuition behind this relationship is that we need to reserve enough resources for each running application in order to run at least one processing task to avoid severe resource contention.

The comparison between the optimal reservation results obtained through experiments and the prediction ones is shown in Table 3.1. As we can observe, the predicted values (i.e., the number of reserved vcores, shown in the parenthesis) are close to the optimal reservation in most cases. However, the amount of resources that need to be reserved is underestimated when the resource requirement of AM is much larger than the resource requirement of normal tasks. Under such a case, the benefit of accelerating each job's execution, i.e., reserving more resources for processing tasks, clearly surpasses the benefit of allowing higher concurrency between jobs, i.e., allowing AMs to occupy more resources. That is because jobs release a large amount of resources that are occupied by their AMs more quickly when they can finish their execution faster. To improve the accuracy of prediction under the extreme cases, we simply set a lower bound for resource reservation as 40% of the total cluster resources according to our observations. New prediction values are shown in Table 3.2.

Furthermore, we find that such a linear relationship still holds under the mixed workloads where jobs can have different resource requirements if we use the average resource requirements of running AMs and processing tasks to calculate the amount of reserved resources, i.e.,

$$R_R = C_R \cdot \frac{AvgTC_R}{AvgAMC_R + AvgTC_R}, \tag{3.2}$$

TABLE 3.2
Compare the predicted and actual (Experiment result) optimal vcore reservation number.

	AMC=1 EXP(PDI)	AMC=2 EXP(PDI)	AMC=3 EXP(PDI)	AMC=4 EXP(PDI)
TC=1	32(32)	30(26)	27(26)	26(26)
TC=2	41(43)	34(32)	28(26)	27(26)
TC=3	46(48)	39(39)	32(32)	29(31)
TC=4	48(52)	40(43)	36(37)	32(32)

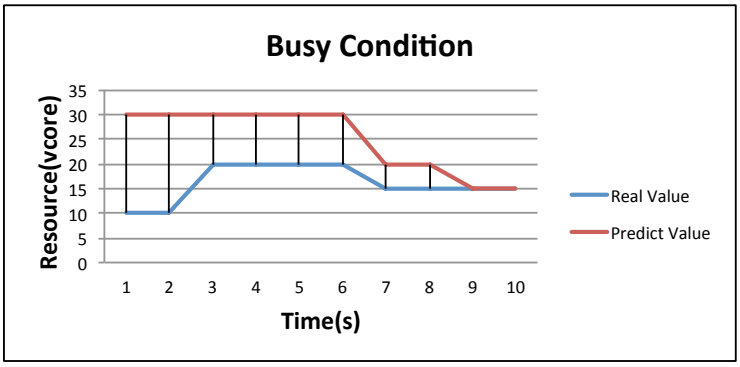

FIG. 3.2. *Compare the predicted reservation resources and the actual available resources.*

where $AvgAMC_R$ and $AvgTC_R$ indicate the average resource requirements of running AMs and processing tasks, respectively. Under the mixed workloads, the prediction value may change over time. For example, the reservation may increase when a new job's AM is submitted for running. However, such an increasing of reservation usually cannot be performed immediately since the resources that are already occupied by AMs cannot be released quickly.

For example, as shown in Figure 3.2, the desired resource reservation for processing tasks is 30 vcores at time period 1. However, the actual amount of remaining resources in the system, i.e., resources that are not occupied by AMs, is 10 vcores. The predicted reservation cannot be achieved until time period 10.

To mitigate the impact of this situation, we further scale up the amount of reserved resources to speed up the execution of processing tasks in the next time period, i.e.,

$$R_R = R_R \cdot \frac{R_R + TotalAMC_R}{C_R}, \tag{3.3}$$

where $TotalAMC_R$ indicates the total amount of resources occupied by AMs. The scale-up is triggered when the summation of resources that are currently occupied by AMs and are needed to be reserved for processing tasks exceeds the resource capacity of the cluster. The algorithm for predicting the reservation amount is shown in Alg. 5, where the scale-up approach is performed in lines 5-6. Figure 3.3 illustrates the summation of resources that are currently occupied by AMs and the desired resource reservation for tasks. The scale-up is triggered when this summation exceeds the capacity of the cluster.

3.3. Application Resource Controller (ARC). The ARC component manages two job queues, i.e., running queue and waiting queue. Each submitted job is inserted into one of these two queues according to the reservation policy. Figure 3.4 illustrates the mechanism of this component. As shown Figure 3.4, when RRP decides to reserve 21 vcores for processing tasks, 6 remaining vcores can then be assigned to AM tasks. The AMs of currently running jobs, i.e., job1 and job2, have already occupied all 6 vcores. Therefore, job3 needs to be inserted into the waiting queue and waits for available resources to start its execution. The algorithm of the ARC component is shown in Alg. 6. In lines 1-6, when a job is submitted to YARN, the ARC component decides if this job can enter the running queue. If the amount of resources for running processing tasks is more

Algorithm 2: Reserved Resource Predictor

Input: Cluster resource: C_R;
Output: Predicted reserved resource: R_R;
while *free resource available on node* **do**
  Get the information from RIC;
  if $N_{AMC} \neq 0$ *and* $N_{TC} \neq 0$ **then**
    $R_R = C_R \cdot \frac{AvgTC_R}{AvgAMC_R + AvgTC_R}$;
    if $R_R > C_R - TotalAMC_R$ **then**
      $R_R = R_R \cdot \frac{R_R + TotalAMC_R}{C_R}$;
    if $R_R < C_R \cdot 40\%$ **then**
      $R_R = C_R \cdot 40\%$;
    if $R_R > C_R - AvgAMC_R$ **then**
      $R_R = C_R - AvgAMC_R$;
  else
    $R_R = C_R \cdot 40\%$;

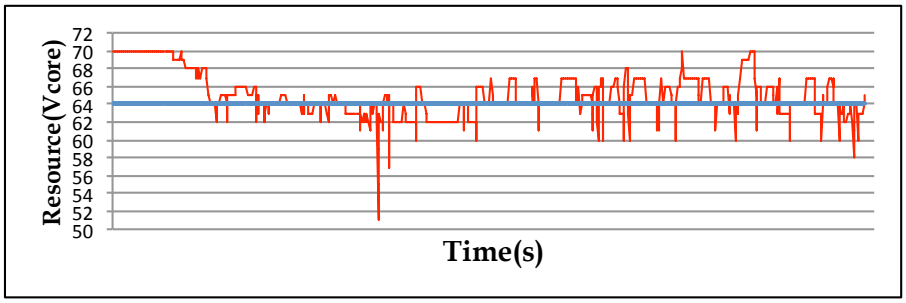

FIG. 3.3. *Illustrations of the total amount of resource (i.e., the resources occupied by AMs and the desired resource reservation for tasks). When the curve is above the overall capacity (i.e., 64 vcores), the reserved resources are then scaled up.*

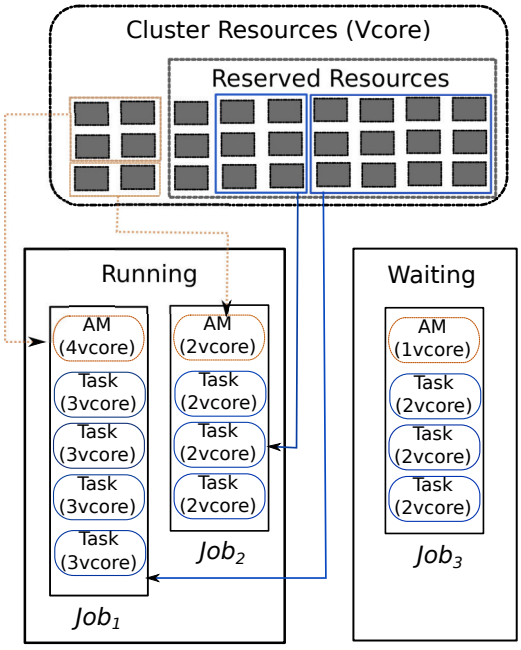

FIG. 3.4. *Application Resource Controller. The controller holds a specific amount of resources to run processing tasks. If there is no resource for processing, then the controller puts incoming jobs into the waiting queue.*

Algorithm 3: Application Resource Controller

Input:
Cluster resource: C_R;
Reserved resource: R_R;
Current occupied resource: $TotalApp_R$;
1 **if** *job J submitted* **then**
2 **if** $C_R - TotalApp_R - AMC_{R_J} \geq R_R$ **then**
3 Push J into APPLIST_RUN;
4 **else**
5 Push J into APPLIST_WAIT;
6 **while** *each node doing NodeUpdate* **do**
7 Get existing available resource in $Node_i$: AVA_R_i;
8 Get the necessary resource to run next waiting job's AM: $WaitingJobAM_R$;
9 $AVA_R = C_R - TotalAPP_R - WaitingJobAM_R$;
10 **if** $AVA_R \geq R_R$ **and** $AVA_R\_i \geq WaitingJobAM_R$ **then**
11 Pop out job J from APPLIST_WAIT;
12 submit ApplicationMaster of J on $Node_i$;
13 Push J into APPLIST_RUN;

than the desired reservation, then the submitted job enters the running queue such that this job's AM can be launched immediately. Furthermore, once work nodes send heartbeat messages to the ResourceManager, the ARC component re-calculates the amount of available resources (AVA_R) and re-submits jobs that are currently waiting in the queue if available resources are enough to run additional AMs, see lines 7-12.

4. Evaluation.

4.1. Experiment Settings. We implement our new admission control mechanism in the Fair scheduler of Hadoop YARN, and build the YARN platform on a local cluster with one master node and 8 worker nodes. Each worker node is configured with 8 vcores and 12GB memory, such that the YARN cluster has the resource capacity of 64 vcores and 96GB memory.

In our experiments, we choose the following four classic MapReduce benchmarks for evaluation.

- **terasort:** a MapReduce implementation of quick sort.
- **wordcount:** a MapReduce program that counts the occurrence times of each word in input files.
- **wordmean:** a MapReduce program that records the average length of words in input files.
- **pi:** a MapReduce program that estimates π value using the Monte Carlo method.

The input files for **terasort** are generated through the `teragen` program, while the input files for **wordcount** and **wordmean** are generated through `randomtextwriter`.

For better understanding how well our new mechanism works, we calculate the relative performance score as follows:

$$Perf.\ Score = \left(1 - \frac{Makespan - Min\_Makespan}{Min\_Makespan}\right) \times 100\%, \tag{4.1}$$

where *Makespan* is the measured makespan (i.e., total completion length) of a batch of MapReduce jobs under our dynamic admission control mechanism, and *Min_Makespan* represents the makespan under the optimal static admission control setting.

4.2. Results Analysis. To better evaluate the robustness of the proposed mechanism, we conduct our experimental evaluation under two sets of workloads, i.e., homogeneous workloads with the same MapReduce jobs and heterogeneous workloads mixing with different MapReduce jobs.

4.2.1. Homogeneous Workloads. In this set of experiments, we submit a batch of 72 **terasort** jobs in each round. All the jobs in the same round have the same resource requirement setting, and each job processes a 100MB randomly generated input file. We further change the resource requirements for jobs in different rounds,

TABLE 4.1
Perf. Scores *under homogeneous workloads.*

	AMC=1	AMC=2	AMC=3	AMC=4
TC=1	90.4%	99.6%	89.3%	91.4%
TC=2	99.3%	95.6%	99.4%	91.7%
TC=3	97.6%	99.2%	96.9%	97.4%
TC=4	88.5%	90.5%	99.7%	98.5%

i.e., from 1 vcore to 4 vcores for both ApplicationMasters and processing tasks. Therefore, there are totally 16 rounds with different resource requirement combinations. The performance (e.g., makespans) under our admission control mechanism which dynamically sets the resource reservations (see red lines) as well as different static reservation configurations (see blue lines) is depicted in Figure 4.1. The corresponding *Perf. Score*s of our new mechanism are also shown in Table 4.1.

We first observe that different resource requirements need different amounts of reserved resources (e.g., numbers of vcores) for running tasks in order to achieve the best performance, i.e., the minimum makespan, see blue curves in Figure 4.1. However, it is inherently difficult to statically find such an optimal reservation level, especially if resource requirements are not fixed. While, by dynamically tuning the resource reservation level, our admission control mechanism always obtains the best performance compared to the results under the static resource reservations under almost all resource requirement configurations, see red lines in the figure. Table 4.1 further demonstrates that our new mechanism achieves high *Perf. Score*s, e.g., under more than half of the cases, *Perf. Score*s are greater than 95%.

4.2.2. Heterogeneous. Now, we turn to evaluate our new mechanism under a more challenging scenario, where we consider heterogeneous workloads which are mixed with different MapReduce jobs. Specifically, we choose more than two MapReduce benchmarks and submit a batch of jobs from these benchmarks which are configured with different resource requirements for running their ApplicationMasters and tasks. We totally conduct 6 sets of experiments with different combinations of MapReduce jobs. Table 4.2 shows the detailed configurations for each set of experiments.

The experimental results (e.g., the makespans and the *Perf. Score*s) under heterogeneous workloads are shown in Figure 4.2 and Table 4.3, respectively. Consistent with the case of homogeneous workloads, we can see that our proposed mechanism can still work well under various heterogeneous MapReduce workloads, which achieves the performance close to those under optimal static resource reservations. On the other hand, the settings for optimal static resource reservations are varying across different heterogeneous workloads. An inappropriate configuration could dramatically degrade the performance. Therefore, our mechanism which dynamically and automatically controls the admission of applications (i.e., reserving resources for running regular tasks) is important for achieving competitive performance of YARN.

5. Related Works. While the original Hadoop MapReduce framework has been extensively studied in recent years, Hadoop YARN is relatively new and has not been widely studied yet. A few preliminary works have been presented to improve the scheduling in Hadoop YARN systems. Dominant resource fairness [14] was proposed to improve the fairness between users when multiple types of resources are required by MapReduce jobs as in YARN framework. Some previous studies [13] [6] designed modified frameworks to handle iterative jobs. These works attempt to achieve performance improvements on share-based scheduling in Hadoop YARN. However, the deadlock problem caused by ApplicationMasters has not been considered yet.

Simple admission control policy that could help avoid deadlocks is supported in Fair [3] and Capacity [2] schedulers of YARN. For example, users can specify the maximum number of jobs for each queue under the Fair scheduler. By manually specifying a small number of jobs that are allowed in each queue concurrently, the ApplicationMasters of these jobs will not occupy all system resources. However, it is difficult for administrators to manually choose a good configuration. Moreover, static configurations cannot work well, especially under dynamic workloads.

Admission control in cloud computing has also been well studied in different aspects. Wu et al. [23] proposed admission control policies that aimed to maximize the SaaS provider's profits based on user SLA

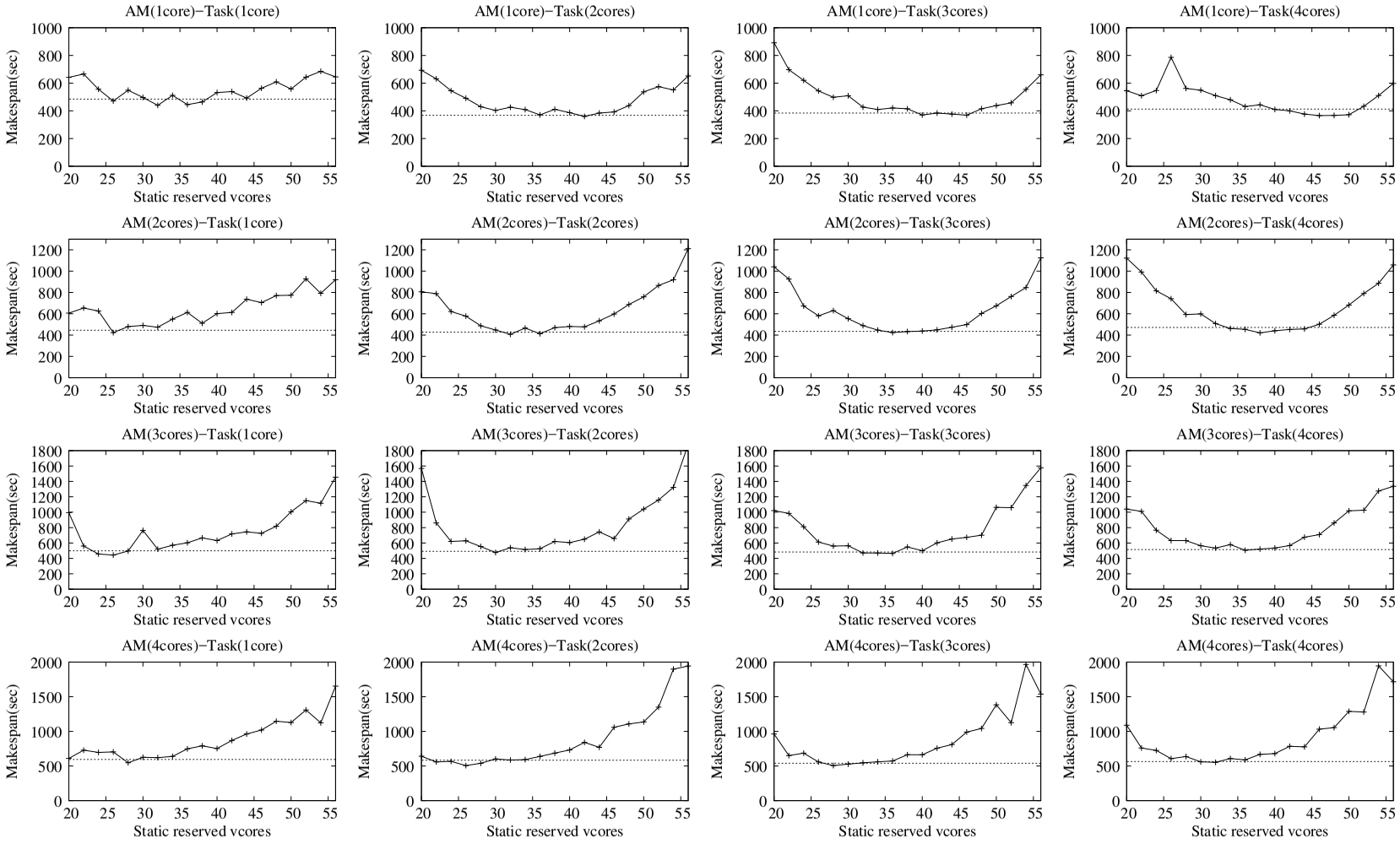

FIG. 4.1. *Makespans under homogeneous workloads, where the solid curves show the results under different static reservation configurations and the red dashed-lines present the results under our mechanism which dynamically sets the resource reservations.*

TABLE 4.2
Experimental setup for heterogeneous workloads.

	Benchmark	Job number	AMC_R	TC_R (Map)	TC_R (Reduce)	Input size
Exp1	Terasort	15	1	2	1	100M
	Wordmean	15	2	1	2	400M
	Wordcount	15	3	3	2	400M
	Pi	15	1	4	1	N/A
Exp2	Terasort	15	3	4	2	400M
	Wordmean	15	1	3	2	200M
	Wordcount	15	2	3	2	200M
	Pi	15	4	2	3	N/A
Exp3	Terasort	15	4	1	3	400M
	Wordmean	15	3	2	4	400M
	Wordcount	15	2	4	1	200M
	Pi	15	1	2	2	N/A
Exp4	Terasort	30	2	3	1	200M
	Wordcount	30	1	3	4	800M
Exp5	Terasort	15	3	1	1	100M
	Wordmean	15	4	1	2	100M
	Wordcount	15	4	1	1	100M
	Pi	15	2	1	1	N/A
Exp6	Terasort	20	1	1	2	200M
	Wordmean	20	2	3	3	400M
	Pi	20	3	2	4	N/A

TABLE 4.3
Perf. Scores *under heterogeneous workloads.*

	Exp1	Exp2	Exp3	Exp4	Exp5	Exp6
Perf. Score	100%	85.9%	94.2%	99.1%	90.6%	95.8%

and IaaS provider SLA. Machine learning based admission control for MapReduce jobs was proposed in [12] to meet job deadlines. Our previous work [24] also proposed a similar admission control mechanism but it does not consider heterogeneous workload use cases. In this work, our primary goal is to avoid the resource deadlocks and meanwhile to improve the makespan of MapReduce jobs [22]. Furthermore, our admission control mechanism only delays jobs instead of declining jobs.

Fine-grained resource management was also well studied for Hadoop systems. ThroughputScheduler [15] was proposed to improve the performance of heterogeneous Hadoop cluster. An explore stage was proposed to learn the resource requirement of tasks and the capabilities of nodes, and the best node was then selected to assign tasks in the scheduler. [18] leveraged job profiling information to dynamically adjust the number of slots on each node, as well as workload placement across nodes, to maximize the resource utilization of the Hadoop cluster. [21] is the first comprehensive study of intermediate data for YARN with Lustre and RDMA. [4] mathematically investigates the scheduling problem which is assigning inputs with various sizes to a set of reducers with capacity. POPI [8] is a lightweight algorithm targeting for efficient processing large outer joins under Hadoop. In order to improve the performance in large distributed environments, a new framework called CCF [9] is proposed to co-optimize application-level data movement and network-level data communications for distributed operators. Rayon [10] is proposed to reserve resources for production jobs and best-effort jobs such that the SLAs for production jobs can be guaranteed and meanwhile the execution time of best-effort jobs can be reduced. We note that our scheduler mainly focuses on how to allocate the reserved resources for best-effort jobs, which is complementary to Rayon in [10]. Zaharia et al. [25] proposed a delay scheduling policy

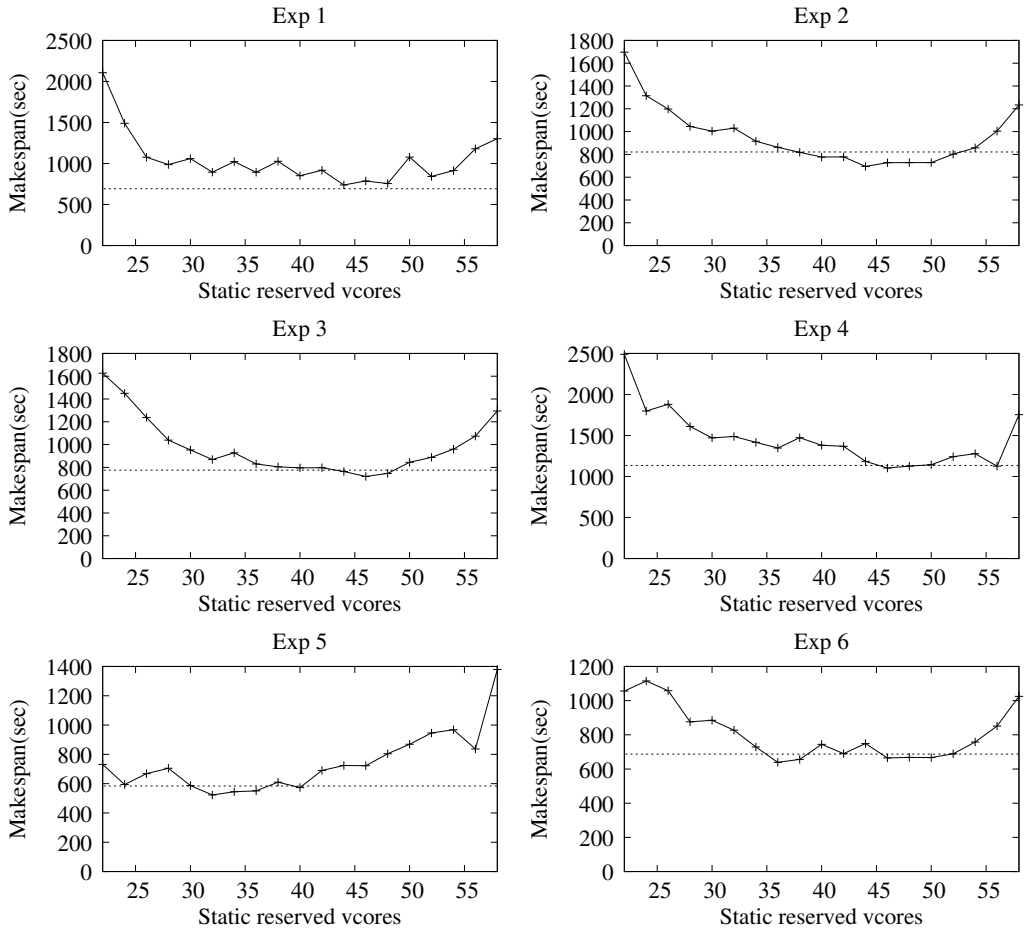

FIG. 4.2. *Makespans under heterogeneous workloads, where the blue curves show the results under different static reservation configurations and the red dashed-lines present the results under our mechanism which dynamically sets the resource reservations.*

to improve the performance of Fair scheduler by increasing the data locality of Hadoop, which is compatible with both Fair scheduler and our proposed scheduling policies. Quincy [16] formulated the scheduling problem in Hadoop as a minimum flow network problem, and decided the slots assignment that obeys the fairness and locality constraints by solving the minimum flow network problem. However, the complexity of this scheduler is high and it was designed for slot based scheduling in the first generation Hadoop. Verma et al. [20] introduced a heuristic method to minimize the makespan of a set of independent MapReduce jobs by applying the classic Johnson's algorithm. However, their evaluation is based on simulation only without real implementation in Hadoop.

6. Conclusions. In this paper, we presented a novel admission control mechanism that integrates with the existing Fair scheduler of Hadoop YARN. The main objective of our work is to automatically and dynamically reserve a specific amount of resources for processing tasks in YARN such that the deadlock problem caused by ApplicationMasters can be avoided. In addition, we aim to achieve better performance by controlling the concurrency level of jobs in the cluster. To meet this goal, the mechanism collects the resource usage information from each work node and leverages this information to predict the optimal amount of reserved resources for processing tasks. A waiting queue is further maintained to hold delayed jobs that will be resubmitted when there are available resources. We implemented our proposed mechanism in Hadoop YARN v2.2.0 and evaluated it with a suite of representative MapReduce benchmarks. The experimental results demonstrate that our mechanism can achieve the near optimal performance. The effectiveness and robustness of this new mechanism

are validated under both homogeneous and heterogeneous workloads. In the future, we will investigate the relationship between job concurrency and system throughput in a YARN cluster and further extend our work to other cloud computing platforms.

REFERENCES

[1] *Apache hadoop users.*
[2] *Hadoop mapreduce next generation - capacity scheduler.*
[3] *Hadoop mapreduce next generation - fair scheduler.*
[4] F. Afrati, S. Dolev, E. Korach, S. Sharma, and J. D. Ullman, *Assignment problems of different-sized inputs in mapreduce*, ACM Transactions on Knowledge Discovery from Data (TKDD), 11 (2016), p. 18.
[5] Apache, *Apache hadoop nextgen mapreduce (yarn).*
[6] Y. Bu, B. Howe, M. Balazinska, and M. D. Ernst, *Haloop: efficient iterative data processing on large clusters*, Proceedings of the VLDB Endowment, 3 (2010), pp. 285–296.
[7] Y. Chen, A. Ganapathi, R. Griffith, and R. Katz, *The case for evaluating mapreduce performance using workload suites*, in Modeling, Analysis & Simulation of Computer and Telecommunication Systems (MASCOTS), 2011 IEEE 19th International Symposium on, IEEE, 2011, pp. 390–399.
[8] L. Cheng and S. Kotoulas, *Efficient large outer joins over mapreduce*, in European Conference on Parallel Processing, Springer, 2016, pp. 334–346.
[9] L. Cheng, Y. Wang, Y. Pei, and D. Epema, *A coflow-based co-optimization framework for high-performance data analytics*, in Parallel Processing (ICPP), 2017 46th International Conference on, IEEE, 2017, pp. 392–401.
[10] C. Curino, D. E. Difallah, C. Douglas, S. Krishnan, R. Ramakrishnan, and S. Rao, *Reservation-based scheduling: If you're late don't blame us!*, in Proceedings of the ACM Symposium on Cloud Computing, ACM, 2014, pp. 1–14.
[11] J. Dean and S. Ghemawat, *Mapreduce: simplified data processing on large clusters*, Communications of the ACM, 51 (2008), pp. 107–113.
[12] J. Dhok, N. Maheshwari, and V. Varma, *Learning based opportunistic admission control algorithm for mapreduce as a service*, in Proceedings of the 3rd India software engineering conference, ACM, 2010, pp. 153–160.
[13] J. Ekanayake, H. Li, B. Zhang, T. Gunarathne, S.-H. Bae, J. Qiu, and G. Fox, *Twister: a runtime for iterative mapreduce*, in Proceedings of the 19th ACM International Symposium on High Performance Distributed Computing, ACM, 2010, pp. 810–818.
[14] A. Ghodsi, M. Zaharia, B. Hindman, A. Konwinski, S. Shenker, and I. Stoica, *Dominant resource fairness: Fair allocation of multiple resource types.*, in NSDI, vol. 11, 2011, pp. 24–24.
[15] S. Gupta, C. Fritz, B. Price, R. Hoover, J. de Kleer, and C. Witteveen, *Throughputscheduler: Learning to schedule on heterogeneous hadoop clusters*, in Proceedings 10th ACM International Conference on Autonomic Computing (ICAC'13), ACM.
[16] M. Isard, V. Prabhakaran, J. Currey, U. Wieder, K. Talwar, and A. Goldberg, *Quincy: fair scheduling for distributed computing clusters*, in Proceedings of the ACM SIGOPS 22nd symposium on Operating systems principles, ACM, 2009, pp. 261–276.
[17] A. Murthy, *Apache hadoop yarn - concepts and applications.*
[18] J. Polo, C. Castillo, D. Carrera, Y. Becerra, I. Whalley, M. Steinder, J. Torres, and E. Ayguadé, *Resource-aware adaptive scheduling for mapreduce clusters*, in Middleware 2011, Springer, 2011, pp. 187–207.
[19] V. K. Vavilapalli, A. C. Murthy, C. Douglas, et al., *Apache hadoop yarn: Yet another resource negotiator*, in Proceedings of the 4th annual Symposium on Cloud Computing, ACM, 2013.
[20] A. Verma, L. Cherkasova, and R. H. Campbell, *Two sides of a coin: Optimizing the schedule of mapreduce jobs to minimize their makespan and improve cluster performance*, in Modeling, Analysis & Simulation of Computer and Telecommunication Systems (MASCOTS), 2012 IEEE 20th International Symposium on, IEEE, 2012, pp. 11–18.
[21] M. Wasi-ur Rahman, N. S. Islam, X. Lu, and D. K. D. Panda, *A comprehensive study of mapreduce over lustre for intermediate data placement and shuffle strategies on hpc clusters*, IEEE Transactions on Parallel and Distributed Systems, 28 (2017), pp. 633–646.
[22] M. Wojnowicz, D. Nguyen, L. Li, and X. Zhao, *Lazy stochastic principal component analysis*, in IEEE International Conference on Data Mining Workshop, 2017.
[23] L. Wu, S. Kumar Garg, and R. Buyya, *Sla-based admission control for a software-as-a-service provider in cloud computing environments*, Journal of Computer and System Sciences, 78 (2012), pp. 1280–1299.
[24] Y. Yao, J. Lin, J. Wang, N. Mi, and B. Sheng, *Admission control in yarn clusters based on dynamic resource reservation*, in Integrated Network Management (IM), 2015 IFIP/IEEE International Symposium on, IEEE, 2015, pp. 838–841.
[25] M. Zaharia, D. Borthakur, J. Sen Sarma, K. Elmeleegy, S. Shenker, and I. Stoica, *Delay scheduling: a simple technique for achieving locality and fairness in cluster scheduling*, in Proceedings of the 5th European conference on Computer systems, ACM, 2010, pp. 265–278.

Edited by: Pradeep Reddy CH
Received: Jun 7, 2017
Accepted: Feb 26, 2018

DOI 10.12694/scpe.v19i1.1394
Scalable Computing: Practice and Experience ISSN 1895-1767
Volume 19, Number 1, pp. 69–77. http://www.scpe.org

AN OPTIMIZED DENSITY-BASED ALGORITHM FOR ANOMALY DETECTION IN HIGH DIMENSIONAL DATASETS

ADEEL SHIRAZ HASHMI*, MOHAMMAD NAJMUD DOJA †, AND TANVIR AHMAD ‡

Abstract. In this study, the authors aim to propose an optimized density-based algorithm for anomaly detection with focus on high-dimensional datasets. The optimization is achieved by optimizing the input parameters of the algorithm using firefly meta-heuristic. The performance of different similarity measures for the algorithm is compared including both L1 and L2 norms to identify the most efficient similarity measure for high-dimensional datasets. The algorithm is optimized further in terms of speed and scalability by using Apache Spark big data platform. The experiments were conducted on publicly available datasets, and the results were evaluated on various performance metrics like execution time, accuracy, sensitivity, and specificity.

Key words: Anomaly detection, outlier detection, optimization, similarity measures, data mining

AMS subject classifications. 68P05, 68W15, 68W25

1. Introduction. In this era of big data, the traditional data mining algorithms are not capable of handling high-dimensional, high-volume datasets efficiently. To handle such datasets, new algorithms need to be proposed or the existing algorithms should be modified. Anomaly/Outlier detection [6][4][1] is a significant field of research in data mining and like other data mining algorithms, anomaly detection algorithms also need to be enhanced to handle such datasets. The algorithm should not only be accurate, but it should also be scalable and fast enough to identify the anomaly in real-time from the vast amount of data that is being generated every second.

This paper discusses how an anomaly detection algorithm can be optimized to make it faster and more accurate, with focus on handling high dimensional datasets. Most of these algorithms provide the results based on some input parameters, and optimization of these parameters is must to obtain high accuracy for the algorithm. These algorithms also make use of some distance/similarity measure to identify the outliers and selection of this distance measure significantly affects the accuracy as well as speed of the algorithm. Further to increase the speed of the algorithm, it can be parallelized to reduce the processing time considerably. So, optimization of the parameters, selection of distance measure, and parallel implementation can collectively have a huge impact on accuracy and speed of the algorithm. This paper aims to propose an efficient anomaly detection algorithm for high-dimensional datasets based on all these fore-mentioned observations.

Local Correlation Integral [13] is a popular anomaly detection algorithm based on identifying the neighborhoods of every instance in the dataset by using a distance/ similarity measure like Euclidean distance, and the instances which are identified as isolated are deemed to be the outliers. In this paper, the authors aim to optimize a LOCI-inspired algorithm for anomaly detection; one of the objectives is to optimize the input parameters, and the only input parameter for this algorithm is the radius of the neighborhood. To optimize this radius threshold, the authors select a swarm intelligence meta-heuristic, which is the firefly algorithm. The second phase of optimization deals with the similarity measure used by the algorithm, where the authors aim to find which similarity measure is optimal while dealing with high dimensional datasets. So, both L1 and L2 norms were compared for accuracy as well as speed. The platform chosen for conducting the experiments is Apache Spark as it guarantees scalability, fault-tolerance and also provides quick results by distributed processing and in-memory analytical abilities.

2. Related Work. In this section, we will review the literature dealing with anomaly detection followed by optimization algorithms which can be utilized to optimize the input parameters.

2.1. Anomaly detection. Anomaly Detection is a field of data mining dealing with finding abnormal data points in the given dataset. The major application areas of anomaly detection are intrusion-detection in the field of network security, fraud detection in financial domain, finding misbehaving node in the wireless

* Department of Computer Engineering, Faculty of Engineering and Technology, Jamia Millia Islamia, New Delhi, India (ashashmi10@gmail.com).
†Department of Computer Engineering, Faculty of Engineering and Technology, Jamia Millia Islamia, New Delhi, India.
‡ Department of Computer Engineering, Faculty of Engineering and Technology, Jamia Millia Islamia, New Delhi, India

sensor networks, medical and healthcare datasets, etc. With the rise of big data, finding anomalies in large datasets in real-time is quite a challenging task. So, we need to develop new faster algorithms or to optimize existing algorithms so that outliers are detected before it is too late in critical real-time environments.

The simplest and fastest anomaly detection algorithm is the AVF (Attribute Value Frequency) [8] which is based on the assumption that the data points with low frequencies are the prime candidates to be the outliers. Another statistical algorithm is the Entropy-based Outlier Detection (EBOD) [9] which assumes that the points whose removal causes the maximum decrease in the entropy of the dataset are the anomalies. There are graphical techniques for outlier detection as well, namely, scatter-plots and box-plots; however these graphical techniques fail for multi-dimensional datasets.

Machine Learning based algorithms are also available for anomaly detection. DBSCAN [7] is a clustering algorithm with ability to identify anomalies, whereas OPTICS-OF [2] is an extension of OPTICS clustering algorithm for anomaly detection. Neural Networks have been utilized in literature in the form of Replicator Neural Networks for finding outliers. LOF (Local Outlier Factor) [3] and LOCI (Local Correlation Integral) [13] are the two most popular algorithms for anomaly detection, provided by most of the machine learning libraries.

2.2. Optimization Algorithms. In artificial intelligence, a metaheuristic is a partial search algorithm which finds a sufficiently good solution when there is no proper information for guiding the search process, and going through all the possible states is not feasible. Metaphor-based metaheuristics are nature-inspired metaheuristics like simulated annealing which is based on a naturally occurring chemical process. Evolutionary algorithms [12] are a category of population-based metaheuristics which start with random solutions and move towards an optimal solution. A category of evolutionary algorithms is swarm-based algorithms which mimic the collective behavior of insects/organisms/animals shown while searching for food, finding mating partner, etc. There are many swarm-based metaheuristics mostly derived from the PSO (Particle Swarm Optimization) and ACO (Ant Colony Optimization) metaheuristics like Firefly Algorithm, Bat Algorithm, Cuckoo Search, Fish School Search, etc. Some of the popular swarm-based metaheuristics are listed in Table 2.1.

The swarm intelligence optimization is based on two processes: exploitation and exploration. The exploitation process deals with finding the best solution among the present candidate solutions (local best), whereas exploration process deals with generating new candidate solutions to reach a global best. The exploration is achieved by a random walk in the search space. Lévy flight [14][17] is a random walk which is used by most of the researchers for exploration in the swarm-based optimization algorithms.

Table 2.1
Swarm-based Metaheuristics

Algorithm	**Year**	**Proposed by**
Ant Colony Optimization	1992	Dorigo, Di Caro
Particle Swarm Optimization	1995	Kennedy, Eberhart, Shi
Harmony Search	2001	Geem, Kim, Loganathan
Bacterial Foraging Algorithm	2002	Passino
Artificial Bee Colony	2007	Karaboga, Basturk
Firefly Algorithm	2008	Xin She-Yang
Cuckoo Search	2009	Xin She-Yang, Deb
Bat Algorithm	2010	Xin She-Yang
Flower Pollination	2012	Xin She-Yang
Cuttlefish Optimization Algorithm	2013	Eesa et al.
Artificial Swarm Intelligence	2014	Louis Resenberg
Grey Wolf Optimizer	2014	Seyedali Mirjalili
Ant Lion Optimizer	2015	Seyedali Mirjalili
Moth Flame Optimization	2015	Seyedali Mirjalili
Dragonfly Algorithm	2015	Seyedali Mirjalili
Whale Optimizer	2016	Seyedali Mirjalili

Most of the swarm-based optimization algorithms are based on the particle swarm optimization algorithm.

PSO mimics the flocking behavior of the birds. The PSO algorithm begins by initializing its population first, which consists of the candidate solutions, called as particles. Each particle has two components position and velocity. The position is the current value of the particle, and the velocity components helps in movement of the particle in the search space. The particles are evaluated using an appropriate fitness function, and the particle which has the highest fitness is labeled as local best. After obtaining the local best, rest of the particles are moved towards this local best particle. This process is repeated in several iterations keeping track of the local best of each iteration and global best among all the iterations, to reach a final global best. The list of algorithms derived from PSO is quite long; artificial bee colony, bat algorithm, firefly algorithm, cuckoo search are among the algorithms which are inspired from PSO.

3. Proposed Work. In this section, we will study how the Local Correlation Integral algorithm identifies the outliers, the shortcomings of LOCI, and how can we optimize our LOCI-inspired algorithm by a metaheuristic. The metaheuristic chosen is a swarm intelligence algorithm based on the behavior of fireflies.

3.1. Density-based Outlier Detection. LOF [3] is a density-based outlier detection algorithm derived from DBSCAN algorithm. In LOF, a local outlier factor score is calculated for each data point. In this method, number of neighborhood points (n) to consider is set a priori. A reachability distance/density is computed (for the data point p under consideration) from the distance to the n nearest neighbors. The reachability density of each of the n nearest neighbors is also calculated. The LOF score of the data point is ratio of the average density of the n nearest neighbor of the point and the density of the point itself. For a normal data point, the density of the point will be similar to that of its neighbors and the LOF value is low, whereas for an outlier LOF score will be high.

LOCI (Local Correlation Integral) [13] addresses the difficulty of selecting the value of n in LOF by using a different criteria for the neighborhood. In LOCI, all the points within a value of r (radius) are considered as neighbors, and the reachability density is calculated *w.r.t* to all these data points. But still the problem that remains is what value of r must be chosen to get optimal results. The LOCI algorithm doesn't provide any mechanism to select a value of r, so either we must know the value of r in advance, or we need to find the value of r by an optimization algorithm. The LOCI algorithm makes use of MDEF (multi-granularity deviation factor) which is the relative density of local neighborhood density of a point and average local neighborhood density of its neighbors; the outliers have a low MDEF score (near zero), whereas normal points have high MDEF score (normally around 1). However, the algorithm used in this paper doesn't utilize the MDEF score; instead it just keeps the basic principle of density-based anomaly detection in mind that low neighborhood density indicates higher probability of the point to be an outlier.

3.2. Firefly Optimization. Firefly metaheuristic [16] is one of the simplest and yet powerful algorithm of swam intelligence, based on flashing behavior of fireflies. The brightest firefly is the most attractive/fittest and rest of fireflies move towards this brightest firefly for mating. This brightest firefly is also not static and it moves randomly in order to further increase its brightness, as its brightness is dependent on brightness of the fireflies in its neighborhood. Firefly metaheuristic begins by initializing a random population of fireflies (solutions). The brightness of each firefly is evaluated by a fitness function, and brightest firefly is identified. The less bright firefly (X_l) is moved towards a brighter firefly (X_b) according to equation (3.1).

$$X_l(t+1) = (1-\beta)X_l(t) + \beta X_b(t) \tag{3.1}$$

where,

$$\beta = \beta_0 e^{-\gamma d^2} \tag{3.2}$$

In equation (3.2), β_0 is a random constant b/w 0-1, and it signifies the convergence rate of the system; high value can jump past the optimal solution and low value can lead to slow convergence, so its value is generally taken to be around 0.2. β signifies the convergence rate b/w a pair of points which depends on the distance d b/w the points. γ is another constant which can be used to control the convergence rate b/w two points, by multiplying it with the distance b/w the two points.

The equation (3.1) deals with exploitation process. For exploration process, the brightest firefly needs to be moved. This random movement of the brightest firefly can be achieved by Lévy flight. Lévy flight is a random

walk in which sudden large steps are taken amidst small steps. The generation of Lévy steps can be achieved by Mantegnas algorithm [10], where the step length S can be calculated by equation (3.3):

$$S = \frac{u}{v^{\frac{1}{\beta}}} \tag{3.3}$$

$$u \approx N(0, \sigma_u^2) \qquad and \qquad v \approx N(0, \sigma_v^2) \tag{3.4}$$

$$\sigma_v = 1 \qquad and \qquad \sigma_u = \left\{ \frac{\Gamma(1+\beta) sin\left(\frac{\pi\beta}{2}\right)}{\Gamma(\frac{1+\beta}{2})\beta 2^{\frac{(\beta-1)}{2}}} \right\}^{\frac{1}{\beta}} \tag{3.5}$$

where β is a parameter b/w interval [1,2] generally taken as 1.5, u and v are drawn from normal distribution, and Γn=(n-1)! is the gamma function.

The firefly metaheuristic can easily be applied for optimizing the value of input parameter r in our anomaly detection algorithm. For optimizing the value of r, the fitness function is k/r and we have to minimize this fitness function. However, the value of r should not be too high so as to include all the points or too low such that every point has small value of k. So, we need to set a lower limit as well as an upper limit on the value of k. So, according to [11] the fitness function that could be used is:

$$\frac{\alpha}{rk} + \frac{k}{r} + \frac{k}{n-k} \tag{3.6}$$

Therefore, the fireflies in our case will be the values of r. For each value of r, the fitness of each point is calculated from equation (3.6).

Steps for anomaly detection by firefly optimized algorithm

Step-1. **Initialization.**
Generate the distance matrix *dist_mat* of the dataset.
Define a *list* with N values of radius r, each value of r corresponding to a firefly.

Step-2. **Calculate brightness of each firefly.**
foreach r in *list* do
    foreach *row* in *dist_max* do
        i. find number of elements less than r (set this value as k).
        ii. find fitness of the row acc. to Eq. 3.6.
    Find the row with minimum value of fitness function. The fitness of this row is the brightness of r/firefly.

Step-3. **Identify brightest firefly.**
In previous step, we get N fitness values corresponding to brightness of each firefly.
The firefly (value of r) with least fitness value is the brightest firefly, denoted by r^*.

Step-4. **Move fireflies.**
foreach r in *list* do
    if(r!=r^*)
        update r acc. to Eq. 3.1.
    else
        update r^* by Lévy flight.

Step-5. **Repeat Steps 3 and 4 for fixed number of iterations.**

Return the value of r^* found to be optimal.

Step-6. **Rank the points for r^*.**
foreach *row* in *dist_max* do
i. find number of elements less than r^*
ii. find fitness of the row acc. to Eq. 3.6.
Rank all the rows (lower the fitness value, higher the rank).

Step-7. **Return the k highest ranked rows/points as outliers and remaining as inliers.**

3.3. Parallelization in Apache Spark. The most popular framework for parallel/distributed computing is Hadoop MapReduce. MapReduce [5] is a distributed/ parallel programming model which runs on a cluster of commodity hardware, where a master node distributes the job to worker nodes for parallel processing. MapReduce model consists of two phases: map and reduce; in the map phase the job in divided into independent sub-tasks and assigned to worker nodes, and in the reduce phase the output returned by each worker is aggregated to give a final result. In MapReduce model, the data is mapped into a list of (key,value) pairs, and then reduce operation is applied over all pairs having the same key.

The Hadoop MapReduce model has a major limitation that it forces a linear dataflow structure on the programs i.e. it doesn't support iterative algorithms. Apache Spark overcomes this limitation through a data structure they call RDD (Resilient Distributed Dataset). RDDs are immutable and their operations are lazy. Fault tolerance is achieved by keeping track of the lineage of each RDD, so that it can be reconstructed in the case of data loss. Apache Spark also has an advanced DAG execution engine that supports acyclic dataflow and in-memory computing. Apache Spark is said to be faster than Apache Hadoop due to its in-memory computation capability and use of Resilient Distributed Database (RDD) on which two types of operations can be performed viz. transformation and action. These transformations and actions contain over 80 high-level operators which make development of parallel applications much easier as compared to other MapReduce based tools like Hadoop.

A Spark job typically contains sequential steps, and those steps which contain independent sub-tasks can be parallelized by executing the sub-tasks in parallel as shown in Figure 3.1. Spark provides APIs with high-level abstractions which provide implicit parallelism over distributed data elements. Spark 2.0 introduced DataFrame API which like RDD is an immutable collection of data, but unlike RDDs, it organizes data into named columns. DataFrame API provides various SQL-like operations which execute in parallel over Spark DataFrame.

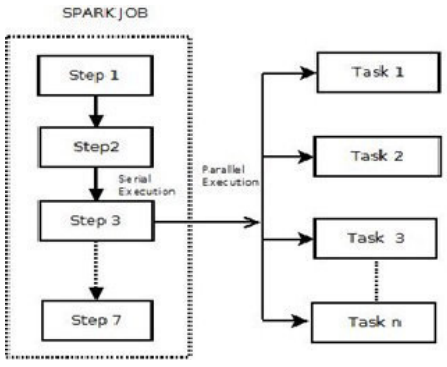

FIG. 3.1. *Spark Job*

The proposed algorithm is implemented using Spark DataFrame API and the hence parallelization is implicit and wasn't needed to be programmed explicitly. The Data- Frame is iterated one row at a time, and its euclidean distance with rest of the rows is calculated in parallel, stored as a temporary distance vector, utilized for counting the number of nearest neighbours and finally the fitness of the row is calculated and stored in a fitness vector.

The fitness vector contains fitness value of each row in the dataset. There are N fitness vectors corresponding to N fireflies (values of r). The process of calculating the distance vector is slow when done sequentially, so parallelization of this step improves the performance of the algorithm considerably.

4. Experimental studies. In this section, the experiments conducted on various publicly available datasets are discussed. The experiments were conducted on i5 processor with 2 cores and 4 GB RAM running Ubuntu 16.10. The algorithm was implemented in PySpark and run over Spark 2.2.0.

4.1. Datasets. The datasets used for experiments are Cardiotocography, Optdigits, Arrhythmia, Musk, Speech and SMTP-KDDCUP99. All these datasets are openly available on UCI/ODDS data repository. The Cardiotocography dataset has 1831 instances with 21 features containing 176 (9.6%) outliers. The Optdigits dataset has 5216 instances with 64 features containing 150 (3%) outliers. The Arrhythmia dataset has 452 instances with 274 features containing 66 (15%) outliers. The Musk dataset has 3062 instances with 166 features containing 97 (3.2%) outliers. Speech dataset has 3686 instances with 400 features containing 61 (1.65%) outliers. SMTP-KDDCUP99 dataset has 95156 instances with 3 features containing 30 (0.03%) outliers.

The Cardiotocography dataset originally has 2126 instances with 23 attributes. The instances are assigned class normal, suspect or pathologic. The points labeled as suspect are discarded, the normal points are considered as inliers and the pathologic points are down-sampled to 176.

The Optdigits dataset is a character recognition dataset for integers 0-9. The 32X32 bitmaps are divided into non-overlapping blocks of 4X4 each, which generates an input matrix of 8X8. The instances for digits 1-9 are treated as inliers whereas the instances of digit 0 are treated as outliers (after down-sampling) to give 150 outliers.

Arrhythmia dataset originally has 279 attributes. There are 5 categorical attributes (age, sex, height, weight, class) which are discarded, giving 274 attributes. The 452 instances are assigned to 16 different labels from 01 to 16. The classes with least instances, i.e., 3, 4, 5, 7, 8, 9, 14, 15 are combined to form the outlier class (66 instances) and the rest of the classes are combined to form the inliers class (386 instances).

Musk dataset describes a set of 102 molecules of which 39 are musks and 63 are non-musks. A single molecule can adopt many shapes due to bond rotations, therefore all the low-energy conformations of the molecules are generated to produce 6598 conformations. The naming convention used for the molecules is MOL_ISO+CONF. These 6598 conformations are reduced to 3062 conformations, keeping molecules j146, j147 and 252 as non-musk (inliers), whereas molecules 213 and 211 are kept as musks (outliers).

The speech dataset consists of 3686 segments of English speech spoken with eight different accents. Most of the segments (98.35%) correspond to American accent whereas only 1.65% (61) of the segments belong to one of the seven other accents. So, the segments belonging to American accent are treated as inliers whereas segments belonging to non-American accent are treated as outliers.

The SMTP-KDDCUP99 dataset is a subset of original KDDCUP99 intrusion detection dataset having 3925651 attacks (80.1%) out of 4898431 records. A smaller set is forged by having only 3377 attacks (0.35%) of 976157 records, where attribute 'logged_in' is positive. From this forged dataset, 95156 instances of 'SMTP' service data is used to construct the SMTP-KDDCUP99 dataset having 30 (0.03%) outliers.

4.2. Evaluation Metrics. To evaluate and compare our results, we need some evaluation metrics. TP (True positives), FP (False Positives), TN (True Negatives) and FN (False Negatives) are the number of normal points correctly detected as inliers, the number of abnormal points that are detected as inliers, the number of abnormal points that are correctly detected as outliers, and the number of normal points that are wrongly detected as outliers, respectively.

Accuracy, sensitivity, and specificity are defined as the following expressions:

$$Accuracy = \frac{TN + TP}{TN + TP + FN + FP} \tag{4.1}$$

$$Sensitivity = \frac{TP}{TP + FN} \tag{4.2}$$

$$Specificity = \frac{TN}{TN + FP} \tag{4.3}$$

4.3. Results. In this section, the results of the experiments are discussed. Analyzing the datasets, the size and feature-to-instance ratio is shown in Table 4.1.

TABLE 4.1
Analysis of datasets

Dataset	Size	Values	Feature-Instance Ratio
Arrhythmia	452 X 274	123,848	0.6061
Cardio	1831 X 21	38,451	0.0114
Musk	3062 X 166	508,292	0.0542
Speech	3686 X 400	1,474,400	0.1085
Optdigits	5216 X 64	333,824	0.0122
SMTP KDDCUP99	95156 X 3	285,468	0.00003

From the literature, it is inferred that Euclidean distance is the similarity measure of choice for ordinary datasets. Table 4.2 provides the execution time to generate the similarity matrices by different similarity measures for our chosen datasets. From Table 4.2, we can infer that execution time is primarily dependent on number of instances rather than total size of the dataset. Further, it is noticed that Manhattan distance is the best choice among the chosen distance measures as far as execution time is concerned; the notable exception is the cardio dataset which has the smallest dimensions among the chosen datasets and for this dataset Euclidean distance has best execution time. It is also noticed that feature-instance ratio has no major impact on choice of similarity measure, as Cardio and Optdigits have nearly same ratio, but results are clearly different. From these results we can conclude that Manhattan distance is the best candidate for similarity measure while dealing with high-dimensional datasets.

TABLE 4.2
Execution Time (in seconds) for distance matrix

Data-base	Distance Measures			
	Euclidean	Cosine Similarity	Manhattan Distance	Hellinger Distance
Arrythmia	0.145	0.141	0.125	0.134
Cardio	1.70	1.66	1.61	1.63
Musk	4.75	4.82	4.50	4.67
Speech	6.58	6.67	6.42	6.51
Optdigits	20.98	14.18	13.74	13.94

Table 4.3 summarizes the accuracy, sensitivity, and specificity of the proposed solution for each dataset. The results show that the algorithm returns highly accurate results for all the datasets. Specificity is the indicator of algorithm's capability of identifying the outliers, whereas sensitivity and accuracy are the indicators of algorithm's capability of identifying normal instances as well as anomalies.

Table 4.4 compares the performance of proposed firefly-optimized algorithm for anomaly detection with state-of-the-art algorithms of anomaly detection viz. K-Means, DBSCAN and LOF. The performance comparison is done on the basis of accuracy metric using euclidean distance as similarity measure. From the results, it is obvious that the firefly optimized algorithm is far superior in terms of accuracy. The major reason for superiority of firefly optimized algorithm is that rest of the algorithms are run with random/default parameters whereas firefly algorithm is self-optimizing (it optimizes the neighbourhood radius "r").

5. Conclusion and Future Scope. From the experiments, we can conclude that optimization achieved by firefly algorithm for the value of "r" was quite fruitful as the results were evaluated to be highly accurate.

TABLE 4.3
Performance Metrics

Dataset	Distance Measure	Accuracy	Sensitivity	Specificity
Cardio dataset	Euclidean Norm	0.9235	0.9564	0.5909
	Cosine Similarity	0.9235	0.9564	0.5909
	Manhattan Distance	0.9213	0.9577	0.6022
	Hellinger Distance	0.9224	0.9564	0.5965
OptDigits dataset	Euclidean Norm	0.9704	0.9848	0.4866
	Cosine Similarity	0.9689	0.9786	0.4600
	Manhattan Distance	0.9635	0.9812	0.4266
	Hellinger Distance	0.9651	0.9820	0.3933
Arrhythmia dataset	Euclidean Norm	0.8362	0.9046	0.4218
	Cosine Similarity	0.8362	0.9046	0.4218
	Manhattan Distance	0.8451	0.9097	0.4531
	Hellinger Distance	0.8407	0.9072	0.4375
Musk dataset	Euclidean Norm	0.9800	0.9895	0.6804
	Cosine Similarity	0.9794	0.9892	0.6700
	Manhattan Distance	0.9794	0.9892	0.6700
	Hellinger Distance	0.9885	0.9781	0.6494
Speech dataset	Euclidean Norm	0.9722	0.9859	0.1475
	Cosine Similarity	0.9722	0.9859	0.1475
	Manhattan Distance	0.9744	0.9870	0.2131
	Hellinger Distance	0.9733	0.9864	0.1803
SMTP KDDCUP99 dataset	Euclidean Norm	0.9996	0.9998	0.4000
	Cosine Similarity	0.9996	0.9998	0.3666
	Manhattan Distance	0.9996	0.9998	0.4000
	Hellinger Distance	0.9996	0.9998	0.3666

TABLE 4.4
Performance Comparison with state-of-the-art

Dataset	K-Means	DBSCAN	LOF	Firefly
Arrhythmia	0.7351	0.6892	0.8543	0.8362
Cardiotocography	0.7916	0.7495	0.8641	0.9235
Musk	0.8512	0.7718	0.9268	0.9800
Optdigits	0.8648	0.8251	0.9375	0.9704
Speech	0.8922	0.8442	0.9416	0.9722
KDDCup99	0.9448	0.9152	0.9657	0.9996

From the discussions above, it is evident that Manhattan L1-norm is most suitable similarity measure for high-dimensional dataset; and as the algorithm was implemented on Apache Spark, therefore the solution is scalable as well as fast.

The future scope of this work is to use other swarm-intelligence algorithms and find a better alternative to firefly algorithm in terms of convergence speed. Parallelization can be done on platforms like GPU which can possibly speed-up the turnaround time even further.

REFERENCES

[1] C. C. AGGARWAL, *Outlier analysis*, in Data mining, Springer, 2015, pp. 237–263.
[2] M. BREUNIG, H.-P. KRIEGEL, R. NG, AND J. SANDER, *Optics-of: Identifying local outliers*, Principles of data mining and knowledge discovery, (1999), pp. 262–270.

[3] M. M. Breunig, H.-P. Kriegel, R. T. Ng, and J. Sander, *Lof: identifying density-based local outliers*, in ACM sigmod record, vol. 29, ACM, 2000, pp. 93–104.
[4] V. Chandola, A. Banerjee, and V. Kumar, *Anomaly detection: A survey*, ACM computing surveys (CSUR), 41 (2009), p. 15.
[5] J. Dean and S. Ghemawat, *Mapreduce: simplified data processing on large clusters*, Communications of the ACM, 51 (2008), pp. 107–113.
[6] D. E. Denning, *An intrusion-detection model*, IEEE Transactions on software engineering, (1987), pp. 222–232.
[7] M. Ester, H.-P. Kriegel, J. Sander, X. Xu, et al., *A density-based algorithm for discovering clusters in large spatial databases with noise.*, in Kdd, vol. 96, 1996, pp. 226–231.
[8] A. Koufakou, J. Secretan, J. Reeder, K. Cardona, and M. Georgiopoulos, *Fast parallel outlier detection for categorical datasets using mapreduce*, in Neural Networks, 2008. IJCNN 2008.(IEEE World Congress on Computational Intelligence). IEEE International Joint Conference on, IEEE, 2008, pp. 3298–3304.
[9] B. Liu, W. Fan, and T. Xiao, *A fast outlier detection method for big data*, in Asian Simulation Conference, Springer, 2013, pp. 379–384.
[10] R. N. Mantegna, *Fast, accurate algorithm for numerical simulation of levy stable stochastic processes*, Physical Review E, 49 (1994), p. 4677.
[11] A. W. Mohemmed, M. Zhang, and W. N. Browne, *Particle swarm optimisation for outlier detection*, in Proceedings of the 12th annual conference on Genetic and evolutionary computation, ACM, 2010, pp. 83–84.
[12] A. Mukhopadhyay, U. Maulik, S. Bandyopadhyay, and C. A. C. Coello, *A survey of multiobjective evolutionary algorithms for data mining: Part i*, IEEE Transactions on Evolutionary Computation, 18 (2014), pp. 4–19.
[13] S. Papadimitriou, H. Kitagawa, P. B. Gibbons, and C. Faloutsos, *Loci: Fast outlier detection using the local correlation integral*, in Data Engineering, 2003. Proceedings. 19th International Conference on, IEEE, 2003, pp. 315–326.
[14] I. Pavlyukevich, *Lévy flights, non-local search and simulated annealing*, Journal of Computational Physics, 226 (2007), pp. 1830–1844.
[15] V. K. Vavilapalli, A. C. Murthy, C. Douglas, S. Agarwal, M. Konar, R. Evans, T. Graves, J. Lowe, H. Shah, S. Seth, et al., *Apache hadoop yarn: Yet another resource negotiator*, in Proceedings of the 4th annual Symposium on Cloud Computing, ACM, 2013, p. 5.
[16] X.-S. Yang, *Firefly algorithm, stochastic test functions and design optimisation*, International Journal of Bio-Inspired Computation, 2 (2010), pp. 78–84.
[17] X.-S. Yang and S. Deb, *Cuckoo search via lévy flights*, in Nature & Biologically Inspired Computing, 2009. NaBIC 2009. World Congress on, IEEE, 2009, pp. 210–214.
[18] M. Zaharia, R. S. Xin, P. Wendell, T. Das, M. Armbrust, A. Dave, X. Meng, J. Rosen, S. Venkataraman, M. J. Franklin, et al., *Apache spark: A unified engine for big data processing*, Communications of the ACM, 59 (2016), pp. 56–65.

Edited by: Gabriel Iuhasz
Received: Dec 11, 2017
Accepted: Mar 11, 2018

AIMS AND SCOPE

The area of scalable computing has matured and reached a point where new issues and trends require a professional forum. SCPE will provide this avenue by publishing original refereed papers that address the present as well as the future of parallel and distributed computing. The journal will focus on algorithm development, implementation and execution on real-world parallel architectures, and application of parallel and distributed computing to the solution of real-life problems. Of particular interest are:

Expressiveness:

- high level languages,
- object oriented techniques,
- compiler technology for parallel computing,
- implementation techniques and their efficiency.

System engineering:

- programming environments,
- debugging tools,
- software libraries.

Performance:

- performance measurement: metrics, evaluation, visualization,
- performance improvement: resource allocation and scheduling, I/O, network throughput.

Applications:

- database,
- control systems,
- embedded systems,
- fault tolerance,
- industrial and business,
- real-time,
- scientific computing,
- visualization.

Future:

- limitations of current approaches,
- engineering trends and their consequences,
- novel parallel architectures.

Taking into account the extremely rapid pace of changes in the field SCPE is committed to fast turnaround of papers and a short publication time of accepted papers.

INSTRUCTIONS FOR CONTRIBUTORS

Proposals of Special Issues should be submitted to the editor-in-chief.

The language of the journal is English. SCPE publishes three categories of papers: overview papers, research papers and short communications. Electronic submissions are preferred. Overview papers and short communications should be submitted to the editor-in-chief. Research papers should be submitted to the editor whose research interests match the subject of the paper most closely. The list of editors' research interests can be found at the journal WWW site (`http://www.scpe.org`). Each paper appropriate to the journal will be refereed by a minimum of two referees.

There is no a priori limit on the length of overview papers. Research papers should be limited to approximately 20 pages, while short communications should not exceed 5 pages. A 50–100 word abstract should be included.

Upon acceptance the authors will be asked to transfer copyright of the article to the publisher. The authors will be required to prepare the text in LaTeX 2ε using the journal document class file (based on the SIAM's `siamltex.clo` document class, available at the journal WWW site). Figures must be prepared in encapsulated PostScript and appropriately incorporated into the text. The bibliography should be formatted using the SIAM convention. Detailed instructions for the Authors are available on the SCPE WWW site at `http://www.scpe.org`.

Contributions are accepted for review on the understanding that the same work has not been published and that it is not being considered for publication elsewhere. Technical reports can be submitted. Substantially revised versions of papers published in not easily accessible conference proceedings can also be submitted. The editor-in-chief should be notified at the time of submission and the author is responsible for obtaining the necessary copyright releases for all copyrighted material.